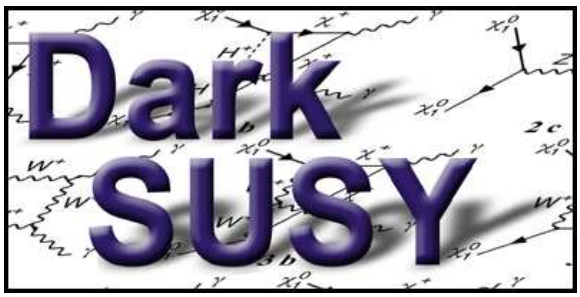

DarkSUSY darksusy-5.1 (rev 806)

Manual and short description of routines

Created automatically by headers2tex.pl
Mon Feb 18 20:40:12 2013

http://www.darksusy.org

Paolo Gondolo[a*], **Joakim Edsjö**[b†], **Lars Bergström**[b‡], **Piero Ullio**[c§], **Mia Schelke**[d¶], **Edward A. Baltz**[e‖], **Torsten Bringmann**[b**] and **Gintaras Duda**[f††]

[a] *Utah*
[b] *Department of Physics, Stockholm University, SCFAB, SE-106 91 Stockholm, Sweden*
[c] *SISSA, via Beirut 4, 34014 Trieste, Italy*
[d] *Torino*
[e] *SLAC*
[f] *Creighton University*

*E-mail address: gondolo@mppmu.mpg.de
†E-mail address: edsjo@physto.se
‡E-mail address: lbe@physto.se
§E-mail address: ullio@he.sissa.it
¶E-mail address: schelke@...
‖E-mail address: eabaltz@physics.columbia.edu
**E-mail address: troms@physto.se
††E-mail address: gkduda@creighton.edu

Abstract

DarkSUSY is a program package for supersymmetric dark matter calculations. This manual describes the theoretical background as well as details about the actual routines. Everything is not covered, but it should hopefully prove useful if you need more information than in our published articles.

Disclaimer. This manual is work in progress.

We try to keep it clear and upto-date with the code, but there will be cases where changes/improvements in the code, for one reason or another, will not have propagated into the manual. Hence, check the actual code if you want to be certain about how a given process/feature is implemented.

Contents

Chapter 1

Introduction

DarkSUSY is a set of Fortran routine to make calculations for supersymmetric dark matter in the Minimal Supersymmetric Standard Model, the MSSM. The physics involved is covered in the DarkSUSY paper [1]. In this manual we will mainly cover the more techincal aspects of DarkSUSY, i.e. how to call different subroutines and how to change switches and options. We will only briefly review the necessary physics involved when needed and refer the reader to [1] and the original papers behind DarkSUSY [2] for more details. If you use DarkSUSY please consider the original physics work behind and give proper credit to [1] and the relevant references in [2]. If you use non-standard options, e.g. a different propagation model for antiprotons, please remember to give proper credit to that model.

Chapter 2

Main programs

DarkSUSY is primarily a library that is intended to be used with your own main programs. However, to get you started, we supply a few sample programs in the test directory. These can be used as they are, but they are also extensively commented to help you understand which routines you are supposed to call for the most typical calculations. The programs in test are

dsmain A main program that asks for MSSM or mSUGRA model parameters and calculates accelerator constraints, relic density and various rates for that model. This program is good as it is for quick calculations for a small set of models. It is also a good starting point for making your own main programs. Just read through the code and its comments.

dstest A test program that performs roughly the same things as **dsmain**, but instead reads a handful of MSSM models from a datafile. This program is mainly intended to test that your installation works as expected, however this program is also as commented as **dsmain** and can be used to learn about which DarkSUSY routines to call.

dstest-isasugra Like **dstest** but for mSUGRA models.

dstest-galprop Like **dstest**, but uses galprop for the charged cosmic ray calculations instead of the internal routines.

dstest-galprop-one A special version of the galprop interface for machines where memory leaks (in galprop) causes **dstest-galprop** to crash before it has calculated all the Green's functions.

Chapter 3

General remarks on notation

In an attempt to keep this manual reasonably easy to follow we will need to specify our notation. We will use the following convention for fonts,

Convention for fonts	
text	This font is used for normal text.
variable	This font is used for variables or other things in the code that is mentioned.
routine	This font is used for subroutine or function names or for header file names.
`dump`	This font will be used for screen dumps of outputs.
input	This font will be used for user input, i.e. where you are supposed to write something.

Subroutines and functions will be described with the following structure

subroutine **example**(in1,in2,in3,in4,in5,in6,in7,out1)		
Purpose:		Here the routine will be explained.
Inputs:		
in1	i	This is an input argument, declared as integer.
in2	r	This is an input argument, declared as real.
in3	r8	This is an input argument, declared as real*8.
in4	c	This is an input argument, declared as complex.
in5	c16	This is an input argument, declared as complex*16.
in6	ch2	This is an input argument, declared as character*2.
in7	ch*	This is an input argument, declared as character*(*).
Outputs		
out1	r8	This is an output argument, declared as real*8

where the shorthand notation for the type of the arguments is indicated. For functions, the type is indicated on the first line,

function **fun**(arg)		r8
Purpose:		Here the function will be explained.
Inputs:		
arg	i	This is an input argument, declared as integer.

i.e., in this case the function is declared as real*8.

The subroutines always reside in a file with the same name as the subroutine/function. Routines that belong together are put in separate subdirectories in the src directory. The different subdirectories are

Subdirectories in src/	
ac	accelerator constraints
an	driver routines for neutralino and chargino annihilation

an1l	1-loop neutralino annihilation amplitudes
anstu	tree-level neutralino and chargino annihilation amplitudes
dd	direct detection and neutralino scattering
ep	positron fluxes from the halo
ge	general routines
ha	yields of halo annihilation products (from Pythia simulations in vacuum)
hm	halo models
hr	driver routines for rates from the halo
ib	internal bremsstrahlung
ini	initialization routines
mh	kinetic decoupling and microhalos
mu	neutrino and muon yields from the neutralino annihilations in the Earth/Sun (from Pythia simulations in medium)
nt	driver routines for rates and fluxes in neutrino telescopes
pb	antiprotons from annihilation in the halo
rd	relic density routines (general)
rn	driver routines for neutralino relic density
su	general MSSM routines, couplings, masses, etc.
xcern	routines from CERNLIB
xcmlib	routines from CMLIB

Common blocks are all declared in header files in the inc directory. When discussing switches and parameters in common blocks we will, instead of describing the common blocks in detail, mention which header file they reside in. If you want to access these variables, you should then include the corresponding header file. E.g., it can look like this

Example parameters in **headerfile.h**

Purpose:		Description of this set of variables.
par1	r8	Description of a real*8 parameter.

Chapter 4

src/ac: Accelerator bounds

4.1 Accelerator bounds

DarkSUSY contains a set of routines to check if a given model is excluded by accelerator constraints. These routines are called **dsacbnd[number]**. The policy is that when we update DarkSUSY with new accelerator constraints, we keep the old routine, and add a new routine with the last number incremented by one. Which routine that is called is determined by calling **dsacset** with a tag determining which routine to call. To check the accelerator constraints, then call **dsacbnd** which calls the right routine for you. Upon return, **dsacbnd** returns an exclusion flag, excl. If zero, the model is OK, if non-zero, the model is excluded. The cause for the exclusion is coded in the bits of excl according to table 4.1

excl			
Bit set	Octal value	Decimal value	Reason for exclusion
0	1	1	Chargino mass
1	2	2	Gluino mass
2	4	4	Squark mass
3	10	8	Slepton mass
4	20	16	Invisible Z width
5	40	32	Higgs mass
6	100	64	Neutralino mass
7	200	128	$b \to s\gamma$
8	400	256	ρ parameter

Table 4.1: The bits of excl are set to indicate by which process this particular model is excluded. Check if a bit is set with btest(excl,bit).

Chapter 5

src/an: Annihilation cross sections (general, χ^0 and $\chi^\pm$)

5.1 Annihilation cross sections – theory

For the relic density calculations, we need all possible (co)annihilation cross sections between neutralinos, charginos and sfermions.

5.1.1 Annihilation cross sections

We have calculated all two-body final state cross sections at tree level for involving netralinos, charginos, sneutrinos, sleptons and squarks in the initial state. A complete list is given below.

Since we have so many different diagrams contributing, we have to use some method where the diagrams can be calculated efficiently. To achive this, we calculate the diagrams with general expressions for vertices, masses etc so that they can be reused for other processes. How we do this in practice differs a bit between different sets of annihilation diagrams.

For neutralino-neutralino, neutralino-chargino and chargino-chargino annihilation, we classify the diagrams according to their topology (s-, t- or u-channel) and to the spin of the particles involved. We then compute the helicity amplitudes for each type of diagram analytically with REDUCE [71] using general expressions for the vertex couplings.

The strength of the helicity amplitude method is that the analytical calculation of a given type of diagram has to be performed only once and the sum of the contributing diagrams for each set of initial and final states can be done numerically afterwards.

For the diagrams involving sfermions, FORM is used to analytically calculate the amplitudes. This output is then converted into Fortran with a PERL script, **form2f** [173].

5.1.2 Coannihilation diagrams

All Feynman diagrams for which we calculate the annihilation cross section are listed in the coming sections. $s(x)$, $t(x)$ and $u(x)$ denote a tree-level Feynman diagram in which particle x is exchanged in the s-, t- and u-channel respectively.

The convention used in this list of included coannihilation diagrams is that if a sfermion is denoted $\tilde{f}$, then it's antiparticle is denoted $\tilde{f}^*$.

5.1.3 Neutralino and chargino annihilation

Indices i, j, k run from 1 to 4, and indices c, d, e from 1 to 2. u, $\tilde{u}$, d, $\tilde{d}$, ν, $\tilde{\nu}$, ℓ, $\tilde{\ell}$, f and $\tilde{f}$ are generic notations for up-type quarks, up-type squarks, down-type quarks, down-type squarks, neutrinos, sneutrinos, leptons, sleptons, fermions and sfermions. A sum of diagrams over (s)fermion generation indices and over the neutralino and chargino indices k and e is understood (no sum over indices i, j, c, d).

Neutralino-neutralino annihilation

Initial state	Final state	Feynman diagrams
$\chi_i^0\chi_j^0$	H_1H_1, H_1H_2, H_2H_2, H_3H_3	$t(\chi_k^0)$, $u(\chi_k^0)$, $s(H_{1,2})$
	H_1H_3, H_2H_3	$t(\chi_k^0)$, $u(\chi_k^0)$, $s(H_3)$, $s(Z^0)$
	H^-H^+	$t(\chi_e^+)$, $u(\chi_e^+)$, $s(H_{1,2})$, $s(Z^0)$
	Z^0H_1, Z^0H_2	$t(\chi_k^0)$, $u(\chi_k^0)$, $s(H_3)$, $s(Z^0)$
	Z^0H_3	$t(\chi_k^0)$, $u(\chi_k^0)$, $s(H_{1,2})$
	W^-H^+, W^+H^-	$t(\chi_e^+)$, $u(\chi_e^+)$, $s(H_{1,2,3})$
	Z^0Z^0	$t(\chi_k^0)$, $u(\chi_k^0)$, $s(H_{1,2})$
	W^-W^+	$t(\chi_e^+)$, $u(\chi_e^+)$, $s(H_{1,2})$, $s(Z^0)$
	$f\bar{f}$	$t(\tilde{f}_{L,R})$, $u(\tilde{f}_{L,R})$, $s(H_{1,2,3})$, $s(Z^0)$

Neutralino-chargino annihilation

Initial state	Final state	Feynman diagrams
$\chi_c^+\chi_i^0$	H^+H_1, H^+H_2	$t(\chi_k^0)$, $u(\chi_e^+)$, $s(H^+)$, $s(W^+)$
	H^+H_3	$t(\chi_k^0)$, $u(\chi_e^+)$, $s(W^+)$
	W^+H_1, W^+H_2	$t(\chi_k^0)$, $u(\chi_e^+)$, $s(H^+)$, $s(W^+)$
	W^+H_3	$t(\chi_k^0)$, $u(\chi_e^+)$, $s(H^+)$
	H^+Z^0	$t(\chi_k^0)$, $u(\chi_e^+)$, $s(H^+)$
	γH^+	$t(\chi_c^+)$, $s(H^+)$
	W^+Z^0	$t(\chi_k^0)$, $u(\chi_e^+)$, $s(W^+)$
	γW^+	$t(\chi_c^+)$, $s(W^+)$
	$u\bar{d}$	$t(\tilde{d}_{L,R})$, $u(\tilde{u}_{L,R})$, $s(H^+)$, $s(W^+)$
	$\nu\bar{\ell}$	$t(\tilde{\ell}_{L,R})$, $u(\tilde{\nu}_L)$, $s(H^+)$, $s(W^+)$

Chargino-chargino annihilation

Initial state	Final state	Feynman diagrams
$\chi_c^+\chi_d^-$	H_1H_1, H_1H_2, H_2H_2, H_3H_3	$t(\chi_e^+)$, $u(\chi_e^+)$, $s(H_{1,2})$
	H_1H_3, H_2H_3	$t(\chi_e^+)$, $u(\chi_e^+)$, $s(H_3)$, $s(Z^0)$
	H^+H^-	$t(\chi_k^0)$, $s(H_{1,2})$, $s(Z^0,\gamma)$
	Z^0H_1, Z^0H_2	$t(\chi_e^+)$, $u(\chi_e^+)$, $s(H_3)$, $s(Z^0)$
	Z^0H_3	$t(\chi_e^+)$, $u(\chi_e^+)$, $s(H_{1,2})$
	H^+W^-, W^+H^-	$t(\chi_k^0)$, $s(H_{1,2,3})$
	Z^0Z^0	$t(\chi_e^+)$, $u(\chi_e^+)$, $s(H_{1,2})$
	W^+W^-	$t(\chi_k^0)$, $s(H_{1,2})$, $s(Z^0,\gamma)$
	$\gamma\gamma$ (only for $c=d$)	$t(\chi_c^+)$, $u(\chi_c^+)$
	$Z^0\gamma$	$t(\chi_d^+)$, $u(\chi_c^+)$
	$u\bar{u}$	$t(\tilde{d}_{L,R})$, $s(H_{1,2,3})$, $s(Z^0,\gamma)$
	$\nu\bar{\nu}$	$t(\tilde{\ell}_{L,R})$, $s(Z^0)$
	$\bar{d}d$	$t(\tilde{u}_{L,R})$, $s(H_{1,2,3})$, $s(Z^0,\gamma)$
	$\bar{\ell}\ell$	$t(\tilde{\nu}_L)$, $s(H_{1,2,3})$, $s(Z^0,\gamma)$
$\chi_c^+\chi_d^+$	H^+H^+	$t(\chi_k^0)$, $u(\chi_k^0)$
	H^+W^+	$t(\chi_k^0)$, $u(\chi_k^0)$
	W^+W^+	$t(\chi_k^0)$, $u(\chi_k^0)$

5.1.4 Squark-squark annihilation

Note: The tables below are not entirely up to date, more processes are included than shown in the tables.

We will here denote squarks as $\tilde{q}_a^i$ and $\tilde{q}_b^j$ where i and j are the family indices and a and b are the mass eigenstate indices (running from 1 to 2). k and l will also be used as family indices for processes including more squarks. Colour indices are suppressed. $\tilde{u}^i$ is used as a generic notation for any up-type squark where i denotes the family index. Down-type squarks are denoted analogously.

Note that we will not (except in rare occations) show processes for $\tilde{\nu}$ and $\tilde{\ell}$ separately since they can easily be obtained from the squark processes by replacing $\tilde{u}$ with $\tilde{\nu}$ and $\tilde{d}$ with $\tilde{\ell}$ (and noting that we only have one mass eigenstate for the $\tilde{\nu}$. Also note that the $\tilde{\nu}-\tilde{\ell}$–sector is assumed not to be flavour-changing.

$\tilde{d}^i_a \tilde{d}^{i*}_b$ annihilation

Initial state	Final state	Diagrams	Note
$\tilde{d}^i_a \tilde{d}^{i*}_b$	$\gamma\gamma$, $Z\gamma$	$t(\tilde{d}^i_{1,2})$, $u(\tilde{d}^i_{1,2})$, p	
$\tilde{d}^i_a \tilde{d}^{i*}_b$	ZZ	$t(\tilde{d}^i_{1,2})$, $u(\tilde{d}^i_{1,2})$, p, $s(H_1, H_2)$	
$\tilde{d}^i_a \tilde{d}^{i*}_b$	W^-W^+	p, $s(H_1, H_2, Z, \gamma)$, $t(\tilde{u}^k_{1,2})$	$k = 1, 2, 3$
$\tilde{d}^i_a \tilde{d}^{i*}_b$	ZH_2, ZH_1	$t(\tilde{d}^i_{1,2})$, $u(\tilde{d}^i_{1,2})$, $s(Z, H_3)$	
$\tilde{d}^i_a \tilde{d}^{i*}_b$	ZH_3	$t(\tilde{d}^i_{1,2})$, $u(\tilde{d}^i_{1,2})$, $s(H_1, H_2)$	
$\tilde{d}^i_a \tilde{d}^{i*}_b$	γH_2, γH_1, γH_3	$t(\tilde{d}^i_{1,2})$, $u(\tilde{d}^i_{1,2})$	
$\tilde{d}^i_a \tilde{d}^{i*}_b$	H_2H_2, H_1H_1, H_1H_2	$t(\tilde{d}^i_{1,2})$, $u(\tilde{d}^i_{1,2})$, p, $s(H_1, H_2)$	
$\tilde{d}^i_a \tilde{d}^{i*}_b$	H_2H_3, H_1H_3	$s(Z, H_3)$, $t(\tilde{d}^i_{1,2})$, $u(\tilde{d}^i_{1,2})$	
$\tilde{d}^i_a \tilde{d}^{i*}_b$	H_3H_3	$s(H_1, H_2)$, p, $t(\tilde{d}^i_{1,2})$, $u(\tilde{d}^i_{1,2})$	
$\tilde{d}^i_a \tilde{d}^{i*}_b$	W^-H^+	$s(H_1, H_2, H_3)$, $t(\tilde{u}^k_{1,2})$	$k = 1, 2, 3$
$\tilde{d}^i_a \tilde{d}^{i*}_b$	H^-H^+	$s(H_1, H_2, Z, \gamma)$, p, $t(\tilde{u}^k_{1,2})$	$k = 1, 2, 3$
$\tilde{d}^i_a \tilde{d}^{i*}_b$	$f\bar{f}$ $(f \neq d^i)$	$s(H^\star_1, H^\star_2, H^\star_3, Z, \gamma^\star, g^\ddagger)$, $t(\chi^+_c)^\dagger$	†) $f = u^k$ $(k = 1, 2, 3)$, $\star$) Not for $f = \nu$, ‡) Only for squarks/quarks
$\tilde{d}^i_a \tilde{d}^{i*}_b$	$d^i\bar{d}^i$	$s(H_1, H_2, H_3, Z, \gamma, g^\dagger)$, $t(\tilde{\chi}^0_k, \tilde{g}^\dagger)$	†) Only for squarks
$\tilde{d}^i_a \tilde{d}^{i*}_b$	Zg	$t(\tilde{d}^i_{1,2}), u(\tilde{d}^i_{1,2}), p$	Only for squarks
$\tilde{d}^i_a \tilde{d}^{i*}_b$	gg	$t(\tilde{d}^i_{1,2}), u(\tilde{d}^i_{1,2}), s(g), p$	Only for squarks
$\tilde{d}^i_a \tilde{d}^{i*}_b$	$g\gamma$	$t(\tilde{d}^i_{1,2}), u(\tilde{d}^i_{1,2}), p$	Only for squarks
$\tilde{d}^i_a \tilde{d}^{i*}_b$	gH_1, gH_2, gH_3	$t(\tilde{d}^i_{1,2}), u(\tilde{d}^i_{1,2})$	Only for squarks

$\tilde{d}^i_a \tilde{d}^{j*}_b$ annihilation $(i \neq j)$

Initial state	Final state	Diagrams	Note
$\tilde{d}^i_a \tilde{d}^{j*}_b$	W^+W^-	$t(\tilde{u}^k_{1,2})^\dagger$	Not included at present
$\tilde{d}^i_a \tilde{d}^{j*}_b$	W^+H^-	$t(\tilde{u}^k_{1,2})^\dagger$	Not included at present
$\tilde{d}^i_a \tilde{d}^{j*}_b$	H^+H^-	$t(\tilde{u}^k_{1,2})^\dagger$	Not included at present
$\tilde{d}^i_a \tilde{d}^{*j}_b$	$d^i\bar{d}^j$	$t(\tilde{\chi}^0_k, \tilde{g}^\dagger)$	†) Only for squarks
$\tilde{d}^i_a \tilde{d}^{*j}_b$	$u^k\bar{u}^l$	$t(\tilde{\chi}^+_c)$	Only $k = i, l = j$ at present

$\tilde{d}^i_a \tilde{d}^i_b$ annihilation

Initial state	Final state	Diagrams	Note
$\tilde{d}^i_a \tilde{d}^i_b$	$d^i d^i$	$t(\tilde{\chi}^0_k, \tilde{g}^\dagger)$, $u(\tilde{\chi}^0_k, \tilde{g}^\dagger)$	†) Only for squarks

$\tilde{d}^i_a \tilde{d}^j_b$ annihilation $(i \neq j)$

Initial state	Final state	Diagrams	Note
$\tilde{d}^i_a \tilde{d}^j_b$	$d^i d^j$	$t(\tilde{\chi}^0_k, \tilde{g}^\dagger)$	†) Only for squarks

$\tilde{u}^i_a \tilde{u}^{i*}_b$ annihilation

Initial state	Final state	Diagrams	Note
$\tilde{u}_a^i \tilde{u}_b^{i*}$	$\gamma\gamma^\dagger$, $Z\gamma^\dagger$	$t(\tilde{u}_{1,2}^i)$, $u(\tilde{u}_{1,2}^i)$, p	†) Not for $\tilde{\nu}$
$\tilde{u}_a^i \tilde{u}_b^{i*}$	ZZ	$t(\tilde{u}_{1,2}^i)$, $u(\tilde{u}_{1,2}^i)$, p, $s(H_1, H_2)$	
$\tilde{u}_a^i \tilde{u}_b^{i*}$	W^-W^+	p, $s(H_1, H_2, Z, \gamma^\dagger)$, $u(\tilde{d}_{1,2}^k)$	$k = 1, 2, 3$, †) Not for $\tilde{\nu}$
$\tilde{u}_a^i \tilde{u}_b^{i*}$	ZH_2, ZH_1	$t(\tilde{u}_{1,2}^i)$, $u(\tilde{u}_{1,2}^i)$, $s(Z, H_3^\dagger)$	†) Not for $\tilde{\nu}$
$\tilde{u}_a^i \tilde{u}_b^{i*}$	ZH_3	$t(\tilde{u}_{1,2}^i)^\dagger$, $u(\tilde{u}_{1,2}^i)^\dagger$, $s(H_1, H_2)$	†) Not for $\tilde{\nu}$
$\tilde{u}_a^i \tilde{u}_b^{i*}$	$\gamma H_2^\dagger$, $\gamma H_1^\dagger$, $\gamma H_3^\dagger$	$t(\tilde{u}_{1,2}^i)$, $u(\tilde{u}_{1,2}^i)$	†) Not for $\tilde{\nu}$
$\tilde{u}_a^i \tilde{u}_b^{i*}$	H_2H_2, H_1H_1, H_1H_2	$t(\tilde{u}_{1,2}^i)$, $u(\tilde{u}_{1,2}^i)$, p, $s(H_1, H_2)$	
$\tilde{u}_a^i \tilde{u}_b^{i*}$	H_2H_3, H_1H_3	$s(Z, H_3^\dagger)$, $t(\tilde{u}_{1,2}^i)^\dagger$, $u(\tilde{u}_{1,2}^i)^\dagger$	†) Not for $\tilde{\nu}$
$\tilde{u}_a^i \tilde{u}_b^{i*}$	H_3H_3	$s(H_1, H_2)$, p, $t(\tilde{u}_{1,2}^i)^\dagger$, $u(\tilde{u}_{1,2}^i)^\dagger$	†) Not for $\tilde{\nu}$
$\tilde{u}_a^i \tilde{u}_b^{i*}$	W^-H^+	$s(H_1, H_2, H_3^\dagger)$, $u(\tilde{d}_{1,2}^k)$	$k = 1, 2, 3$, †) Not for $\tilde{\nu}$
$\tilde{u}_a^i \tilde{u}_b^{i*}$	H^+H^-	$s(H_1, H_2, Z, \gamma^\dagger)$, p, $t(\tilde{d}_{1,2}^k)$	$k = 1, 2, 3$, †) Not for $\tilde{\nu}$
$\tilde{u}_a^i \tilde{u}_b^{i*}$	$f\bar{f}$ $(f \neq u^i)$	$s(H_1^\times, H_2^\times, H_3^{\dagger\times}, Z, \gamma^{\dagger\times}, g^\ddagger), t(\chi_c^+)^\star$	†) Not for $\tilde{\nu}$, $\star$) If $f = d^k$ $(k = 1, 2, 3)$, ‡) Only for squarks/quarks, $\times$) Not for ν
$\tilde{u}_a^i \tilde{u}_b^{i*}$	$u^i\bar{u}^i$	$s(H_1^\times, H_2^\times, H_3^\times, Z, \gamma^\times, g^\ddagger)$, $t(\tilde{\chi}_k^0, \tilde{g}^\ddagger)$	$\times$) Not for ν, ‡) Only for squarks
$\tilde{u}_a^i \tilde{u}_b^{i*}$	Zg	$t(\tilde{u}_{1,2}^i), u(\tilde{u}_{1,2}^i), p$	Only for squarks
$\tilde{u}_a^i \tilde{u}_b^{i*}$	gg	$t(\tilde{u}_{1,2}^i), u(\tilde{u}_{1,2}^i), s(g), p$	Only for squarks
$\tilde{u}_a^i \tilde{u}_b^{i*}$	$g\gamma$	$t(\tilde{u}_{1,2}^i), u(\tilde{u}_{1,2}^i), p$	Only for squarks
$\tilde{u}_a^i \tilde{u}_b^{i*}$	gH_1, gH_2, gH_3	$t(\tilde{u}_{1,2}^i), u(\tilde{u}_{1,2}^i)$	Only for squarks

$\tilde{u}_a^i \tilde{u}_b^{j*}$ annihilation $(i \neq j)$

Initial state	Final state	Diagrams	Note
$\tilde{u}_a^i \tilde{u}_b^{j*}$	W^+W^-	$t(\tilde{d}_{1,2}^k)^\dagger$	Not included at present, †) Not for $\tilde{\ell}$
$\tilde{u}_a^i \tilde{u}_b^{j*}$	W^+H^-	$t(\tilde{d}_{1,2}^k)^\dagger$	Not included at present, †) Not for $\tilde{\ell}$
$\tilde{u}_a^i \tilde{u}_b^{j*}$	H^+H^-	$t(\tilde{d}_{1,2}^k)^\dagger$	Not included at present, †) Not for $\tilde{\ell}$
$\tilde{u}_a^i \tilde{u}_b^{j*}$	$u^i\bar{u}^j$	$t(\tilde{\chi}_k^0, g^\dagger)$	†) Only for squarks
$\tilde{u}_a^i \tilde{u}_b^{j*}$	$d^k\bar{d}^l$	$t(\tilde{\chi}_c^+)$	Only $k = i, l = j$ at present

$\tilde{u}_a^i \tilde{u}_b^i$ annihilation

Initial state	Final state	Diagrams	Note
$\tilde{u}_a^i \tilde{u}_b^i$	$u^i u^i$	$t(\tilde{\chi}_k^0, \tilde{g}^\dagger)$, $u(\tilde{\chi}_k^0, \tilde{g}^\dagger)$	†) Only for squarks

$\tilde{u}_a^i \tilde{u}_b^j$ annihilation $(i \neq j)$

Initial state	Final state	Diagrams	Note
$\tilde{u}_a^i \tilde{u}_b^j$	$u^i u^j$	$t(\tilde{\chi}_k^0, \tilde{g}^\dagger)$	†) Only for squarks

$\tilde{u}_a^i \tilde{d}_b^{i*}$ annihilation

Initial state	Final state	Diagrams	Note
$\tilde{u}_a^i \tilde{d}_b^{i*}$	H^+H_1, H^+H_2	$t(\tilde{d}_{1,2}^i)$, $u(\tilde{u}_{1,2}^i)$, p, $s(W^+, H^+)$	
$\tilde{u}_a^i \tilde{d}_b^{i*}$	H^+H_3	$t(\tilde{d}_{1,2}^i)$, $u(\tilde{u}_{1,2}^i)^\dagger$, p, $s(W^+)$	†) Not for $\tilde{\ell}$
$\tilde{u}_a^i \tilde{d}_b^{i*}$	γH^+	$t(\tilde{u}_{1,2}^i)^\dagger$, $u(\tilde{d}_{1,2}^i)$, $s(H^+)$	†) Not for $\tilde{\ell}$
$\tilde{u}_a^i \tilde{d}_b^{i*}$	ZH^+	$t(\tilde{u}_{1,2}^i)$, $u(\tilde{d}_{1,2}^i)$, $s(H^+)$	
$\tilde{u}_a^i \tilde{d}_b^{i*}$	W^+H_1, W^+H_2	$t(\tilde{d}_{1,2}^i)$, $u(\tilde{u}_{1,2}^i)$, $s(W^+, H^+)$	
$\tilde{u}_a^i \tilde{d}_b^{i*}$	W^+H_3	$t(\tilde{d}_{1,2}^i)$, $u(\tilde{u}_{1,2}^i)^\dagger$, $s(H^+)$	†) Not for $\tilde{\ell}$
$\tilde{u}_a^i \tilde{d}_b^{i*}$	$W^+\gamma$	$t(\tilde{d}_{1,2}^i)$, $u(\tilde{u}_{1,2}^i)^\dagger$, $s(W^+)$, p	†) Not for $\tilde{\ell}$
$\tilde{u}_a^i \tilde{d}_b^{i*}$	W^+Z	$t(\tilde{d}_{1,2}^i)$, $u(\tilde{u}_{1,2}^i)$, $s(W^+)$, p	
$\tilde{u}_a^i \tilde{d}_b^{i*}$	$u^k \bar{d}^l$	$s(H^+, W^+)^\star$, $t(\tilde{\chi}_m^0, \tilde{g}^\dagger)\delta^{ik}\delta^{il}$	†) Not for $\tilde{\ell}$, $\star$) Only $k = l$ at present
$\tilde{u}_a^i \tilde{d}_b^{i*}$	W^+g	$t(\tilde{d}_{1,2}^i)$, $u(\tilde{u}_{1,2}^i)$, p	Only for squarks
$\tilde{u}_a^i \tilde{d}_b^{i*}$	gH^+	$t(\tilde{u}_{1,2}^i)$, $u(\tilde{d}_{1,2}^i)$	Only for squarks

$\tilde{u}_a^i \tilde{d}_b^{j*}$ annihilation ($i \neq j$)

For squarks we can have the following processes

Initial state	Final state	Diagrams	Note
$\tilde{u}_a^i \tilde{d}_b^{j*}$	H^+H_1, H^+H_2	$t(\tilde{d}_{1,2}^j)$, $u(\tilde{u}_{1,2}^i)$, p, $s(W^+, H^+)$	Not included at present
$\tilde{u}_a^i \tilde{d}_b^{j*}$	H^+H_3	$t(\tilde{d}_{1,2}^j)$, $u(\tilde{u}_{1,2}^i)$, p, $s(W^+)$	Not included at present
$\tilde{u}_a^i \tilde{d}_b^{j*}$	$H^+\gamma$	$t(\tilde{d}_{1,2}^j)$, $u(\tilde{u}_{1,2}^i)$, $s(H^+)$	Not included at present
$\tilde{u}_a^i \tilde{d}_b^{j*}$	H^+Z	$t(\tilde{d}_{1,2}^j)$, $u(\tilde{u}_{1,2}^i)$, $s(H^+)$	Not included at present
$\tilde{u}_a^i \tilde{d}_b^{j*}$	W^+H_1, W^+H_2	$t(\tilde{d}_{1,2}^j)$, $u(\tilde{u}_{1,2}^i)$, $s(W^+, H^+)$	Not included at present
$\tilde{u}_a^i \tilde{d}_b^{j*}$	W^+H_3	$t(\tilde{d}_{1,2}^j)$, $u(\tilde{u}_{1,2}^i)$, $s(H^+)$	Not included at present
$\tilde{u}_a^i \tilde{d}_b^{j*}$	$W^+\gamma$	$t(\tilde{d}_{1,2}^j)$, $u(\tilde{u}_{1,2}^i)$, $s(W^+)$, p	Not included at present
$\tilde{u}_a^i \tilde{d}_b^{j*}$	W^+Z	$t(\tilde{d}_{1,2}^j)$, $u(\tilde{u}_{1,2}^i)$, $s(W^+)$, p	Not included at present
$\tilde{u}_a^i \tilde{d}_b^{j*}$	$u^k \bar{d}^l$	$s(H^+, W^+)^\dagger$, $t(\tilde{\chi}_m^0, \tilde{g})\delta^{ik}\delta^{jl}$	†) Not included at present

whereas for sneutrinos and sleptons, we can only have the process

Initial state	Final state	Diagrams	Note
$\tilde{\nu}^i \tilde{\ell}_b^{j*}$	$\nu^i \bar{\ell}^j$	$t(\tilde{\chi}_k^0)$	

$\tilde{u}_a^i \tilde{d}_b^i$ annihilation

Initial state	Final state	Diagrams	Note
$\tilde{u}_a^i \tilde{d}_b^i$	$u^k d^l$	$t(\tilde{\chi}_m^0, \tilde{g}^\dagger)\delta^{ik}\delta^{il}$, $u(\tilde{\chi}_c^+)^\star$	†) Only for squarks, $\star$) Only $i = k = l$ at present

$\tilde{u}_a^i \tilde{d}_b^j$ annihilation ($i \neq j$)

Initial state	Final state	Diagrams	Note
$\tilde{u}_a^i \tilde{d}_b^j$	$u^k d^l$	$t(\tilde{\chi}_m^0, \tilde{g}^\dagger)\delta^{ik}\delta^{jl}$, $u(\tilde{\chi}_c^+)^{\times\star}$	†) Only for squarks, $\times$) For $\tilde{\nu}\tilde{\ell}$ only when $i = l, j = k$, $\star$) Only included when $i = l, j = k$ at present

5.1.5 Squark-neutralino annihilation

Note: The tables below are not entirely up to date, more processes are included than shown in the tables.

We will here denote squarks as $\tilde{u}_a^i$ and $\tilde{d}_a^i$ where i is the family index and a is the mass eigenstate index (running from 1 to 2).

$\tilde{u}_a^i\tilde{\chi}_j^0$ annihilation

Initial state	Final state	Diagrams	Note
$\tilde{u}_a^i\tilde{\chi}_j^0$	γu^i	$s(u^i)$, $t(\tilde{u}_{1,2}^i)$	Only for squarks
$\tilde{u}_a^i\tilde{\chi}_j^0$	Zu^i	$s(u^i)$, $t(\tilde{u}_{1,2}^i)$, $u(\tilde{\chi}_k^0)$	
$\tilde{u}_a^i\tilde{\chi}_j^0$	H_1u^i, H_2u^i	$s(u^i)^\dagger$, $t(\tilde{u}_{1,2}^i)$, $u(\tilde{\chi}_k^0)$	†) Only for squarks
$\tilde{u}_a^i\tilde{\chi}_j^0$	H_3u^i	$s(u^i)^\dagger$, $t(\tilde{u}_{1,2}^i)^\dagger$, $u(\tilde{\chi}_k^0)$	†) Only for squarks
$\tilde{u}_a^i\tilde{\chi}_j^0$	W^+d^k	$s(u^i)$, $t(\tilde{d}_{1,2}^k)$, $u(\tilde{\chi}_c^+)$	$k = 1,2,3$, $\tilde{u}_a^{i*}\tilde{\chi}_j^0 \to W^-\bar{d}^k$ in the code
$\tilde{u}_a^i\tilde{\chi}_j^0$	H^+d^k	$s(u^i)$, $t(\tilde{d}_{1,2}^k)$, $u(\tilde{\chi}_c^+)$	$k = 1,2,3$, $\tilde{u}_a^{i*}\tilde{\chi}_j^0 \to H^-\bar{d}^k$ in the code
$\tilde{u}_a^i\tilde{\chi}_j^0$	gu^i	$s(u^i)$, $t(\tilde{u}_{1,2}^i)$	

$\tilde{d}_a^i\tilde{\chi}_j^0$ annihilation

Initial state	Final state	Diagrams	Note
$\tilde{d}_a^i\tilde{\chi}_j^0$	γd^i	$s(d^i)$, $t(\tilde{d}_{1,2}^i)$	
$\tilde{d}_a^i\tilde{\chi}_j^0$	Zd^i	$s(d^i)$, $t(\tilde{d}_{1,2}^i)$, $u(\tilde{\chi}_k^0)$	
$\tilde{d}_a^i\tilde{\chi}_j^0$	H_1d^i, H_2d^i	$s(d^i)$, $t(\tilde{d}_{1,2}^i)$, $u(\tilde{\chi}_k^0)$	
$\tilde{d}_a^i\tilde{\chi}_j^0$	H_3d^i	$s(d^i)$, $t(\tilde{d}_{1,2}^i)$, $u(\tilde{\chi}_k^0)$	
$\tilde{d}_a^i\tilde{\chi}_j^0$	W^-u^k	$s(d^i)$, $t(\tilde{u}_{1,2}^k)$, $u(\tilde{\chi}_c^+)$	$k = 1,2,3$
$\tilde{d}_a^i\tilde{\chi}_j^0$	H^-u^k	$s(d^i)$, $t(\tilde{u}_{1,2}^k)$, $u(\tilde{\chi}_c^+)$	$k = 1,2,3$
$\tilde{d}_a^i\tilde{\chi}_j^0$	gd^i	$s(d^i)$, $t(\tilde{d}_{1,2}^i)$	

5.1.6 Squark-chargino annihilation

Note: The tables below are not entirely up to date, more processes are included than shown in the tables.

We will here denote squarks as $\tilde{q}_a^i$ where i is the family index and a is the mass eigenstate index (running from 1 to 2).

$\tilde{u}_a^i\tilde{\chi}_c^+$ annihilation

Initial state	Final state	Diagrams	Note
$\tilde{u}_a^i\tilde{\chi}_c^+$	W^+u^k	$t(\tilde{d}_{1,2}^l)$, $u(\tilde{\chi}_c^0)\delta^{ik}$	Only $k = l = i$ at present
$\tilde{u}_a^i\tilde{\chi}_c^+$	H^+u^k	$t(\tilde{d}_{1,2}^l)$, $u(\tilde{\chi}_c^0)\delta^{ik}$	Only $k = l = i$ at present

$\tilde{u}_a^{i*}\tilde{\chi}_c^+$ annihilation

Initial state	Final state	Diagrams	Note
$\tilde{u}_a^{i*}\tilde{\chi}_c^+$	$Z\bar{d}^k$	$s(\bar{d}^k)$, $t(\tilde{u}_{1,2}^i)$, $u(\tilde{\chi}_c^+)$	$k = 1, 2, 3$
$\tilde{u}_a^{i*}\tilde{\chi}_c^+$	$\gamma\bar{d}^k$	$s(\bar{d}^k)$, $t(\tilde{u}_{1,2}^i)^\dagger$, $u(\tilde{\chi}_c^+)$	$k = 1, 2, 3$, †) Only for squarks
$\tilde{u}_a^{i*}\tilde{\chi}_c^+$	$H_1\bar{d}^k$, $H_2\bar{d}^k$	$s(\bar{d}^k)$, $t(\tilde{u}_{1,2}^i)$, $u(\tilde{\chi}_c^+)$	$k = 1, 2, 3$
$\tilde{u}_a^{i*}\tilde{\chi}_c^+$	$H_3\bar{d}^k$	$s(\bar{d}^k)$, $t(\tilde{u}_{1,2}^i)^\dagger$, $u(\tilde{\chi}_c^+)$	$k = 1, 2, 3$, †) Only for squarks
$\tilde{u}_a^{i*}\tilde{\chi}_c^+$	$W^+\bar{u}^k$	$s(\bar{d}^l)$, $u(\tilde{\chi}_c^0)\delta^{ik}$	Only $k = l = i$ at present
$\tilde{u}_a^{i*}\tilde{\chi}_c^+$	$H^+\bar{u}^k$	$s(\bar{d}^l)$, $u(\tilde{\chi}_c^0)\delta^{ik}$	Only $k = l = i$ at present
$\tilde{u}_a^{i*}\tilde{\chi}_c^+$	$g\bar{d}^k$	$s(\bar{d}^k)$, $t(\tilde{u}_a^i)$	$k = 1, 2, 3$, only for squarks

$\tilde{d}_a^i\tilde{\chi}_c^+$ annihilation

Initial state	Final state	Diagrams	Note
$\tilde{d}_a^i\tilde{\chi}_c^+$	Zu^k	$s(u^k)$, $t(\tilde{d}_{1,2}^i)$, $u(\tilde{\chi}_c^+)$	Only $k = i$ at present
$\tilde{d}_a^i\tilde{\chi}_c^+$	γu^k	$s(u^k)^\dagger$, $t(\tilde{d}_{1,2}^i)$, $u(\tilde{\chi}_c^+)$	Only $k = i$ at present, †) Only for squarks
$\tilde{d}_a^i\tilde{\chi}_c^+$	H_1u^k, H_2u^k	$s(u^k)^\dagger$, $t(\tilde{d}_{1,2}^i)$, $u(\tilde{\chi}_c^+)$	Only $k = i$ at present, †) Only for squarks
$\tilde{d}_a^i\tilde{\chi}_c^+$	H_3u^k	$s(u^k)^\dagger$, $t(\tilde{d}_{1,2}^i)$, $u(\tilde{\chi}_c^+)$	Only $k = i$ at present, †) Only for squarks
$\tilde{d}_a^i\tilde{\chi}_c^+$	W^+d^k	$s(u^l)$, $u(\tilde{\chi}_c^0)\delta^{ik}$	Only $k = l = i$ at present
$\tilde{d}_a^i\tilde{\chi}_c^+$	H^+d^k	$s(u^l)$, $u(\tilde{\chi}_c^0)\delta^{ik}$	Only $k = l = i$ at present
$\tilde{d}_a^i\tilde{\chi}_c^+$	gu^k	$s(u^k)$, $t(\tilde{d}_a^i)$	Only $k = i$ at present, only for squarks

$\tilde{d}_a^{i*}\tilde{\chi}_c^+$ annihilation

Initial state	Final state	Diagrams	Note
$\tilde{d}_a^{i*}\tilde{\chi}_c^+$	$W^+\bar{d}^k$	$t(\tilde{u}_{1,2}^l)$, $u(\tilde{\chi}_c^0)\delta^{ik}$	Only $k = l = i$ at present
$\tilde{d}_a^{i*}\tilde{\chi}_c^+$	$H^+\bar{d}^k$	$t(\tilde{u}_{1,2}^l)$, $u(\tilde{\chi}_c^0)\delta^{ik}$	Only $k = l = i$ at present

5.1.7 Degrees of freedom

We have to be careful with the internal degrees of freedom, g, of the particles. We can either treat e.g. a χ_i^+ and a χ_i^- as two separate particles with two degrees of freedom each, or we can treat them as one particle $\chi_i^\pm$ with four degrees of freedom. The latter approach has an advantage that we simplify our expressions for the effective annihilation cross sections when coannihilations are needed. Hence, we use that approach here. For a more detailed discussion about this, see Section 24.1.4.

5.2 Annihilation routines - general remarks

The annihilation cross section routines is divided into several parts, mostly for historical reasons. The layout is roughly as follows:

src/an Here we keep the main routins for both neutralino- neutralino annihilation cross sections and the effective annihilation cross section in the relic density calculations. The steering routines for neutralino and chargino coannihilations are also kept here.

src/anstu Here keep the $t-$, $u-$ and $s-$ diagram expressions for fermion-fermion coannihilations (i.e. neutralino and chargino coannihilations).

src/as Here all the coannihilation cross sections including sfermions are kept.

We will here describe the src/an-routines.

5.2.1 General routines

The general routine to call for an effective annihilation cross section (to be used for relic density calculations) is **dsanwx**, which returns the invariant annihilation rate (integrated over $\cos\theta$). The actual cross section, differential in $\cos\theta$ is calculated by **dsandwdcos** which includes all the coannihilations needed. This is set up in **rn/dsrdomega** which determines which coannhilating particles to include.

For other applications where the annihilation rate is needed, e.g. annihilation in the galactic halo, one can call the specific annihilation rate routine directly. The main one is **dsandwdcosnn** for neutralino-neutralino annihilation. To simplify this task, we supply a routine **dssigmav** which calls **dsandwdcosnn** for neutralino-neutralino annihilation at zero relative velocity and returns the result, either as the total annihilation cross section, or the cross section for a specific channel. See the header of **dssigmav** for details.

5.2.2 Neutralino and chargino (co)annihilation cross sections

The routines **dsandwdcosnn**, **dsandwdcoscn** and **dsandwdcoscc** calculate the annihilation cross sections (returning the invariant annihilation rate) for neutralino-neutralino, neutralino-chargino and chargino-chargino annihilations. Which particles the cross section is calculated for is given by particle indices as defined in **inc/dsmssm.h**.

All the annihilation routines return the invariant rate instead of the cross section. The invariant annihilation rate between particle i and j is defined as

$$W_{ij} = 4p_{ij}\sqrt{s}\sigma_{ij} = 4\sigma_{ij}\sqrt{(p_i \cdot p_j)^2 - m_i^2 m_j^2} = 4E_i E_j \sigma_{ij} v_{ij}. \tag{5.1}$$

See chapter 24 for more details.

Chapter 6

src/an1l: Annihilation cross sections (1-loop)

6.1 Annihilation cross sections at 1-loop – general

The annihilation cross sections at 1-loop that we have implemented in DarkSUSY are those to $\gamma\gamma$, $Z\gamma$ and gg. The derivation of these is described in the works [**?**, 175].

To see how these routines are called, see the file **src/an/dsandwdcosnn.f** where the $\gamma\gamma$, $Z\gamma$ and gg contributions are added to the annihilation cross section at the end.

Chapter 7

src/anstu: t, u and s diagrams for ff-annihilation

7.1 Annihilation amplitudes for fermion-fermion annihilation

In this directory, all the helicity amplitudes needed for neutralino-neutralino, neutralino-chargino and chargino-chargino annihilation are calculated. The helicity amplitudes have been calculated with general expressions for vertices, masses etc. in Reduce and converted to Fortran files. The calculation of these are described in more detail in [35].

Each routine here adds the contribution to the helicity amplitudes from one particular diagram and the sum over contributed diagrams is done in the routines **an/dsandwdcosnn**, **an/dsandwdcoscn** and **an/dsandwdcoscc**. The naming convention for the routines here is the following: The first part of the routine name is **dsan** to indicate that they deal with annihilations in DarkSUSY. The next character tells which kind of process it is s-, t- or u-channel and the next two caracters tell which initial state particles we have (**f** for fermion), the next character is the kind of propagating particle (**f** for fermion, **s** for scalar and **v** for vector boson), and finally, the last two characters tell the kind of final state particles. So, to take an example, the routine **dsansffsvv** calculates the helicity amplitudes for annihilation of two fermions to two vector bosons via s-channel exchange of a scalar. There are also a few special cases (routines ending in **ex** or **in**) for diagrams with clashing arrows.

Chapter 8

src/as: Annihilation cross sections (with sfermions)

8.1 Annihilation cross sections with sfermions – general

In this directory, all the (co)annihilation cross sections involving one or more sfermions in the initial state are calculated. The code here is based upon the work described in [177]. All the cross sections are calculated with Form and converted to Fortran with a script **form2f** [173].

The main routines here are

Routine	Purpose
dsasdwdcossfsf	Calculates the invariant annihilation rate between two sfermions in the initial state.
dsasdwdcossfchi	Calculates the invariant annihilation rate between one sfermion and one fermion (neutralino or chargino) in the iniital state.

Chapter 9

src/bsg:
$b \to s\gamma$

9.1 $b \to s\gamma$ – theory

The rare decay $b \to s\gamma$ can have large contributions from loops of supersymmetric particles and one therefore has to check that a particular supersymmetric model does not violate the observed branching ratio for b decay to $s\gamma$. In DarkSUSY we have several expressions for calculations of the $b \to s\gamma$ decay. In **src/ac**, some older obsolte expressions are found (kept only for historical reasons). In this directory, **bsg/**, we have our best (and next-to-best) implementation of the $b \to s\gamma$ decay.

Our best estimate of this process includes the complete next-to-leading order (NLO) correction for the SM contribution and the dominant NLO corrections for the SUSY term. Until 2006, the NLO QCD SM calculation was performed following the analysis in Ref. [178], modified according to [179], and gave a branching ratio $\mathrm{BR}[B \to X_s\,\gamma] = 3.72 \times 10^{-4}$ for a photon energy greater than $m_b/20$. However, there was a big shift in the theoretical calculation of the SM branching ratio in 2006. We thus now instead have implemented the new results [196] which instead give a SM branching ratio of $\mathrm{BR}[B \to X_s\,\gamma] = (3.15 \pm 0.23) \times 10^{-4}$

In the SUSY contribution, we include the NLO contributions in the two Higgs doublet model, following [180], and the corrections due to SUSY particles. The latter are calculated under the assumption of minimal flavour violation, with the dominant LO contributions from Ref. [181], and with the NLO QCD term with expressions of [182] modified in the large $\tan\beta$ regime according to [181]. In the mSUGRA framework (see, e.g., [183]), the largest discrepancy between the LO and the NLO SUSY corrections are found for sign$\mu > 0$, large $\tan\beta$ and low values of $m_{1/2}$: in this case the SUSY contribution to the decay rate is negative, and the discrimination of models based on the NLO analysis is less restrictive than the one in the LO analysis.

We will assume as allowed range of branching ratios $2.71 \times 10^{-4} \leq \mathrm{BR}[B \to X_s\,\gamma] \leq 4.39 \times 10^{-4}$, which is obtained adding a theoretical uncertainty of $\pm 0.23 \times 10^{-4}$ (both for the SM and for the SUSY calculation) to the experimental value quoted by [197].

9.2 $b \to s\gamma$ – routines

The main routines is **dsbsgammafull** which calls the latest routine **dsbsg2007full**. For historical reasons, the old (pre-2007) calculations are available in **dsbsgpre2007full**.

The main routine **dsbsgammafull** returns the $b \to s\gamma$ branching ratio. The routine can calculate either only the standard model contribution or also include the SUSY contribution (which is of course the default when this routine is called from **dsacbnd**). The reaming (large) set or routines are the various contributions to the decay as given in the references listed above.

Chapter 10

src/db:
Anti-deuteron fluxes from the halo

10.1 Anti-deuteron fluxes from annihilation in the halo

The anti-deuteron fluxes are calculated here following the approach of [185]. This means that we calculate the anti-deuteron fluxes based on a merging model of antiprotons and antineutrons in quark jets. Apart from this, the anti-deuterons are propagated in the same way as antiprotons.

Chapter 11

src/dd: Direct detection

11.1 Direct detection – theory

NOTE: The description below is outdated. DarkSUSY now includes much better form factors.

If neutralinos are indeed the CDM needed on galaxy scales and larger, there should be a substantial flux of these particles in the Milky Way halo. Since the interaction strength is essentially given by the same weak couplings as, e.g., for neutrinos there is a non-negligible chance of detecting them in low-background counting experiments [78]. Due to the large parameter space of MSSM, even with the simplifying assumptions above, there is a rather wide span of predictions for the event rate in detectors of various types. It is interesting, however, that the models giving the largest rates are already starting to be probed by present direct detection experiments [46, 79].

The rate for direct detection of galactic neutralinos, integrated over deposited energy assuming no energy threshold, is

$$R = \sum_i N_i n_\chi \langle \sigma_{i\chi} v \rangle, \tag{11.1}$$

where N_i is the number of nuclei of species i in the detector, n_χ is the local galactic neutralino number density, $\sigma_{i\chi}$ is the neutralino-nucleus elastic cross section, and the angular brackets denote an average over v, the neutralino speed relative to the detector as described in Section 16.1.

In DarkSUSY, the basic quantities computed are the neutralino-nucleon cross sections, which are free of complications related to nuclear structure, and various experimental details like energy threshold, efficiencies etc. However, as a crude estimate of the expected rates in realistic detectors, the total neutralino-nucleus scattering rates can be obtained for ^{76}Ge, Al_2O_3 (sapphire) and NaI. Usually, it is the spin-independent interaction that gives the most important contribution in target materials such as Na, Cs, Ge, I, or Xe, due to the enhancement caused by the coherence of all nucleons in the target nucleus.

The neutralino-nucleus elastic cross section can be written as

$$\sigma_{i\chi} = \frac{1}{4\pi v^2} \int_0^{4m_{i\chi}^2 v^2} \mathrm{d}q^2 G_{i\chi}^2(q^2), \tag{11.2}$$

where $m_{i\chi}$ is the neutralino-nucleus reduced mass, q is the momentum transfer and $G_{i\chi}(q^2)$ is the effective neutralino-nucleus vertex. We write

$$G_{i\chi}^2(q^2) = A_i^2 F_S^2(q^2) G_S^2 + 4\Lambda_i^2 F_A^2(q^2) G_A^2, \tag{11.3}$$

which shows the coherent enhancement factor A_i^2 for the spin-independent cross section (often Λ_i^2 is written as $\lambda^2 J(J+1)$). We assume gaussian nuclear form factors [80]

$$F_S(q^2) = F_A(q^2) = \exp(-q^2 R_i^2/6\hbar^2), \tag{11.4}$$

$$R_i = (0.3 + 0.89 A_i^{1/3})\text{fm}, \tag{11.5}$$

which should provide us with a good approximation of the integrated detection rate [83], in which we are only interested. (To obtain the differential rate with reasonable accuracy, better approximations are needed [84].)

Using heavy-squark effective lagrangians [85], we get

$$G_S = \sum_{q=\text{u,d,s,c,b,t}} \langle \bar{q}q \rangle \left(\sum_{h=H_1,H_2} \frac{g_{h\chi\chi} g_{hqq}}{m_h^2} - \frac{1}{2} \sum_{k=1}^{6} \frac{g_{L\tilde{q}_k \chi q} g_{R\tilde{q}_k \chi q}}{m_{\tilde{q}_k}^2} \right) \tag{11.6}$$

and

$$G_A = \sum_{q=\text{u,d,s}} \Delta q \left(\frac{g_{Z\chi\chi} g_{Zqq}}{m_Z^2} + \frac{1}{8} \sum_{k=1}^{6} \frac{g_{L\tilde{q}_k \chi q}^2 + g_{R\tilde{q}_k \chi q}^2}{m_{\tilde{q}_k}^2} \right). \tag{11.7}$$

The g's are elementary vertices involving the particles indicated by the indices, and they read

$$g_{h\chi\chi} = \begin{cases} (gZ_{\chi 2} - g_y Z_{\chi 1})(-Z_{\chi 3}\cos\alpha + Z_{\chi 4}\sin\alpha), & \text{for } H_1, \\ (gZ_{\chi 2} - g_y Z_{\chi 1})(Z_{\chi 3}\sin\alpha + Z_{\chi 4}\cos\alpha), & \text{for } H_2, \end{cases} \tag{11.8}$$

$$g_{hqq} = \begin{cases} -Y_q \cos\alpha/\sqrt{2}, & \text{for } H_1, \\ +Y_q \sin\alpha/\sqrt{2}, & \text{for } H_2, \end{cases} \tag{11.9}$$

$$g_{Z\chi\chi} = \frac{g}{2\cos\theta_W}\left(Z_{\chi 3}^2 - Z_{\chi 4}^2\right) \tag{11.10}$$

$$g_{Zqq} = -\frac{g}{2\cos\theta_W} T_{3q}, \tag{11.11}$$

$$g_{L\tilde{q}_k \chi q} = g_{LL}\Gamma_{QL}^{kq} + g_{RL}\Gamma_{QR}^{kq}, \tag{11.12}$$

$$g_{R\tilde{q}_k \chi q} = g_{LR}\Gamma_{QL}^{kq} + g_{RR}\Gamma_{QR}^{kq}, \tag{11.13}$$

with

$$g_{LL} = -\frac{1}{\sqrt{2}}\left(T_{3q} g Z_{\chi 2} + \frac{1}{3} g_y Z_{\chi 1}\right), \tag{11.14}$$

$$g_{RR} = \sqrt{2} e_q g_y Z_{\chi 1}, \tag{11.15}$$

$$g_{LR} = g_{RL} = \begin{cases} -Y_q Z_{\chi 3}, & \text{for } q = \text{u, c, t}, \\ -Y_q Z_{\chi 4}, & \text{for } q = \text{d, s, b}, \end{cases} \tag{11.16}$$

and

$$Y_q = \begin{cases} m_q/v_2, & \text{for } q = \text{u, c, t}, \\ m_q/v_1, & \text{for } q = \text{d, s, b}. \end{cases} \tag{11.17}$$

Defining ($N = n, p$)

$$f_{Tq}^N \equiv \frac{\langle N | m_q \bar{q} q | N \rangle}{m_N}, \tag{11.18}$$

we take in DarkSUSY the numerical values [86]

$$\begin{aligned} f_{Tu}^p &= 0.023, & f_{Td}^p &= 0.034, \\ f_{Tc}^p &= 0.0595, & f_{Ts}^p &= 0.14, \\ f_{Tt}^p &= 0.0595, & f_{Tb}^p &= 0.0595 \end{aligned} \tag{11.19}$$

and

$$\begin{aligned} f_{Tu}^n &= 0.019, \qquad f_{Td}^n = 0.041, \\ f_{Tc}^n &= 0.0592 \qquad f_{Ts}^n = 0.14, \\ f_{Tt}^n &= 0.0592, \qquad f_{Tb}^n = 0.0592. \end{aligned} \tag{11.20}$$

For the quark contributions to the nucleon spin we take [87]

$$\Delta\mathrm{u} = 0.77, \qquad \Delta\mathrm{d} = -0.40, \qquad \Delta\mathrm{s} = -0.12. \tag{11.21}$$

However, the older set of data [88]

$$\Delta\mathrm{u} = 0.77, \qquad \Delta\mathrm{d} = -0.49, \qquad \Delta\mathrm{s} = -0.15 \tag{11.22}$$

can optionally be used.

Moreover, we take for the Λ factors

$$\Lambda_{\mathrm{Al}}^2 = 0.087, \qquad \Lambda_{\mathrm{Na}}^2 = 0.041 \quad \text{and} \quad \Lambda_{\mathrm{I}}^2 = 0.007, \tag{11.23}$$

according to the odd-group model [89].

11.2 Direct detection – routines

subroutine **dsddneunuc**(sigsip,sigsin,sigsdp,sigsdn)

Purpose: Calculate the spin-independent and spin-dependent scattering cross sections for neutralinos on neutrons and protons.

Output:

sigsip	r8	The spin-independent neutralino-proton scattering cross section, $\sigma_{\chi p}^{SI}$, in units of $\mathrm{cm}^3\ \mathrm{s}^{-1}$.
sigsin	r8	The spin-independent neutralino-neutron scattering cross section, $\sigma_{\chi n}^{SI}$, in units of $\mathrm{cm}^3\ \mathrm{s}^{-1}$.
sigsip	r8	The spin-dependent neutralino-proton scattering cross section, $\sigma_{\chi p}^{SD}$, in units of $\mathrm{cm}^3\ \mathrm{s}^{-1}$.
sigsin	r8	The spin-dependent neutralino-neutron scattering cross section, $\sigma_{\chi n}^{SD}$, in units of $\mathrm{cm}^3\ \mathrm{s}^{-1}$.

Chapter 12

src/ep: Positron fluxes from the halo

12.1 Positrons from the halo – theory

Neutralino annihilations in the halo will give rise to positrons either directly or from decaying mesons in hadron jets. We thus expect to get both monochromatic positrons (at an energy of m_χ) from direct annihilation into e^+e^- and continuum positrons from the other annihilation channels. In general, the branching ratio for annihilation directly into e^+e^- is rather small due to the helicity-flip suppression $\propto m_e$ for S-wave annihilation in the halo, but for some classes of models one can still obtain a large enough branching ratio for the line to be observable.

The computation of the positron flux from neutralino annihilations used in DarkSUSY resembles the calculation of the antiproton flux, with some important changes due to other mechanisms of energy loss with different energy dependence. Due to the fact that energy losses for positrons are more rapid than for antiprotons, the computed signal is less sensitive to the global structure of the dark matter halo. (On the other hand, it is more sensitive to possible local sources of background, such as supernova remnants etc.)

The calculation of the neutralino-induced positron flux performed in DarkSUSY follows the analysis in [121]. For continuum positrons, we have again simulated the decay and/or hadronization with the Lund Monte Carlo Pythia as described in section **??**. We have included all two-body final states in DarkSUSY (except the three lightest quarks which are completely negligible) at tree level and the $Z\gamma$ [176] and gg [112] final states which arise at one-loop level.

12.1.1 Propagation and the interstellar flux

We consider a standard diffusion model, somewhat less sophisticated than in the case of antiprotons, for the propagation of positrons in the galaxy. Charged particles move under the influence of the galactic magnetic field. For the relevant energies the magnetic gyroradii of the particles are quite small. However, the magnetic field is tangled, and even with small gyroradii, particles can jump to nearby field lines which will drastically alter their courses. This entire process can be modeled as a random walk, which can be described by a diffusion equation.

Positron propagation is complicated by the fact that light particles lose energy quickly due to inverse Compton and synchrotron processes. Diffuse starlight and the Cosmic Microwave Background (CMB) both contribute appreciably to the energy loss rate of high energy electrons and positrons via inverse Compton scattering. Electrons and positrons also lose energy by synchrotron radiation as they spiral around the galactic magnetic field lines.

Our detailed treatment of positron diffusion employed in DarkSUSY is as follows. First define

a dimensionless energy variable $\varepsilon = E/(1\text{ GeV})$, and the dimensionless mass $\tilde{m}_\chi = m_\chi/(1\text{ GeV})$. The standard diffusion-loss equation for the space density of cosmic rays per unit energy, $dn/d\varepsilon$, is then given by

$$\frac{\partial}{\partial t}\frac{dn}{d\varepsilon} = \vec{\nabla}\cdot\left[K(\varepsilon,\vec{x})\vec{\nabla}\frac{dn}{d\varepsilon}\right] + \frac{\partial}{\partial\varepsilon}\left[b(\varepsilon,\vec{x})\frac{dn}{d\varepsilon}\right] + Q(\varepsilon,\vec{x}), \tag{12.1}$$

where K is the diffusion constant, b is the energy loss rate and Q is the source term. We consider only steady state solutions, setting the left hand side of Eq. (12.1) to zero.

We assume that the diffusion constant K is constant in space throughout a "diffusion zone", but it may vary with energy. At energies above a few GeV, we can represent the diffusion constant as a power law in energy [123],

$$K(\varepsilon) = K_0\varepsilon^\alpha \approx 3\times 10^{27}\varepsilon^{0.6}\text{cm}^2\text{ s}^{-1}. \tag{12.2}$$

However, at energies below about 3 GeV, there is a cutoff in the diffusion constant that can be modeled as

$$K(\varepsilon) = K_0\left[C+\varepsilon^\alpha\right] \approx 3\times 10^{27}\left[3^{0.6}+\varepsilon^{0.6}\right]\text{cm}^2\text{ s}^{-1}. \tag{12.3}$$

Both of these models for the diffusion constant can be used in DarkSUSY but the second expression is the default.* The function $b(\varepsilon)$ represents the (time) rate of energy loss. We allow energy loss via synchrotron emission and inverse Compton scattering. The rms magnetic field in the diffusion zone is about 3 μG, an energy density of about 0.2 eV cm^{-3}. We allow inverse Compton scattering on both the cosmic microwave background and diffuse starlight, which have energy densities of 0.3 and 0.6 eV cm^{-3} respectively. These two processes combined give an energy loss rate [125]

$$b(\varepsilon)_{e^\pm} = \frac{1}{\tau_E}\varepsilon^2 \approx 10^{-16}\varepsilon^2\text{ s}^{-1}, \tag{12.4}$$

where we have neglected the space dependence of the energy loss rate. Lastly, the function Q is the source of positrons in units of cm^{-3} s^{-1}.

We model the diffusion zone as a slab of thickness $2L$. We fix L to be 3 kpc, which fits observations of the cosmic ray flux [123]. We impose free escape boundary conditions, namely that the cosmic ray density drops to zero on the surfaces of the slab, which we let be the planes $z = \pm L$. We neglect the radial boundary usually considered in diffusion models. This is justified when the sources of cosmic rays are nearer than the boundary, as is usually the case with galactic sources. We will see that the positron flux at Earth, especially at higher energies, mostly originates within a few kpc and hence this approximation is well justified in our case. (This is different from the case of antiprotons, where the flux from the Galactic center can be very important at the Earth's location [108].) The spatial part of the Green's function is performed once, independently of the supersymmetric model, yielding an energy dependent diffusion time

$$\tau_D(\varepsilon,\varepsilon') = \frac{1}{4K_0\Delta v}\sum_{n=-\infty}^{\infty}\sum_{\pm}\text{erf}\left(\frac{(-1)^n L + 2Ln \pm z}{\sqrt{4K_0\tau_E\Delta v}}\right)\times \tag{12.5}$$

$$\int_0^\infty dr'\, r' f(r') I_0\left(\frac{2rr'}{4K_0\tau_E\Delta v}\right)\exp\left(\frac{r^2+r'^2}{4K_0\tau_E\Delta v}\right)\theta(\Delta v),$$

where $f(r)$ is the effective halo profile squared, and the expression is evaluated for r and z appropriate for the observer. The function $v(\varepsilon)$ depends on the diffusion model: the default model has $v(\varepsilon) = C/\varepsilon + \varepsilon^{\alpha-1}/(1-\alpha)$. The function τ_D is the effective diffusion time for particles emitted at energy ε' and observed at energy ε. Of course if the observed energy is larger than the emitted energy, $\tau_D = 0$. The spatial integrand is smooth, and is computed for a range of values, equally spaced in $\log(\Delta v)$ for use in DarkSUSY. Likewise, the series of image charges used in the Green's

*In fact, a third option can be chosen in DarkSUSY as well, employing the propagation model of [124].

function converges rapidly, and with the range of Δv values we are concerned with, need not be taken past $n = \pm 10$. The total positron spectrum is now given by

$$\frac{dn}{d\varepsilon} = n_0^2 \langle \sigma v \rangle_{\rm tot} \frac{1}{\varepsilon^2} \left\{ B_{\rm line} \tau_D \left(\varepsilon, \tilde{m}_\chi \right) + \int_\varepsilon^{\tilde{m}_\chi} d\varepsilon' \left. \frac{d\phi}{d\varepsilon} \right|_{\rm cont.} \tau_D(\varepsilon, \varepsilon') \right\}, \tag{12.6}$$

where $B_{\rm line}$ is the branching ratio directly to e^+e^-, and $d\phi/d\varepsilon|_{\rm cont.}$ is the spectrum of continuum positrons per annihilation. Remembering that this is an expression for the number density of positrons, the flux is given by

$$\frac{d\Phi}{d\varepsilon} = \frac{\beta c}{4\pi} \frac{dn}{d\varepsilon} \simeq \frac{c}{4\pi} \frac{dn}{d\varepsilon}, \tag{12.7}$$

where βc is the velocity of a positron of energy ε. For the energies we are interested in, $\beta c \simeq c$ is a very well justified approximation.

12.1.2 Solar modulation

Again there is a complication in that interactions with the solar wind and magnetosphere, solar modulation, alter the spectrum. This can be neglected at high energies, but at energies below about 10 GeV, the effects of solar modulation become important. However, its effects can be reduced by considering the positron fraction, $e^+/(e^+ + e^-)$, instead of the absolute positron fluxes. This is possible to obtain from DarkSUSY, since included in the package is an estimate of the background e^+ and e^- flux taken from [126].

12.2 Positrons from the halo – routines

.....

Chapter 13

src/ep2: Positron fluxes from the halo (alternative solution)

Chapter 14

src/ge: General routines

14.1 General routines

In **ge/**, we collect routines that are of general interest to many other routines in DarkSUSY. E.g., we have routins to find elements in arrays (used for interpolation), Bessel functions, error functions, spline routines, etc.

Chapter 15

src/ha: Halo annihilation yields

15.1 Annihilation in the halo, yields – theory

Here we calculate yields from annihilation in the halo.

15.1.1 Monte Carlo simulations

We need to evaluate the yield of different particles per neutralino annihilation. The hadronization and/or decay of the annihilation products are simulated with PYTHIA [90] 6.154. The simulations are done for a set of 18 neutralino masses, $m_\chi = 10$, 25, 50, 80.3, 91.2, 100, 150, 176, 200, 250, 350, 500, 750, 1000, 1500, 2000, 3000 and 5000 GeV. We tabulate the yields and then interpolate these tables in DarkSUSY.

The simulations are here simpler than those for annihilation in the Sun/Earth since we don't have a surrounding medium that can stop the annihilation products. We here simulate for 8 'fundamental' annihilation channels $c\bar{c}$, $b\bar{b}$, $t\bar{t}$, $\tau^+\tau^-$, W^+W^-, Z^0Z^0, gg and $\mu^+\mu^-$. Compared to the simulations in the Earth and the Sun, we now let pions and kaons decay and we also let antineutrons decay to antiprotons. For each mass we simulate 2.5×10^6 annihilations and tabulate the yield of antiprotons, positrons, gamma rays (not the gamma lines), muon neutrinos and neutrino-to-muon conversion rates and the neutrino-induced muon yield, where in the last two cases the neutrino-nucleon interactions has been simulated with PYTHIA as outlined in section 21.1.1

With these simulations, we can calculate the yield for any of these particles for a given MSSM model. For the Higgs bosons, which decay in flight, an integration over the angle of the decay products with respect to the direction of the Higgs boson is performed. Given the branching ratios for different annihilation channels it is then straightforward to compute the muon flux above any given energy threshold and within any angular region around the Sun or the center of the Earth.

Chapter 16

src/hm: Halo models

16.1 Halo models – theory

All the dark matter detection rates depend in one way or another on the properties of the Milky Way dark matter halo. We will here outline the halo model that by default is included with DarkSUSY.

The mass distribution in the Milky Way and the relative importance of its three components, the bulge, the disk and the halo, are poorly constrained by available observational data. Although the dynamics of the satellites of the galaxy clearly indicates the presence of a non-luminous matter component, a discrimination among the different radial dark matter halo profiles proposed in the literature is not possible at the time being [127]. One approach is to assume that dark matter profiles are of a universal functional form and to infer the Milky Way dark matter distribution from the results of N-body simulations of hierarchical clustering in cold dark matter cosmologies. The predicted profiles in these scenarios have been tested to a sample of dark matter dominated dwarf and low-surface brightness galaxies which provide the best opportunities to test the spatial distribution of dark matter. Actually this field of research is in rapid evolution and slightly discrepant results have recently been presented [113, 128, 129, 130].

In DarkSUSY, we include a dark matter halo profile of the form

$$\rho(r) \propto \frac{1}{(r/a)^{\gamma}\,[1+(r/a)^{\alpha}]^{(\beta-\gamma)/\alpha}}. \tag{16.1}$$

With this family of profiles, we have a parameterization of most spherically symmetric profiles in the literature. In Table 16.1 we list the corresponding values of α, β and γ for some popular profiles.

One should keep in mind that some of these profiles are very steep at the center of the galaxy which might be in conflict with observations. In fact, this is a topic under rapid evolution at present. Some researchers have taken the view that the steep profiles seen in simulations are impossible to match with observations, and therefore drastic modifications of the cold dark matter scenario have

Model	(α, β, γ)	a **(kpc)**
Isothermal sphere [129]	$(2, 2, 0)$	
Kravtsov et al. [129]	$(2, 3, 0.2-0.4)$	
Navarro, Frenk and White [113]	$(1, 3, 1)$	
Moore et al. [130]	$(?, ?, ?)$	

Table 16.1: Different halo dark matter profiles and their corresponding parameters.

been proposed. Examples are self-interacting [136] or strongly self-annihilating [137] dark matter models. None of these proposals can be made to work in MSSM models, so we do not consider them in DarkSUSY. It should also be noted that there could be other, astrophysics-related solutions to these problems, which involve the interplay between the baryons and the dark matter.

Our galactocentric distance R_0 is not entirely known. Estimates for R_0 range from 7.1 kpc to 8.5 kpc [145, 144, **?**] and in DarkSUSY we use $R_0 = 8.5$ kpc as a default. We also choose the modified isothermal distribution as a default, but this can be changed by the user.

As a further uncertainty, it is unknown precisely how the black hole at the galactic center would have interacted with the halo neutralino distribution. In fact, there are indications that a profile more singular than NFW would cause a very steep cusp (a "spike") near the Galactic center, with a high enough density that even the flux of neutrinos from that population could be detected [138]. If this really exists, essentially all MSSM models may already be excluded through the non-detection of radio emission from electrons and positrons generated in the annihilations [139]. It should be noted though that these estimates involve many uncertainties.

We only consider spherical profiles; introducing a flattening parameter may enhance the value of the flux but the effect is not expected to be dramatic for this neutralino detection method and we prefer not to introduce another factor of uncertainty.

We also need to specify the normalization constant of the halo profile, which we choose as the value of the halo density ρ_0 at our galactocentric distance R_0, the core radius a and R_0. One should keep in mind that there is correlation between the allowed values of a and ρ_0 and the chosen halo profile [176, 140] due to constraints on e.g. the total mass of the galaxy within 100 pc and the dark matter contribution to the local rotation curve. In Table **??** we list typical values of a and ρ_0 that we have chosen based on these constraints for the different profiles. For more details about these arguments, see [176, 140]. The DarkSUSY default value for ρ_0 is 0.3 GeV/cm^3.

Usually, the local galactic dark matter velocity distribution is taken to be a truncated gaussian, which in the detector frame moving at speed v_O relative to the galactic halo reads

$$f(v) = \frac{1}{\mathcal{N}_{\rm cut}} \frac{v^2}{u v_O \sigma} \left\{ \exp\left[-\frac{(u - v_O)^2}{2\sigma^2} \right] - \exp\left[-\frac{\min(u + v_O, v_{\rm cut})^2}{2\sigma^2} \right] \right\} \tag{16.2}$$

for $v_{\rm esc} < v < \sqrt{v_{\rm esc}^2 + (v_O + v_{\rm cut})^2}$ and zero otherwise, with $u = \sqrt{v^2 + v_{\rm esc}^2}$ and

$$\mathcal{N}_{\rm cut} = \frac{v_{\rm cut}}{\sigma} \exp\left(-\frac{v_{\rm cut}^2}{2\sigma^2} \right) - \sqrt{\frac{\pi}{2}} {\rm erf}\left(\frac{v_{\rm cut}}{\sqrt{2}\sigma} \right). \tag{16.3}$$

As default, we have taken the halo line-of-sight (one-dimensional) velocity dispersion σ =120 km/s,* the galactic escape speed $v_{\rm cut} = 600$ km/s, the relative Earth-halo speed $v_O = 264$ km/s (a yearly average) and the Earth escape speed $v_{\rm esc} = 11.9$ km/s. These parameters can be changed by the user. In some instances, like neutralino capture in the Earth, the user can specify an arbitrary velocity distribution by providing a subroutine.

16.1.1 Rescaling of the neutralino density

It is natural to assume that the neutralinos make up most of the dark matter in our galaxy. One may therefore only consider MSSM models which are cosmologically interesting, i.e. where the neutralinos can make up a major fraction of the dark matter in the Universe without overclosing it. This range is usually chosen to be $0.025 < \Omega_\chi h^2 < 1$. However, the user may want to either enlarge or narrow this range. If, as is perhaps most natural, the neutralino alone contributes the major fraction of non-baryonic dark matter in the Universe, one may want to refer to the current values of cosmological parameters and fix $\Omega_\chi h^2$ to be in the interval between, say 0.1 and 0.3. If there are other components of the dark matter, one may want to tolerate smaller numbers. If one

*Other authors write $\exp(-3v^2/2\overline{v}^2)$, in which case $\overline{v} = \sqrt{3}\sigma$.

makes use of the poor knowledge of how galaxy halos were formed, all the range down to 0.025 may be taken as acceptable. However, if $\Omega_\chi h^2$ drops below 0.025, it cannot account for all the dark matter associated with galaxy halos. A frequently used recipe is then to rescale the estimated local dark matter density $\rho_0 \sim 0.3$ GeV/cm^3 by $\Omega_\chi h^2/0.025$, giving a lower local density in the form of neutralinos. Although this may seem a harmless procedure, one should keep in mind that it is very *ad hoc* and that it may overestimate the preponderance of models with large direct detection rates. This is because of the general result that $\Omega_\chi h^2 \sim 1/\sigma_{ann} v$, and crossing symmetry generally relates a large annihilation cross section to a large scattering cross section. (For indirect detection in the halo, the effect is moderated by the fact that the rates are proportional to the square of the density, which thus involves the square of the rescaling factor.) In DarkSUSY, the user can set the value of the local dark matter density (the default is 0.3 GeV/cm^3) and determine whether rescaling is to be used or not, and in that case the lowest tolerable $\Omega_\chi^{\rm min} h^2$ below which rescaling should take place. If rescaling is used, all output detection rates are computed with the rescaled value when appropriate.

16.2 Halo model – routines

The most important routine is dshmset which sets the chosen halo profile.

Chapter 17

src/hr: Halo rates from annihilation

17.1 Gamma rays from the halo – theory

Among the yields of pair annihilations of halo dark matter particles, the role played by gamma-rays could be a major one. Unlike the cases involving charged particles, for gamma-rays it is straightforward to relate the distribution of sources and the expected flux at the earth. Most flux estimated can be obtained just by summing over the contributions along lines of sight (or better, geodesics): gamma-rays have a low enough cross section on gas and dust and therefore the Galaxy is essentially transparent to them (except perhaps in the innermost part, very close to the region where a massive black hole is inferred); absorption by starlight and infrared background becomes effecient only for very far away sources (redshift larger than about 1).

It follows that in case the gamma-ray signal is detectable, this might be the only chance for mapping the fine structure of a dark halo, with a much better resolution for inomogenities (clumps) with respect what is accevable through dynamical measurements or lensing effects. Turning the latter argument around, if the fine structure of the Galactic halo is clumpy, or if a large density enhancement is present towards the Galactic center, as seen in N-body simulations of dark matter halos, this dark matter detection tecnique is much more promising than indicated by the earliest estimates in which smooth non-singular halo scenarios were considered (recall that the fluxes per unit volume are proportional to the square of the dark matter density locally in space).

A further reason to examine in details this detection methods is that we are approaching what will probably be the golden age for gamma-ray observations, with a several new experiments that are going to map the gamma-ray sky. These experiments will have unprecendented sensitivities and cover an energy range, namely 10 GeV – few hundred GeV, in which very scarce data are available at the time being and which may turn out to be the most interesting for dark matter detection. The hypothesis of a gamma-ray signal from neutralino annihilations will be tested for both by the upcoming space experiments (GLAST, AMS, AGILE) and by the new generation of ground-based air cherenkov telescopes (ACTs) being built (Magic, Hess, Veritas).

The bulk of the gamma-ray yield from neutralino annihilations arise in the decay of neutral pions produced in the fragmetation processes initiated by tree level final states [148, 73, 155] (analogously to the other halo signals, in DarkSUSY we include all tree level final states and make use of a Monte Carlo simulation for fragmentation and decay processes, see Section **??**). Unfortunately the π^0 intermediate state is common to other astrophysical processes, and this may turn out to be a limiting factor to disentangle dark matter sources. At the same time, however, a relevant gamma-ray contribution may arise directly (at one-loop level) in two body final states; although such photons are much fewer than those from π^0 decays they have a much better signature: neutralinos annihilating

in the galactic halos move with a velocity of the order $v/c \sim 10^{-3}$, hence these outgoing photons (as any particle in any of the allowed two body final states) will then be nearly monochromatic, with energy of the order of the neutralino mass[149, 150, 151, 112, 110, 73]. There is no other known astrophysical source with such a signature: the detection of a line signal out of a spectrally smooth gamma-ray background would be a spectacular confirmation of the existence of dark matter in form of exotic massive particles.

If dark matter is in form of neutralinos, there are two processes givin rise to line signals, the annihilation into two photons and into one photon and a Z boson. Both of them are included in the DarkSUSY package, as well as the contribution with a continuum energy spectrum. We review them briefly here, focussing first on annihilation rates and giving then expressions for gamma-ray fluxes.

17.1.1 $\chi\chi \to \gamma\gamma$

In DarkSUSY the full expression for the annihilation cross section of the process

$$\tilde{\chi}_1^0 + \tilde{\chi}_1^0 \to \gamma + \gamma \tag{17.1}$$

is computed at full one loop level, in the limit of vanishing relative velocity of the neutralino pair, i.e. the case of interest for neutralinos in galactic halos; the outgoing photons have an energy equal to the mass of χ_1^0:

$$E_\gamma = M_\chi. \tag{17.2}$$

The neutralino pair must be in an S wave state with pseudoscalar quantum numbers; projecting out of the amplitude the $^1S_0$ state simplifies the calculation, and a further simplification is obtained by computing the amplitude in the non linear gauge defined in [152], which is a slight variant of the usual linear R-gauge (or 't Hooft gauge).

The amplitude of the annihilation process can be factorized in the form

$$\mathcal{A} = \frac{e^2}{2\sqrt{2}\,\pi^2} \epsilon\left(\epsilon_1, \epsilon_2, k_1, k_2\right)\, \tilde{\mathcal{A}} \tag{17.3}$$

where ϵ_1, ϵ_2 and k_1, k_2 are respectively the polarization tensors and the momenta of the two outgoing photons. The cross section is then given, as a function of $\tilde{\mathcal{A}}$, by the formula

$$v\sigma_{2\gamma} = \frac{\alpha^2 M_\chi^2}{16\pi^3} \left| \tilde{\mathcal{A}} \right|^2 \quad . \tag{17.4}$$

The total amplitude is implemented in DarkSUSY as the sum of the contributions obtained from four different classes of diagrams:

$$\tilde{\mathcal{A}} = \tilde{\mathcal{A}}_{f\tilde{f}} + \tilde{\mathcal{A}}_{H^+} + \tilde{\mathcal{A}}_W + \tilde{\mathcal{A}}_G,$$

where the indices label the particles in the internal loops, i.e., respectively, fermions and sfermions, charged Higgs and charginos, W-bosons and charginos, and, in the gauge we chose, charginos and Goldstone bosons. For every $\mathcal{A}$ term, real and imaginary parts are splitted; the full set of analytic formulas are given in [112], following the notation of [168], where some of the contributions were first computed. They are rather lengthy expressions with non trivial dependences on various combinations of parameters in the MSSM. We reproduce here, as an example, the formulas for the diagrams with W bosons and charginos, which, in most cases, give the dominant contribution to the cross section as discovered in [112]. The sum over χ_i^+ includes the two chargino eigenstates:

$$Re\,\tilde{\mathcal{A}}_W \;=\; \sum_{\chi_i^+} \frac{1}{M_\chi^2} \left[2\,\frac{(a-b)\;S_{\chi W}}{1+a-b}\; I_1\left(a,b\right) + \frac{S_{\chi W} - 2\sqrt{a}\,D_{\chi W}}{1-a-b}\; I_1\left(a,1\right) \right.$$

$$+\left(2\,\frac{S_{\chi W}-2\sqrt{a}\,D_{\chi W}}{1-a-b}-\frac{3\,S_{\chi W}-4\sqrt{a}\,D_{\chi W}}{1-b}\right)\,I_2\,(a,b)$$
$$+\left(\frac{(2+b)\;S_{\chi W}-4\sqrt{a}\,D_{\chi W}}{1-b}-2\,\frac{(1-a+b)\;S_{\chi W}}{1+a-b}\right)\,I_3\,(a,b)\Bigg] \qquad (17.5)$$

$$Im\,\tilde{\mathcal{A}}_W \;=\; -\pi\sum_{\chi_i^+}\frac{1}{M_\chi^2}\,\left(2\,\frac{(a-b)\;S_{\chi W}}{1+a-b}\right)\cdot$$
$$\cdot\,\log\left(\frac{1+\sqrt{1-b/a}}{1-\sqrt{1-b/a}}\right)\theta\left(1-m_W^2\,/\,M_\chi^2\right) \qquad (17.6)$$

where we defined:

$$a=\frac{M_{\chi_1^0}^2}{M_{\chi_i^+}^2}\qquad b=\frac{m_W^2}{M_{\chi_i^+}^2}$$

$$S_{\chi W}=\frac{1}{2}\;\left(g_{W1i}^L\,g_{W1i}^{L\,*}+g_{W1i}^R\,g_{W1i}^{R\,*}\right)\qquad D_{\chi W}=\frac{1}{2}\;\left(g_{W1i}^L\,g_{W1i}^{R\,*}+g_{W1i}^R\,g_{W1i}^{L\,*}\right)\;\;,$$

and the functions $I_1\,(a,b)$, $I_2\,(a,b)$ and $I_3\,(a,b)$, which arise from the loop integrations, are given by:

$$I_1\,(a,b)=\int_0^1\frac{d\,x}{x}\;\log\left(\left|\frac{4\,a\,x^2-4\,a\,x+b}{b}\right|\right) \qquad (17.7)$$

$$I_2\,(a,b)=\int_0^1\frac{d\,x}{x}\;\log\left(\left|\frac{-a\,x^2+(a+b-1)\,x+1}{a\,x^2+(-a+b-1)\,x+1}\right|\right) \qquad (17.8)$$

$$I_3\,(a,b)=\int_0^1\frac{d\,x}{x}\;\log\left(\left|\frac{-a\,x^2+(a+1-b)\,x+b}{a\,x^2+(-a+1-b)\,x+b}\right|\right). \qquad (17.9)$$

$I_1\,(a,b)$ is the well known three point function that appears in triangle diagrams; it is an analytic function of a/b. $I_2\,(a,b)$ and $I_3\,(a,b)$ may be expressed in terms of dilogarithms. In DarkSUSY, they are computed in the integral form as, for any physically interesting value of the parameters a and b, the integrands are smooth functions of x.

The branching ratio for neutralino annihilations into 2γ is typically not larger than 1%, with the largest values of $v\sigma_{2\gamma}$, for neutralinos with a cosmologically significant relic aboundance, in the range 10^{-29}–10^{-28} cm^{3}s^{-1}. Such values may be large enough for the discovery of this signal in upcoming measurements; at the same time it should be kept in mind that very low values for the cross section are feasible as well.

17.1.2 $\chi\chi \to Z\gamma$

The process of neutralino annihilation into a photon and a Z^0 boson [110]

$$\tilde{\chi}_1^0+\tilde{\chi}_1^0\to\gamma+Z^0 \qquad (17.10)$$

also gives a nearly monochromatic line (with a small smearing caused by the finite width of the Z^0 boson), with energy

$$E_\gamma=M_\chi-\frac{m_Z^2}{4\,M_\chi}. \qquad (17.11)$$

The steps followed in DarkSUSY to compute the cross section are essentially the same as those described for the 2γ case. Again the total amplitude is obtained by summing the contribution from four classes of diagrams and by splitting for each of them real and imaginary parts. The analytic formulas were derived in [110], and are much less compact than those obtained for the process of neutralino annihilation into two photons.

The maximum value of $v\sigma_{Z\gamma}$, for neutralinos with a cosmologically significant relic aboundance, is around $2{\cdot}10^{-28}$ cm^{3}s^{-1} and occurs for a nearly pure Higgsinos. In the heavy mass range, the value of $v\sigma_{Z\gamma}$ reaches a plateau of around $0.6 \cdot 10^{-28}$ cm^{3}s^{-1}. This interesting effect of a non-diminishing cross section with higgsino mass (which is due to a contribution to the real part of the amplitude) is also valid for the 2γ final state in the corresponding limit, with a value of $1 \cdot 10^{-28}$ cm^{3}s^{-1} [112]. Since the gamma-ray background drops rapidly with increasing photon energy, these processes may be interesting for detecting dark matter neutralinos near the upper range of allowed neutralino masses.

Whenever the lightest neutralino contain a significant Wino or Higgsino component the value of $v\sigma_{Z\gamma}$ maybe as large as, or even larger than, twice the value of $v\sigma_{2\gamma}$. It is therefore usually not a good approximation to neglect the $Z\gamma$ state compared to 2γ.

17.1.3 Gamma rays with continuum energy spectrum

The advantage with the gamma-ray lines discussed in the previous Sections is the distinctive spectral signature, which has no plausible astrophysical counterpart.

Compared to the monochromatic flux, the gamma-ray flux produced in π^0 decays is much larger but has less distinctive features. The photon spectrum in the process of a pion decaying into 2γ is, independent of the pion energy, peaked at half of the π^0 mass, about 70 MeV, and symmetric with respect to this peak if plotted in logaritmic variables. Of course, this is true both for pions produced in neutralino annihilations and, e.g., for those generated by cosmic ray protons interacting with the interstellar medium.

When considered together with to the cosmic ray induced Galactic gamma-ray background, the neutralino induced signal looks like a component analogous to the secondary flux due to nucleon nucleon interactions: it is drowned into the Bremsstrahlung component at low energy, while it may be the dominant contribution at energies above 1 GeV or so. In fact, if the exotic component is indeed significant an option to disentangle it would be to search for a break in the energy spectrum at about the neutralino mass, where the line feature might be present as well: while the maximal energy for a photon emitted in neatralino pair annihilations is equal to the neutralino mass, the component from cosmic ray protons extends to much higher energies, essentially with the same spectral index as for the proton spectrum (the role played by the third main background component, inverse Compton emission, has still to settled at the time being and may worsen the problem of discrimitation against background).

Besides this (weak) spectral feature, another way to disentangle the dark matter signal may be to exploit a directional signature: data with a wide angular coverage should be analyzed to seach for a gamma-ray flux component following the shape and density profile of the dark halo, including eventual contributions from clumps.

17.1.4 Sources and fluxes

Given a density distribution of dark matter neutralinos along some line of sight l, the monochromatic gamma-ray flux per unit solid angle in that direction is:

$$\frac{d\Phi_\gamma(\psi)}{d\Omega} = \frac{N_\gamma \, v\sigma_{X^0\gamma}}{8\pi M_\chi^2} \int_{line\ of\ sight} \rho_\chi^2(l) \, d\, l(\psi) \, , \tag{17.12}$$

where ψ is an angle to label the direction of observation and where $N_\gamma = 2$ for $\chi\,\chi \to \gamma\,\gamma$, $N_\gamma = 1$ for $\chi\,\chi \to Z\,\gamma$. Analogously, the gamma-ray flux with continuum energy spectrum is obtained

by replacing $N_\gamma \ v\sigma_{X^0\gamma}$ with $\sum_f dN_\gamma^f/dE \ v\sigma_f$, where the sum is over all tree level final states. Separating the dependence on the dark matter distribution from the part which is related to values of the cross section and the neutralino mass, we rewrite Eq. (17.12) as:

$$\frac{d\Phi_\gamma(\psi)}{d\Omega} \simeq 9.395 \cdot 10^{-12} \left(\frac{N_\gamma \ v\sigma_{X^0\gamma}}{10^{-29} \ \mathrm{cm^3 s^{-1}}}\right) \left(\frac{10\,\mathrm{GeV}}{M_\chi}\right)^2 \cdot J\left(\psi\right) \ \mathrm{cm^{-2}\ s^{-1}\ sr^{-1}} \ , \tag{17.13}$$

where we have defined the dimensionless function

$$J\left(\psi\right) = \frac{1}{8.5\,\mathrm{kpc}} \cdot \left(\frac{1}{0.3\,\mathrm{GeV/cm^3}}\right)^2 \int_{line\ of\ sight} \rho_\chi^2(l) \ d\,l(\psi) \ . \tag{17.14}$$

The relevant quantity for a measurement is, rather than $J\left(\psi\right)$, the integral of $J\left(\psi\right)$ over the solid angle given by the angular acceptance $\Delta\Omega$ of a detector which is pointing in the direction ψ. Defining:

$$\langle J\left(\psi\right)\rangle_{\Delta\Omega} = \frac{1}{\Delta\Omega} \int_{\Delta\Omega} d\Omega' J\left(\psi'\right) \ , \tag{17.15}$$

the flux measured in a detector is:

$$\Phi_\gamma(\psi, \Delta\Omega) = 9.395 \cdot 10^{-12} \left(\frac{N_\gamma \ v\sigma_{X^0\gamma}}{10^{-29} \ \mathrm{cm^3 s^{-1}}}\right) \left(\frac{10\,\mathrm{GeV}}{M_\chi}\right)^2 \langle J\left(\psi\right)\rangle_{\Delta\Omega} \times \Delta\Omega \ \mathrm{cm^{-2}\ s^{-1}\ sr^{-1}} \ . \tag{17.16}$$

Finally, the formalism we introduced can be used also to estimate the flux in the simple case of a single source which, for the given detector, can be approximated as point-like (see examples below). If such source is in the direction ψ at a distance d, Eq. (17.15) becomes:

$$\langle J\left(\psi\right)\rangle_{\Delta\Omega} = \frac{1}{8.5\,\mathrm{kpc}} \cdot \left(\frac{1}{0.3\,\mathrm{GeV/cm^3}}\right)^2 \cdot \frac{1}{d^2} \cdot \frac{1}{\Delta\Omega} \int d^3r \ \rho_\chi^2(\vec{r}) \tag{17.17}$$

where the integral is over the extention of the source (much smaller than d).

Several targets have been discussed as sources of gamma-rays from the annihilation of dark matter particles. An obvious source is the dark halo of our own galaxy [153] and in particular the Galactic center, as the dark matter density profile is expected, in most models, to be picked towards it, possibly with huge enhancements close to te central black hole. The Galactic center is an ideal target for both ground- and space-based gamma-ray telescopes. As satellite experiments have much wider field of views and will provide a full sky coverage, they will test the hypothesis of gamma-rays emitted in clumps of dark matter which may be present in the halo [154, 155, 114, 156]. Another possibility which has been considered is the case of gamma-ray fluxes from external nearby galaxies [157]. Furthermore, it has been proposed to search for an extragalactic flux originated by all cosmological annihilations of dark matter particles [158, 159].

DarkSUSY is suitable to compute the gamma-ray flux from all these (and possibly other) sources. Two cases are fully included in the package: assuming neutralinos are smoothly distributed in the Galactic halo with ρ_χ equal to the dark matter density profile, in DarkSUSY Eq. 17.15 is computed for a specified halo profile and any given ψ and $\Delta\Omega$ [73]. The second option deals with the case of a portion of dark matter being in the form of clumps, each of which is treated as a non-resolvable source in the detector, distributed in the Galaxy according to a probability distribution which follows the dark matter density profile (see [114] for details). It is straightforward to extend this to all other astrophysical sources; in case of cosmological sources one has just to pay attention to include redshift effects and absoption on starlight and infrared background, see [159].

17.2 Neutrinos from halo – theory

Usually, the flux of neutrinos from annihilation of neutralinos in the Milky Way halo is too small to be detectable, but for some clumpy or cuspy models, it might be detectable. The calculation of

the neutrino-flux follows closely the calculation of the continuous gamma ray flux, with the main addition that neutrino interactions close to the detector are also included. Hence, both the neutrino flux and the neutrino-induced muon flux can be obtained. The neutrino to muon conversion rate in the Earth can also be obtained.

Chapter 18

src/ib: Internal Bremsstrahlung

18.1 Internal Bremsstrahlung (IB) – theory

Whenever WIMPs annihilate into pairs of charged particles $X\bar{X}$, this process will inevitably be accompanied by internal bremsstrahlung (IB), i.e. the emission of an additional photon in the final state (note that in contrast to ordinary, or external, bremsstrahlung no external electromagnetic field is required for the emission of the photon). In many cases, IB photons completely dominate the annihilation spectrum at the highest accessible energies. The resulting, characteristic sharp step at an energy corresponding to the dark matter particle's mass, often accompanied by a bump-like feature at slightly smaller energies, is a spectral signature that is hard to mimic by astrophysical sources and in that respect similar to monochromatic photons. In fact, being an $\mathcal{O}(\alpha_{\rm em})$ correction to the tree-level annihilation rate, one would generically expect IB photons to be more copiously produced than the loop-suppressed [i.e. $\mathcal{O}(\alpha_{\rm em}^2)$] monochromatic photons; this has been confirmed in [191] for a large part of the supersymmetric parameter space, not the least due to the appearance of efficient enhancement mechanisms.

18.1.1 General considerations

For didactic purposes, one may follow [191] and distinguish between photons directly radiated off the external legs (*final state radiation*, FSR) and photons radiated from virtual charged particles (*virtual internal bremsstrahlung*, VIB). The IB photons are thus the total contribution from both FSR and VIB photons.

For relativistic charged final states, FSR diagrams are always dominated by photons emitted *collinearly* with X or $\bar{X}$. This is a purely kinematical effect and related to the fact that the propagator of the corresponding outgoing particle,

$$D(p) \propto \left((k+p)^2 - m_X^2\right)^{-1}, \tag{18.1}$$

diverges in this situation. Here, k and p denote the momenta of the photon and the outgoing particle, respectively. The resulting photon spectrum turns out to be of a universal form, almost independent of the underlying particle physics model (see, e.g., [193]):

$$\frac{dN_{\gamma,\rm FSR}^{X\bar{X}}}{dx} \approx \frac{\alpha Q_X^2}{\pi} \mathcal{F}_X(x) \log\left(\frac{s(1-x)}{m_X^2}\right). \tag{18.2}$$

Here, Q_X and m_X are the electric charge and mass of X; the splitting function $\mathcal{F}(x)$ depends only

on the spin of the final state particles and takes the form

$$\mathcal{F}_{\rm fermion}(x) = \frac{1+(1-x)^2}{x} \tag{18.3}$$

for fermions and

$$\mathcal{F}_{\rm boson}(x) = \frac{1-x}{x} \tag{18.4}$$

for bosons. Due to the logarithmic enhancement that becomes apparent in Eq. (18.2), FSR photons are often the main source for IB. A prominent example where FSR in this universal form not only dominates IB but in fact the total gamma-ray spectrum from WIMP annihilations, is the case of Kaluza-Klein dark matter [192].

In general, one can single out two situations where photons emitted from virtual charged particles may give an even more important contribution to the total IB spectrum than FSR: i) the three-body final state $X\bar{X}\gamma$ satisfies a symmetry of the initial state that cannot be satisfied by the two-body final state $X\bar{X}$ or ii) X is a boson and the annihilation into $X\bar{X}$ is dominated by t-channel diagrams, with the t-channel particle almost degenerate in mass with the annihilating WIMP. In contrast to FSR, the contribution from VIB photons can not be given in a model-independent way but is very sensitive to the underlying short-distance physics. For more details, see [191].

18.1.2 IB from neutralino annihilations

For supersymmetric dark matter annhilations, the relevant final states for IB are W^+W^-, $W^\pm H^\mp$, H^+H^- and $f\bar{f}$; both of the situations just mentioned above can arise, and *VIB* contributions become important in considerable regions of the parameter space.

Let us first note that for neutralino annihilations, in contrast to the situation for, e.g., Kaluza-Klein dark matter, we cannot in general expect very large *FSR* contributions. This is because the lightest charged final states, for which the logarithmic enhancement shown in Eq. (18.2) would be most effective, are fermionic and therefore strongly helicity suppressed. Fermion final states containing an additional photon, however, are not subject to such a suppression [194]. In the limit of vanishing fermion mass, and assuming that both corresponding sfermions have the same mass, the photon multiplicity is given by [191]

$$\begin{aligned}\frac{{\rm d}N^{f^+f^-}}{{\rm d}x} &= \alpha_{\rm em} Q_f^2 \frac{|\tilde{g}_R|^4 + |\tilde{g}_L|^4}{64\pi^2}\Big(m_\chi^2 \langle\sigma v\rangle_{\chi\chi\to f\bar{f}}\Big)^{-1} \\ &\times(1-x)\left\{\frac{4x}{(1+\mu)(1+\mu-2x)} - \frac{2x}{(1+\mu-x)^2} - \frac{(1+\mu)(1+\mu-2x)}{(1+\mu-x)^3}\log\frac{1+\mu}{1+\mu-2x}\right\},\end{aligned} \tag{18.5}$$

where $\mu \equiv m^2_{\tilde{f}_R}/m^2_\chi = m^2_{\tilde{f}_L}/m^2_\chi$ and $\tilde{g}_R P_L$ ($\tilde{g}_L P_R$) denotes the coupling between neutralino, fermion and right-handed (left-handed) sfermion. In the above expression, a large factor m^2_χ/m^2_f due to the lifted helicity suppression (from $\langle\sigma v\rangle_{\chi\chi\to f\bar{f}} \propto m_f^2 m\chi^{-4}$) appears, and another enhancement at high photon energies for sfermions degenerate with the neutralino.

For large neutralino masses $m_\chi \gg m_W$ and charginos almost degenerate with the neutralino, W^+W^- and $W^\pm H^\mp$ final states are affected by the second of the mechanisms for VIB enhancement that were discussed in the previous subsection. Of these two channels, IB from W^+W^- nearly always dominates; for pure Higgsinos (or Winos), the resulting photon multiplicity in this limit is well approximated by [191, 195]:

$$\frac{{\rm d}N^{W^+W^-}}{{\rm d}x} \approx \frac{\alpha_{\rm em}}{\pi}\frac{4(1-x+x^2)^2}{(1-x+\epsilon/2)x}\left[\log\left(2\frac{1-x+\epsilon/2}{\epsilon}\right) - 1/2 + x - x^3\right], \tag{18.6}$$

where $\epsilon \equiv m_W/m_\chi$.

Charged Higgs pairs H^+H^-, finally, provide yet another interesting example where the two-body final state is not allowed due to symmetry restrictions; in this case, in the limit $v \to 0$, enforced by CP conservation. The annihilation into $H^+H^-\gamma$, on the other hand, *is* possible. However, since charged Higgs bosons in most models have considerably larger masses than gauge bosons, they are expected to give negligible IB contributions compared to the latter.

18.1.3 The implementation in DarkSUSY

Let us now briefly describe how IB is implemented in DarkSUSY. The total gamma-ray spectrum from WIMP annihilations is given by

$$\frac{dN_{\gamma,\mathrm{tot}}}{dx} = \sum_f B_f \left(\frac{dN^f_{\gamma,\mathrm{sec}}}{dx} + \frac{dN^f_{\gamma,\mathrm{IB}}}{dx} + \frac{dN^f_{\gamma,\mathrm{line}}}{dx} \right) , \tag{18.7}$$

where B_f denotes the branching ratio into the annihilation channel f. The first term encodes the contribution from secondary photons, mainly produced through the decay of neutral pions, as described in Section 17.1. We recall here that these contributions are included by using the Monte Carlo code Pythia [90] to simulate the decay of a hypothetical particle with mass $2m\chi$ and user-specified branching ratios B_f. In this way, also FSR associated to this decay is automatically included in $dN^f_{\gamma,\mathrm{sec}}/dx$ (the main contribution here comes from photons directly radiated off the external legs, but also photons radiated from other particles in the decay cascade are taken into account).

Of course, IB from the decay of such a hypothetical particle cannot in general be expected to show the same characteristics as IB from the actual annihilation of two WIMPs and for this reason an additional term $dN^f_{\gamma,\mathrm{IB}}/dx$ is included that accounts for the difference between the full IB contribution and the FSR part already taken into account for by Pythia. For details regarding the implemented procedure of separating these two contributions in a consistent way, see [191]. The contributions $dN^f_{\gamma,\mathrm{IB}}/dx$, in contrast to $dN^f_{\gamma,\mathrm{sec}}/dx$, are generically highly model-dependent. At the moment, they are fully implemented only for neutralino annihilations and included by default. However, one may easily switch to a user-defined contribution, choose to neglect IB completely or, for comparison, to only include the FSR part (for details, see **dshaib**).

For the supersymmetric case, the full expressions for all relevant three-body final states are implemented, i.e. not just the approximations given in the last subsection, which only apply to the limits described there. For performance reasons, IB is only included when virtual t-channel particles are sufficiently degenerate in mass that large IB contributions to the total spectrum can be expected. With a call to **dsIBset**, this default behaviour can be customized. Finally, radiative corrections to the annihilation into charged particles $X\bar{X}$ of course also change the number of $X\bar{X}$ pairs per annihilation and thus the corresponding yield of particles in the further decay of the annihilation products. At the moment, apart from the photon yield, only the IB positron yield is implemented in DarkSUSY. By default, only the annihilation into the dominating channel $e^+e^-\gamma$ is taken into account in this case; again, this behaviour can be modified by a call to **dsIBset**.

Chapter 19

src/ini: Initialization routines

19.1 Initialization routines

Before DarkSUSY is used for some calculations, it needs to be initialized. This is done with a call to **dsinit**. This routine makes sure that all standard parameters are defined, such as standard model parameters and particle codes. It also calls the different **ds*set** routines with the argument default. E.g., the halo model is set to the default choice with a call to **dshmset**('default'). Analogously, all other routines with a **ds*set** routine is also called to set them up to the default model/parameters.

This means that the call to **dsinit** should be the first call in any program using DarkSUSY. Any calls the user makes to other routines, either to calculte things or select a different model (e.g. a different halo model) should come after the call to **dsinit**.

Chapter 20

src/mh: Kinetic decoupling and microhalos

20.1 Kinetic decoupling and microhalos (mh) – theory

Even after *chemical decoupling*, which sets the DM relic density (see Section 24.1.1), DM frequently scatters with the very abundant standard model particles and thereby stays in local thermal equilibrium with the heat bath until the temperature has dropped by another factor of between 10 and a few 1000; after *kinetic decoupling*, even these scattering events cease and DM no longer interacts with standard model particles. Inhomogeneities in the DM density can only develop after this has happenened, and the DM particles have sufficiently cooled down so that free streaming becomes negligible. The scale of kinetic decoupling can therefore directly be translated into a cutoff in the power spectrum of (dark) matter fluctuations and thus the size of the smallest (at least when not taking into account primordial black holes) gravitationally bound objects in the universe.

20.1.1 Kinetic decoupling

The process of kinetic decoupling is governed by the full Boltzmann equation for the WIMP distribution function $f(\mathbf{x}, \mathbf{p})$, which in a flat Friedmann-Robertson Walker spacetime reads

$$E(\partial_t - H\,\mathbf{p}\cdot\nabla_{\mathbf{p}})\,f = C[f]\,, \tag{20.1}$$

where $C[f]$ is known as the collision term. The Boltzmann equation quoted in Eq. (24.1) for the description of the (chemical) DM freeze-out process is actually just the first moment of this expression, i.e. obtained by integrating it over $\int d^3p$ (after dividing it by E). As was realized int [205, 206], kinetic decoupling can be decribed to a very high precision by considering, instead, the *second* moment of Eq. (20.1). For this purpose, one introduces the WIMP "temperature" T_χ,

$$\int \frac{d^3p}{(2\pi)^3}\mathbf{p}^2 f(\mathbf{p}) \equiv 3\,m_\chi T_\chi n_\chi\,, \tag{20.2}$$

as a parameter that characterizes the deviation from thermal equilibrium (for which $T_\chi = T$ holds). Multiplying Eq.(20.1) by $\mathbf{p}^2/E$, integrating it over $\mathbf{p}$ and keeping only the leading order terms in $\mathbf{p}^2/m_\chi^2$ then results in [206]

$$(\partial_t + 5H)\,T_\chi = 2\,m_\chi\,c(T)\,(T - T_\chi)\ , \tag{20.3}$$

where

$$c(T) = \sum_i \frac{g_{\rm SM}}{6(2\pi)^3 m_\chi^4 T}\int dk\,k^5\omega^{-1}\,g^\pm\left(1\mp g^\pm\right)\ \overline{|\mathcal{M}|}^2_{\substack{t=0\\ s=m_\chi^2+2m_\chi\omega+m_i^2}}\ . \tag{20.4}$$

In the above expression, the sum runs over all standard model scattering partners with 4-momentum $(\omega, \mathbf{k})$ and (thermal) distribution $g(\omega)$ (note, however, that no assumption has been made about the form of the WIMP distribution function f).

For practical purposes, one may now further introduce

$$x \equiv m_\chi/T\,, \tag{20.5}$$

$$y \equiv m_\chi g_{\rm eff}^{-1/2} T_\chi/T^2\,, \tag{20.6}$$

and bring Eq. (20.3) into a form that can more easily be integrated numerically:

$$\frac{dy}{dx} = 2\frac{m_\chi\, c(T)}{H\tilde{g}^{-1/2}}\left(1-\frac{T_\chi}{T}\right)\,, \tag{20.7}$$

with $\tilde{g}^{1/2} \equiv g_{\rm eff}^{1/2}/(1+\frac{1}{4}\frac{g'_{\rm eff}}{g_{\rm eff}}T)$. This form of the equation is also very convenient in that it allows to directly read off its asymptotic behaviour: At large T, the factor in front of the right-hand side is much larger than unity, thus enforcing $T_\chi = T$; when T becomes small, the WIMPs completely decouple from the thermal bath and y stays constant, i.e. $T_\chi \propto T^2 g_{\rm eff}^{1/2} \propto a^{-2}$. Since this transition happens on a rather short time scale, a sensible definition of the *kinetic decoupling* temperature $T_{\rm kd}$ is thus given by equating these two regimes (as if the decoupling process were to occur instantaneously – see [206] for a more detailed discussion):

$$x_{\rm kd} = \frac{m_\chi}{T_{\rm kd}} \equiv g_{\rm eff}(T_{\rm kd})\ y|_{x\to\infty}\ . \tag{20.8}$$

20.1.2 The smallest protohalos

Before kinetic decoupling, WIMPs are tightly coupled to the heat bath, so any small-scale perturbations in the DM fluid would immediately be washed out. For temperatures $T \lesssim T_{\rm kd}$, however, this is no longer the case and perturbations in the DM density start to devolop under the influence of gravity; however, the remaining viscous coupling between the two fluids and, subsequently, the free-streaming of the WIMPs generate an exponential cutoff in the power spectrum [207], with a characteristic comoving damping scale $k_{\rm fs}$. The WIMP mass contained in a sphere of the corresponding size is thus given by [206]

$$M_{\rm fs} \approx \frac{4\pi}{3}\rho_\chi\left(\frac{\pi}{k_{\rm fs}}\right)^3 = 4.0\times10^{-6}\left(\frac{1+\ln\left(g_{\rm eff}^{1/4}T_{\rm kd}/30\ {\rm MeV}\right)/18.6}{(m_\chi/100\ {\rm GeV})^{1/2}\, g_{\rm eff}^{1/4}\,(T_{\rm kd}/30\ {\rm MeV})^{1/2}}\right)^3 M_\odot\,. \tag{20.9}$$

Acoustic oscillations also have to be taken into account as a damping mechanism and lead to a similar exponential cutoff in the power spectrum [208, 209]. In this case, the characteristic damping mass is given by the total amount of DM inside the horizon at the time of kinetic decoupling:

$$M_{\rm ao} \approx \frac{4\pi}{3}\left.\frac{\rho_\chi}{H^3}\right|_{T=T_{\rm kd}} = 3.4\times10^{-6}\left(\frac{T_{\rm kd}g_{\rm eff}^{1/4}}{50\,{\rm MeV}}\right)^{-3} M_\odot\,. \tag{20.10}$$

In general, the actual cutoff in the power spectrum is given by $M_{\rm cut} = \max\left[M_{\rm fs}, M_{\rm ao}\right]$; which of the two physically independent damping mechanisms is more efficient depends on the particle nature of the WIMP. The expected mass for the smallest gravitationally bound objects in the universe is then also simply given by $M_{\rm cut}$. Numerically, the formation of protohalos with masses down to the cutoff scale has been confirmed and their evolution could be followed until a redshift of $z \sim 26$ [210]; the further survival probabilities of these objects, however, as well as the resulting consequences for the indirect detection of DM, are subject to a presently still ongoing discussion.

20.1.3 Implementation in DarkSUSY

Before using any of the routines provided in `src/mh` for the first time, one has to call **dsmhset** in order to choose the DM model and to make some necessary initilizations; currently, both the case of neutralino DM in the general SUSY case as well as Kaluza-Klein DM in minimal universal extra dimensions (mUED) are implemented. However, it is straightforward to add any additional, user-defined DM model by extending the relevant routines and following the comments given in the correponding files. For the average user, the subroutines of greatest interest will be **dsmhtkd** and **dsmhmcut**, and there should be no need to call any of the other routines directly.

dsmhtkd numerically solves the Boltzmann equation (20.3) and returns $T_{\rm kd}$ as given in the definition of Eq. (20.8). Here, special care is taken to accurately handle potential resonances in the scattering amplitude; to this end, **dsmhboltz_init** identifies the location of all relevant resonances and passes this information to **dsmhboltz** where the integral of Eq. (20.4) is perfomed.

Finally, **dsmhmcut** returns the mass cutoff in the power spectrum, with an input parameter determining whether it is $M_{\rm fs}$ or $M_{\rm ao}$; the default call results in $M_{\rm cut} = \max[M_{\rm fs}, M_{\rm ao}]$, i.e. the mass of the smallest protohalos.

Chapter 21

src/wa: Yields from WIMP annihilation in the Sun/Earth

21.1 Muon yields from annihilation in the Earth/Sun – theory

We need to take into account all processes that yield muon neutrinos from annihilation in the Earth/Sun. To do this, we use a Monte Carlo, WimpSim [198], to simulate annihilations in the center of the Sun/Earth, neutrino oscillations and neutrino interactions on the way out of the Sun/Earth and to the detector.

21.1.1 Monte Carlo simulations with WimpSim

We need to evaluate the yield of different particles per neutralino annihilation. The hadronization and/or decay of the annihilation products are simulated with PYTHIA [90] 6.414 and we here describe how the simulations are done. For annihilation in the Sun/Earth the simulations are done for a set of 22 neutralino masses, m_χ = 3, 6, 10, 25, 50, 80.3, 91.2, 100, 150, 176, 200, 250, 350, 500, 750, 1000, 1500, 2000, 3000, 5000, 7500 and 10000 GeV. We tabulate the yields and then interpolate these tables in DarkSUSY.

We are mainly interested in the flux of high energy muon neutrinos and neutrino-induced muons at a neutrino telescope. We simulate 13 'fundamental' annihilation channels, for each mass (where kinematically allowed) above. In Table 21.1 we list the 'fundamental' channels for which simulations are run and the full set of more complex channels. Pions and kaons get stopped before they decay and are thus made stable in the PYTHIA simulations so that they don't produce any neutrinos. For annihilation channels containing Higgs bosons, we can calculate the yield from these fundamental channels by letting the Higgs bosons decaying in flight (see below). We also take into account the energy losses of B-mesons in the Sun and the Earth by following the approximate treatment of [91] but with updated B-meson interaction cross sections as given in [76]. We also take neutrino-interactions on the way out of the Sun into account by considering the charged-current interaction as a neutrino-loss and the neutral current interactions are simulated with nusigma [199]. The neutrino-nucleon charged current interactions close to the detector are also simulated with nusigma and finally the multiple Coulomb scattering of the muon on its way to the detector is calculated using distributions from [55]. We have used the CTEQ6 structure functions in these simulations. We also take into account neutrino oscillations with a full three-neutrino Monte Carlo. All of these

processes are put into the simulation package WimpSim wimpsim that can be downloaded separately. Results from simulation runs with this package are included with DarkSUSY. For more details on these simulations, see [200].

For each annihilation channel and mass we simulate 10^7 annihilations and tabulate the final results as a neutrino-yield, neutrino-to-lepton conversion rate, a muon yield and hadronic shower yields differential in energy and angle from the center of the Sun/Earth. We also tabulate the integrated yield above a given threshold and below an opening angle θ. We assumed throughout that the surrounding medium is water with a density of 1.0 g/cm^3. Hence, the neutrino-to-muon conversion rates have to be multiplied by the density of the medium. In the muon fluxes, the density cancels out (to within a few percent). All results are summarized as yield tables that can be loaded and interpolated in with DarkSUSYThis is done with the function dswayieldf. There are three kinds of yields (two-dimensional in opening angle θ and energy), kind=1 gives integrated yields, kind=2 gives differential yields and kind=3 gives yields integrated in angle, but differential in θ. For each kind, there are 26 different types of yield available according to Table 21.4. As a default, only type 3–4, 9–10 and 13–14 are included in the DarkSUSY download, as these are the most commonly used types. If you need any other types, download the auxiliary data files from `http://www.darksusy.org`, unpack them in share/DarkSUSY in the DarkSUSY root directory, and then do a usual configure and make to install them. Also note that the kind=3 yields are not tabulated directly, but are instead calculated and tabulated when the simulation tables are read in during DarkSUSY initialization.

With these simulations, we can calculate the yield for any of these particles for a given MSSM model. For the Higgs bosons, which decay in flight, an integration over the angle of the decay products with respect to the direction of the Higgs boson is performed. Given the branching ratios for different annihilation channels it is then straightforward to compute the yield above any given energy threshold and within any angular region around the Sun or the center of the Earth. The routine dswayieldone calculates the yield for one channel, i.e. even these complex channels containing Higgs bosons, whereas the main routine dswayield calculates the total yield for a given model. Note that the WIMP annihilation yield routines do not know about SUSY at all, so before they are called, a routine dswasetup is called to set up the annihilation branching ratios for the WIMP and decay channels for the Higgs bosons. In Tables 21.2 and 21.3, the Higgs decay width channels are given. If these routines are used with other particle physics models, replace dswasetup with a routine appropriate for your particle physics model and then call dswayield as usual.

Annihilation channel ch	Particles	Internal channel chi	Internal channel array index chii
1	$S_1^0 S_1^0$	-	-
2	$S_1^0 S_2^0$	-	-
3	$S_2^0 S_2^0$	-	-
4	$S_3^0 S_3^0$	-	-
5	$S_1^0 S_3^0$	-	-
6	$S_2^0 S_3^0$	-	-
7	$S^- S^+$	-	-
8	$Z^0 S_1^0$	-	-
9	$Z^0 S_2^0$	-	-
10	$Z^0 S_3^0$	-	-
11	$W^- S^+ / W^+ W^-$	-	-
12	$Z^0 Z^0$	9	9
13	$W^+ W^-$	8	8
14	$\nu_e \bar{\nu}_e$	12	11
15	$e^+ e^-$	-	-
16	$\nu_\mu \bar{\nu}_\mu$	13	12
17	$\mu^+ \mu^-$	10	-
18	$\nu_\tau \bar{\nu}_\tau$	14	13
19	$\tau^+ \tau^-$	11	10
20	$u\bar{u}$	2	2
21	$d\bar{d}$	1	1
22	$c\bar{c}$	4	4
23	$s\bar{s}$	3	3
24	$t\bar{t}$	6	6
25	$b\bar{b}$	5	5
26	gg	7	7
27	qqg	-	-
28	$\gamma\gamma$	-	-
29	$Z^0\gamma$	-	-

Table 21.1: The annihilation channels ch used in dswayieldone. Also shown are the internal channel numbers chi used for the fundamental channels used in the simulations (used by routine dswayieldf). To save some additional space with the data files in memory, there are also array index channel numbers chii that are only used internally to access the right elements of the yield arrays. S denotes scalars (Higgs bosons).

Decay width channel dch	Particles
1–29	Same as the annihilation channels in Table 21.1.
30	Sfermions
31	Neutralinos
32	Charginos

Table 21.2: The neutral scalar (Higgs) decay width channels used. In DarkSUSY these are stored in the array hdwidth(i,j) where i is the decay channel index above and j is the Higgs number (1–3 for H_1^0, H_2^0 and H_3^0 respectively). For the wa routines, these decay branching ratios (partial width divided by total width) are stored in dswas0br(i,j).

Decay width channel dch	Particles
1	ud
2	$u\bar{s}$
3	$u\bar{b}$
4	$c\bar{d}$
5	$c\bar{s}$
6	$c\bar{b}$
7	$t\bar{d}$
8	$t\bar{s}$
9	$t\bar{b}$
10	$\nu_e e^+$
11	$\nu_\mu \mu^+$
12	$\nu_\tau \tau^+$
13	$W^+ S_1^0$
14	$W^+ S_2^0$
15	$W^+ S_3^0$
20	Sfermions
21	Neutralinos and charginos

Table 21.3: The (positively) charged scalar (Higgs) decay width channels used. In DarkSUSY these are stored in the array hdwidth(i,4) where i is the decay channel index above. For the wa routines, these decay branching ratios (partial width divided by total width) are stored in dswascbr(i).

Yield type type	Yield	Unit
1	ν_e	10^{-30} m^{-2} annihilation^{-1}
2	$\bar{\nu}_e$	10^{-30} m^{-2} annihilation^{-1}
3	ν_μ	10^{-30} m^{-2} annihilation^{-1}
4	$\bar{\nu}_\mu$	10^{-30} m^{-2} annihilation^{-1}
5	ν_τ	10^{-30} m^{-2} annihilation^{-1}
6	$\bar{\nu}_\tau$	10^{-30} m^{-2} annihilation^{-1}
7	e^- at neutrino-nucleon vertex	10^{-30} m^{-3} annihilation^{-1}
8	e^+ at neutrino-nucleon vertex	10^{-30} m^{-3} annihilation^{-1}
9	μ^- at neutrino-nucleon vertex	10^{-30} m^{-3} annihilation^{-1}
10	μ^+ at neutrino-nucleon vertex	10^{-30} m^{-3} annihilation^{-1}
11	τ^- at neutrino-nucleon vertex	10^{-30} m^{-3} annihilation^{-1}
12	τ^+ at neutrino-nucleon vertex	10^{-30} m^{-3} annihilation^{-1}
13	μ^- at an imaginary plane at detector	10^{-30} m^{-2} annihilation^{-1}
14	μ^+ at an imaginary plane at detector	10^{-30} m^{-2} annihilation^{-1}
15	hadronic shower from ν_e CC int. at neutrino-nucleon vertex	10^{-30} m^{-3} annihilation^{-1}
16	hadronic shower from $\bar{\nu}_e$ CC int. at neutrino-nucleon vertex	10^{-30} m^{-3} annihilation^{-1}
17	hadronic shower from ν_μ CC int. at neutrino-nucleon vertex	10^{-30} m^{-3} annihilation^{-1}
18	hadronic shower from $\bar{\nu}_\mu$ CC int. at neutrino-nucleon vertex	10^{-30} m^{-3} annihilation^{-1}
19	hadronic shower from ν_τ CC int. at neutrino-nucleon vertex	10^{-30} m^{-3} annihilation^{-1}
20	hadronic shower from $\bar{\nu}_\tau$ CC int. at neutrino-nucleon vertex	10^{-30} m^{-3} annihilation^{-1}
21	hadronic shower from ν_e NC int. at neutrino-nucleon vertex	10^{-30} m^{-3} annihilation^{-1}
22	hadronic shower from $\bar{\nu}_e$ NC int. at neutrino-nucleon vertex	10^{-30} m^{-3} annihilation^{-1}
23	hadronic shower from ν_μ NC int. at neutrino-nucleon vertex	10^{-30} m^{-3} annihilation^{-1}
24	hadronic shower from $\bar{\nu}_\mu$ NC int. at neutrino-nucleon vertex	10^{-30} m^{-3} annihilation^{-1}
25	hadronic shower from ν_τ NC int. at neutrino-nucleon vertex	10^{-30} m^{-3} annihilation^{-1}
26	hadronic shower from $\bar{\nu}_\tau$ NC int. at neutrino-nucleon vertex	10^{-30} m^{-3} annihilation^{-1}

Table 21.4: The yield types available from the wa routines. All of these yields are at the detector (currently IceCube). Note that the units are for integrated yields (kind=1), for differential yields (kind=2), the units should be multiplied by GeV^{-1} degree^{-1}. CC int. = charged current interactions. NC int. = neutral current interactions.

Chapter 22

src/nt: Neutrino and muon rates from annihilation in the Sun/Earth

22.1 Neutrinos from the Sun and Earth – theory

There are several indirect methods for detection of neutralinos. One of the most promising [94] is to make use of the fact that scattering of halo neutralinos by the Sun and the planets, in particular the Earth, during the several billion years that the Solar system has existed, will have trapped these neutralinos within these astrophysical bodies. Being trapped within the Solar or terrestrial material, they will sink towards the center, where a considerable enrichment and corresponding increase of annihilation rate will occur.

Searches for neutralino annihilation into neutrinos will be subject to extensive experimental investigations in view of the new neutrino telescopes (AMANDA, IceCube, Baikal, NESTOR, ANTARES) planned or under construction [95]. A high-energy neutrino signal in the direction of the centre of the Sun or Earth is an excellent experimental signature which may stand up against the background of neutrinos generated by cosmic-ray interactions in the Earth's atmosphere.

There are several different approximations one could do, or processes to include when calculating the capture rates in the Earth/Sun and many of these are coded into DarkSUSY. The default in DarkSUSY is always to use the best calculations available, but more approximate (older) routines are also available, as well as more speculative signals, like the Damour-Krauss signal (not included by default). If you want to use something else than the defaults, or want to call more internal rotuines (more internal than dsntrates or dsntdiffrates), you should read the following sections carefully.

22.1.1 Neutrino yield from annihilations

The differential neutrino flux from neutralino annihilation is

$$\frac{dN_\nu}{dE_\nu} = \frac{\Gamma_A}{4\pi D^2} \sum_f B_\chi^f \frac{dN_\nu^f}{dE_\nu} \tag{22.1}$$

where Γ_A is the annihilation rate, D is the distance of the detector from the source (the central region of the Earth or the Sun), f is the neutralino pair annihilation final states, and B_χ^f are the branching ratios into the final state f. dN_ν^f/dE_ν are the energy distributions of neutrinos generated by the final state f and are obtained from the PYTHIA simulations described in section **??**.

In comparison with calculations using the results of [91] (e.g. [96]), this Monte Carlo treatment of the neutrino propagation through the Sun does not need the simplifying assumptions previously

made, namely neutral currents are no more assumed to be much weaker than charged currents and energy loss is no more considered continuous.

The neutrino-induced muon flux may be detected in a neutrino telescope by measuring the muons that come from the direction of the centre of the Sun or Earth. For a shallow detector, this usually has to be done in the case of the Sun by looking (as always the case for the Earth) at upward-going muons, since there is a huge background of downward-going muons created by cosmic-ray interactions in the atmosphere. There is always in addition a more isotropic background coming from muon neutrinos created on the other side of the Earth in such cosmic-ray events (and also from cosmic-ray interactions in the outer regions of the Sun). The flux of muons at the detector is given by

$$\frac{dN_\mu}{dE_\mu} = N_A \int_{E_\mu^{\rm th}}^{\infty} dE_\nu \int_0^\infty d\lambda \int_{E_\mu}^{E_\nu} dE'_\mu \; P(E_\mu, E'_\mu; \lambda) \; \frac{d\sigma_\nu(E_\nu, E'_\mu)}{dE'_\mu} \; \frac{dN_\nu}{dE_\nu} \,, \tag{22.2}$$

where λ is the muon range in the medium (ice or water for the large detectors in the ocean or at the South Pole, or rock which surrounds the smaller underground detectors), $d\sigma_\nu(E_\nu, E'_\mu)/dE'_\mu$ is the weak interaction cross section for production of a muon of energy E'_μ from a parent neutrino of energy E_ν, and $P(E_\mu, E'_\mu; \lambda)$ is the probability for a muon of initial energy E'_μ to have a final energy E_μ after passing a path–length λ inside the detector medium. $E_\mu^{\rm th}$ is the detector threshold energy, which for "small" neutrino telescopes like Baksan, MACRO and Super-Kamiokande is around 1 GeV. Large area neutrino telescopes in the ocean or in Antarctic ice typically have thresholds of the order of tens of GeV, which makes them sensitive mainly to heavy neutralinos (above 100 GeV) [97].

The integrand in Eq. (22.2) is weighted towards high neutrino energies, both because the cross section σ_ν rises approximately linearly with energy and because the average muon energy, and therefore the range λ, also grow approximately linearly with E_ν. Therefore, final states which give a hard neutrino spectrum (such as heavy quarks, τ leptons and W or Z bosons) are usually more important than the soft spectrum arising from light quarks and gluons.

22.1.2 Evolution of the number density in the Earth/Sun

Neutralinos are steadily being trapped in the Sun or Earth by scattering, whereas annihilations take them away. Let $N(t)$ be the total number of neutralinos trapped, at time t, in the core of, for example, the Earth. The annihilation rate of neutralino pairs can be written as

$$\Gamma_a(t) = \frac{1}{2} \, C_a \, N^2(t) \,. \tag{22.3}$$

The evolution of $N(t)$ is the result of the competition between capture and annihilation:

$$\frac{dN}{dt} = C_c(t) - C_a \, N^2 \tag{22.4}$$

The constant C_c is the capture rate, and C_a entering equations (22.3) and (22.4) is linked to the annihilation cross-section σ_a, and to some effective volumes V_j, $j = 1, 2$, taking into account the quasi-thermal distribution of neutralinos in the Earth core:

$$C_a = \langle \sigma_a \, v \rangle \, \frac{V_2}{V_1^2} \,, \tag{22.5}$$

$$V_j \simeq 2.3 \times 10^{25} \left(\frac{j \, m_X}{10 \, \mathrm{GeV}} \right)^{-3/2} \mathrm{cm}^3 \,. \tag{22.6}$$

This has the solution for the annihilation rate implemented in DarkSUSY

$$\Gamma_A = \frac{C_c}{2} \tanh^2 \left(\frac{t}{\tau} \right) , \tag{22.7}$$

where the equilibration time scale $\tau = 1/\sqrt{C_c C_a}$. In most cases for the Sun, and in the cases of observable fluxes for the Earth, τ is much smaller than a few billion years, and therefore equilibrium is often a good approximation ($\dot{N}(t) = 0$). This means that it is the capture rate which is the important quantity that determines the neutrino flux. However, in the program we keep the exact formula (22.7), with some modifications discussed in Sec. 22.1.8).

22.1.3 Approximate capture rate expressions

The capture rate induced by scalar (spin-independent) interactions between the neutralinos and the nuclei in the interior of the Earth or Sun is the most difficult one to compute, since it depends sensitively on the Higgs mass, form factors, and other poorly known quantities. However, this spin-independent capture rate calculation is the same as for direct detection treated in Section **??**. Therefore, there is a strong correlation between the neutrino flux expected from the Earth (which is mainly composed of spin-less nuclei) and the signal predicted in direct detection experiments [97, 98]. It seems that even the large (kilometer-scale) neutrino telescopes planned, when searching for neutralino annihilation in the Earth, will not be competitive with the next generation of direct detection experiments when it comes to detecting neutralino dark matter. However, the situation concerning the Sun is more favourable. Due to the low counting rates for the spin-dependent interactions in terrestrial detectors, high-energy neutrinos from the Sun constitute a competitive and complementary neutralino dark matter search. Of course, even if a neutralino is found through direct detection, it will be extremely important to confirm its identity and investigate its properties through indirect detection. In particular, the mass can be determined with reasonable accuracy by looking at the angular distribution of the detected muons [99, 100].

For the Sun, dominated by hydrogen, the axial (spin-dependent) cross section is important and relatively easy to compute. A reasonably good approximation is given by [3]

$$\frac{C_\odot^{\rm sd}}{(1.3\cdot 10^{23}\,{\rm s}^{-1})\,(270\ {\rm km\,s}^{-1}/\bar{v})} = \left(\frac{\rho_\chi}{0.3\ {\rm GeV\,cm}^{-3}}\right)\left(\frac{100\,{\rm GeV}}{m_\chi}\right)\left(\frac{\sigma_{p\chi}^{\rm sd}}{10^{-40}\ {\rm cm}^2}\right) \tag{22.8}$$

where $\sigma_{p\chi}^{\rm sd}$ is the cross section for neutralino-proton elastic scattering via the axial-vector interaction, $\bar{v}$ is the dark-matter velocity dispersion, and ρ_χ is the local dark matter mass. The capture rate in the Earth is dominated by scalar interactions, where there may be kinematic and other enhancements, in particular if the mass of the neutralino almost matches one of the heavy elements in the Earth. For this case, a more detailed analysis is called for, which is available in [80] with convenient approximations in [3]. In fact, also for the Sun the spin-independent contribution can be important, in particular iron may contribute non-negligibly. For the Sun, the approximation in [3] is also available,

$$\frac{C_\odot^{\rm si}}{(4.8\cdot 10^{22}\,{\rm s}^{-1})\,(270\ {\rm km\,s}^{-1}/\bar{v})} = \left(\frac{\rho_\chi}{0.3\ {\rm GeV\,cm}^{-3}}\right)\left(\frac{100\,{\rm GeV}}{m_\chi}\right)\times \sum_A \left(\frac{\sigma_A^{\rm si}}{10^{-40}\ {\rm cm}^2}\right) F_A(m_\chi) f_A \phi_A S\left(m_\chi/m_A\right)/m_A, \tag{22.9}$$

where f_A is the mass fraction of element A and ϕ_A is the typical gravitational potential (relative to the surface) for that element. I.e. an element that is concentrated in the core will have a higher ϕ_A than an element at the surface. A is the atomic number of the element and M_A is its mass. The factor S is a kinematical suppression factor [3, 161]. In the next subsection we will go through the compositions of the Earth/Sun that we use.

The approximate capture rate expressions above are coded into the routines dsntcapsun and dsntcapearth. More accurate expressions will follow in the coming subsections.

		Average parameters	
Element	Mass number (A)	f_i	ϕ_i
Hydrogen, H	1	0.670	3.15
Helium-4, ^{4}He	4	0.311	3.40
Carbon, C	12	0.00237	2.85
Nitrogen, N	14	0.00188	3.83
Oxygen, O	16	0.00878	3.25
Neon, Ne	20	0.00193	3.22
Magnesium, Mg	24	0.000733	3.22
Silicon, Si	28	0.000798	3.22
Sulphur, S	32	0.000550	3.22
Iron, Fe	56	0.00142	3.22

Table 22.1: The composition of the Sun with average parameters to be used in the approximative relations given in [3]. These values are updated with the solar model of [190] and differs slightly from the values used in [3].

	Mass	Mass fraction		Average parameters	
Element	number (A)	Core	Mantle	f_i	ϕ_i
Oxygen, O	16	0.0	0.440	0.298	1.20
Silicon, Si	28	0.06	0.210	0.162	1.24
Magnesium, Mg	24	0.0	0.228	0.154	1.20
Iron, Fe	56	0.855	0.0626	0.319	1.546
Calcium, Ca	40	0.0	0.0253	0.0171	1.20
Phosphor, P	30	0.002	0.00009	0.00071	1.56
Sodium, Na	23	0.0	0.0027	0.00183	1.20
Sulphur, S	32	0.019	0.00025	0.0063	1.59
Nickel, Ni	59	0.052	0.00196	0.0181	1.57
Aluminum, Al	27	0.0	0.0235	0.0159	1.20
Chromium, Cr	52	0.009	0.0026	0.0047	1.44

Table 22.2: The composition of the Earth's core and mantle. The core mass fractions are from [172][Table 4] and the mantle mass fractions are from [172][Table 2]. The average mass fractions and potentials in the last two columns are weighted averages assuming a core mass of $1.93 \cdot 10^{24}$ kg and a mantle mass of $4.04 \cdot 10^{24}$ kg with average potentials (relative to the surface) of 1.6 in the core and 1.2 in the mantle [80].

22.1.4 Earth and Sun composition

When the capture rates are calculated, we need to know the composition and density of the Earth/Sun as a function of depth.

In [3] they used average mass fractions and potentials for the location of the various elements in the Sun. We have updated these to the BP2000 [190] values instead, as given in Table 22.1

For the Earth, we have also implemented more accurate density profiles and more up-to date chemical distributions within the Earth. We use the estimates for the Earth composition given in [172][Table 2 for the mantle and Table 4 for the core]. In Table 22.2 we list these values together with the average parameters f_i and ϕ_i that should be used in the expressions for the approximate capture rates in the previous section. Note that using these average parameters instead of integrating over the full radius is equivalent to putting all the elements of the give type at the gravitational potential ϕ_i.

We also need the density profile of the Earth, and for this we use the values in [107]. Using this density profile, we can calculate the gravitational potential, $\phi(r)$ inside the Earth and from this one

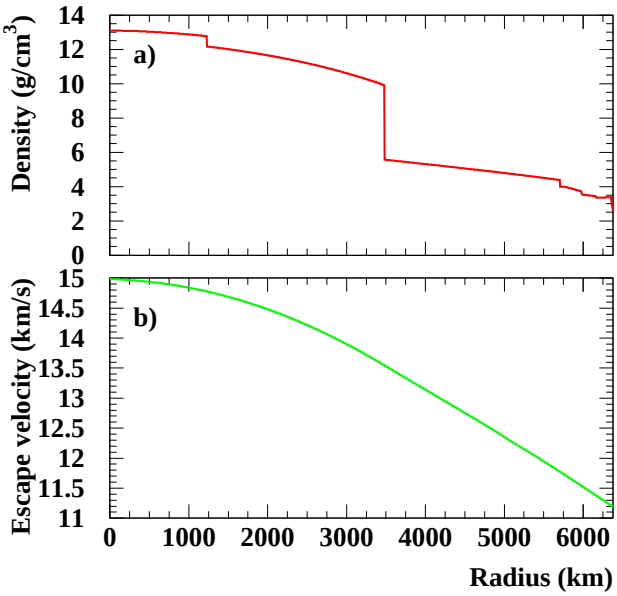

Figure 22.1: In a) the density profile and in b) the escape velocity in the Earth is shown.

the escape velocity v inside the Earth,

$$v = 11.2\sqrt{\frac{\phi(r)}{\phi(R_\oplus)}}\ \text{km/s}. \tag{22.10}$$

In Fig. 22.1 we show the density profile and escape velocity inside the Earth.

22.1.5 More accurate capture rate expressions

Another complicating factor when calculating the capture rates is the integration over the velocity distribution. In [80], parts of the integrations are performed analytically for a Gaussian veolocity distributions. These expressions are also coded in DarkSUSYfor the Earth and give a more accurate calculation of the capture rate in the Earth than the approximations given above. The routine dsntcapearth2 performs these calculations for the Earth.

22.1.6 Accurate capture rates in the Earth for general velocity distributions

If one wants even more accurate and general expressions for the capture rates in the Sun/Earth, we have also implemented the full expressions in [80], but without assuming that the velocity distribution is a Gaussian (or Maxwell-Boltzmann). These routines are now the default in DarkSUSY.

We will here outline how these expressions look like for the Earth and how they can be used both for a Maxwell-Boltzmann distribution and for a general velocity distribution. The expressions will of course look analogously for the Sun. We start with the general case and study the special case of a Maxwell-Boltzmann distribution in the next section.

We will divide the Earth into shells and calculate the capture from element i in each shell individually. At the end we will integrate over all the shells and sum over all the elements in the

Earth. The capture rate from element i per unit shell volume is given by [80][Eq. (2.8)]

$$\frac{dC_i}{dV} = \int_0^{u_{max}} du \frac{f(u)}{u} w\Omega^-_{v,i}(w) \tag{22.11}$$

where $f(u)$ is the velocity distribution (normalized such that $\int_0^\infty f(u) = n_\chi$ where n_χ is the number density of WIMPs. The expression $\Omega^-_{v,i}(w)$ is related to the probability that we scatter to orbits below the escape velocity. w is the velocity at the given shell and it is related to the velocity at infinity u and the escape velocity v by

$$w = \sqrt{u^2 + v^2}. \tag{22.12}$$

The upper limit of integration is a priori set to $u_{max} = \infty$, but we will see below that due to kinematical reasons we can set it to a lower value (Eq. (22.17) below). If we allow for a form factor suppression of the form [80][Eq. (A3)]

$$|F(q^2)|^2 = \exp\left(-\frac{\Delta E}{E_0}\right) \tag{22.13}$$

with [80][Eq. (A4)]

$$E_0 = \frac{3\hbar^2}{2m_\chi R^2} \tag{22.14}$$

we can evaluate $w\Omega^-_{v,i}(w)$ and arrive at the expression [80][Eq. (A6)]

$$w\Omega^-_{v,i}(w) = \sigma_i n_i \frac{\mu_+^2}{\mu} 2E_0 \left[e^{-\frac{m_\chi u^2}{2E_0}} - e^{-\frac{\mu}{\mu_+^2} m_\chi \frac{u^2+v^2}{2E_0}}\right] \Theta\left(\frac{\mu}{\mu_+^2} - \frac{u^2}{u^2+v^2}\right) \tag{22.15}$$

where we have introduced

$$\mu = \frac{m_\chi}{m_i} \quad ; \quad \mu_\pm = \frac{\mu \pm 1}{2} \tag{22.16}$$

with m_i the mass of element i. The Heaviside step function Θ plays the role of only including WIMPs that can scatter to a velocity lower then the escape velocity v. To simplify our calculations we can drop this step function in Eq. (22.15) and instead set the upper limit of integration in Eq. (22.11) to

$$u_{max} = \sqrt{\frac{\mu}{\mu_-^2}} v \tag{22.17}$$

We also need the scattering cross section on element i, which can be written as [3][Eq. (9-25)]

$$\sigma_i = \sigma_p A_i^2 \frac{(m_\chi m_i)^2}{(m_\chi + m_i)^2} \frac{(m_\chi + m_p)^2}{(m_\chi m_p)^2} \tag{22.18}$$

where A_i is the atomic number of the element, m_p is the proton mass and σ_p is the scattering cross section on protons.

We now have what we need to calculate the capture rate. In Eq. (22.11) we integrate over the velocity for our chosen velocity distribution. We then integrate this equation over the radius of the Earth and sum over all the different elements in the Earth,

$$C = \int_0^{R_\oplus} dr \sum_i \frac{dC_i}{dV} 4\pi r^2 \tag{22.19}$$

Note that we have not assumed anything special about our velocity distribution, it doesn't even have to be isotropic since the distribution of elements evenly in the shells will make an anisotropic distribution on average to behave as an isotropic one.

The routines that calculate the capture rates with these general (and accurate) expressions are dsntcapearthnum and dsntcapsunnum. As these calculations are somewhat time-consuming, we have also added a possibility to tabulate the result and interpolate in these tables. To use (or create, if the table files are missing) instead call dsntcapearthtab and dsntcapsuntab. These last two routines are the default in DarkSUSY. The velocity distribution used is determined by a switch when the halo model is set (i.e. when dshmset is called).

22.1.7 Accurate capture rates for the Earth for a Maxwell-Boltzmann velocity distribution

We will here give some more information on how the approximations introduced in the beginning of this chapter are derived from the general expressions in the preceeding section.

If the velocity distribution is of Maxwell-Boltzmann type we can greatly simplify our expressions above as we can perform the integration over velocity analytically. The integration over radius can also be further simplified by using the average mass fractions f_i and potentials ϕ_i in Tables 22.1–22.2.

If the velocity distribution in the halo is Maxwell-Boltzmann, it looks like

$$f_h(u)du = n_\chi \frac{4}{\sqrt{\pi}} \left(\frac{3}{2}\right)^{\frac{3}{2}} \frac{u^2}{\bar{v}^3} e^{-\frac{3}{2}\frac{u^2}{\bar{v}^2}} du \tag{22.20}$$

where $\bar{v}$ is the three-dimensional velocity dispersion and n_χ is the number density of WIMPs in the halo. However, the solar system moves through the halo with a velocity v_* and the distribution on observer with this velocity through the halo will see is

$$f_*(u) = f_h(u) e^{-\frac{3}{2}\frac{v_*^2}{\bar{v}^2}} \frac{\sinh\left(\frac{3uv_*}{\bar{v}^2}\right)}{\frac{3uv_*}{\bar{v}^2}} = n_\chi \sqrt{\frac{3}{2\pi}} \frac{u}{\bar{v}v_*} \left[e^{-\frac{3}{2}\frac{(u-v_*)^2}{\bar{v}^2}} - e^{-\frac{3}{2}\frac{(u+v_*)^2}{\bar{v}^2}} \right] \tag{22.21}$$

Now one would naively believe that this is not the distribution that an observer at the Earth will see. First of all, the Earth is moving with respect to the Sun and secondly, the WIMPs have gained speed by the gravitational attraction of the Sun when they reach the Earth. Both of these arguments are true and the distribution of WIMPs in the halo will not look like Eq. (22.21) to an observer on the Earth. However, Gould [104] showed that WIMPs from the halo can diffuse into the solar system due to gravitational interactions with the planets and this distribution of WIMPs will roughly look like as if the Earth was in free space moving through the halo with the velocity of the solar system, i.e. Eq. (22.21). We will later scrutinize this statement, as it turns out that it does not quite hold, but as a first guess it is a reasonable approximation. For the Sun, though, the velocity distribution give above is the correct one for a Maxwell-Boltzmann distribution.

With the distribution Eq. (22.21) we can analytically perform the integration over velocity in Eq. (22.11). After some algebra we arrive at [80][Eq. (A10)]

$$\begin{aligned} \frac{dC_i}{dV} &= \left(\frac{8}{3\pi}\right)^{\frac{1}{2}} \frac{\sigma_i n_i n_\chi \bar{v}}{2b\eta} \\ &\quad \left[\frac{e^{-a\hat{\eta}^2}}{\sqrt{1+a}} \left[2\widetilde{\mathrm{erf}}(\hat{\eta}) - \widetilde{\mathrm{erf}}(\hat{A}_+) + \widetilde{\mathrm{erf}}(\hat{A}_-) \right] \right. \\ &\quad \left. - \frac{e^{-b\check{\eta}^2}}{\sqrt{1+b}} e^{-(a-b)A^2} \left[2\widetilde{\mathrm{erf}}(\check{\eta}) - \widetilde{\mathrm{erf}}(\check{A}_+) + \widetilde{\mathrm{erf}}(\check{A}_-) \right] \right] \end{aligned} \tag{22.22}$$

where $\widetilde{\mathrm{erf}}$ is the modified error function,

$$\widetilde{\mathrm{erf}}(x) = \frac{\sqrt{\pi}}{2}\mathrm{erf}(x) \qquad ; \qquad \mathrm{erf}(x) = \frac{2}{\sqrt{\pi}} \int_0^x e^{-y^2} dy. \tag{22.23}$$

Following Gould [80], we have in Eq. (22.22) introduced the following shorthand notation:

$$\begin{array}{lll} \eta = \sqrt{\frac{3}{2}\frac{v_*^2}{\bar{v}^2}} & ; \quad a = \frac{m_c h i \bar{v}^2}{3E_0} & ; \quad b = \frac{\mu}{\mu_+^2} a \\ \hat{\eta} = \frac{\eta}{\sqrt{1+a}} & ; \quad \check{\eta} = \frac{\eta}{\sqrt{1+b}} & \\ A^2 = \frac{3}{2}\frac{v_*^2}{\bar{v}^2}\frac{\mu}{\mu_-^2} & ; \quad \hat{A} = A\sqrt{1+a} & ; \quad \check{A} = A\sqrt{1+b} \\ \hat{A}_\pm = \hat{A} \pm \hat{\eta} & ; \quad \check{A}_\pm = \check{A} \pm \check{\eta} & \end{array} \tag{22.24}$$

If we wish, we can now integrate Eq. (22.22) over radius just like in the previous section, but we can without loosing too much accuracy, replace this integration with a sum over the elements in the Earth with their respective typical location. I.e. we can write

$$C = \sum_i \frac{dC_i}{dV}\frac{1}{n_i}\frac{f_i M_\oplus}{m_i} \tag{22.25}$$

where we instead of the number density n_i use the total number of atoms of the given type $f_i M_\oplus / m_i$. Note that for each element in the sum we should evaluate this expression at the given typical gravitational potential ϕ_i of the element, i.e. with the escape velocity given by Eq. (22.10). The mass fractions f_i and typical potentials ϕ_i are listed in Table 22.2 (and analogously in Table 22.1 for the Sun). This approximation introduces an error of no more than about 1–2% for a Maxwell-Boltzmann distribution*

The capture rate evaluated with the expressions shown here are encoded into the routine dsntcapearth2. Note that we have not coded the corresponding approximate expressions for the Sun. Instead, as given in the preceeding section, we now have more accurate expressions for both the Sun and the Earth.

22.1.8 A possible new population of neutralinos

Recently, it has been shown that the scattering process in the Sun can populate orbits which subsequently result in a bound Solar System population of WIMPs [101, 102] and which can be comparable in spectral density, in the region of the Earth, to the Galactic halo WIMP population. This new population consists of WIMPs that have scattered in the outer layers of the Sun and due to perturbations by the other planets (mainly Venus and Jupiter) evolve into bound orbits which do not cross the Sun but do cross the Earth's orbit. This population of WIMPs should have a completely different velocity distribution than halo WIMPs and will thus have quite different capture probabilities in the Earth. The predicted WIMP abundance, and spectrum, relevant for direct detection have been calculated in [101, 102], where it was shown that although the total rates may not change by a large amount, there could be a striking directional effect, which could be of impoertance once detectors with directional sensitivity are built. Also for capture in the Earth, and the predicted indirect neutrino signature, there are poissibly large effects, incorporated as an optional choice in DarkSUSY, coming from this new population [77]. (Other studies of solar system populations of WIMPs can be found in [103, 104]. See also the comments in [105] about the uncertainties involved in estimating these effects.)

The enhancement caused by the new population is only important for neutralino mass less than 150 - 170 GeV (the exact number depending on details about the angular momentum distribution [77]).

Following the notation of [101, 102] one can write the contribution from the new population of neutralinos to the usual halo neutralino density as

$$\delta_E \equiv \frac{n(a_1)}{n_X} \equiv \frac{\text{(secondary) neutralino density at the Earth}}{\text{halo neutralino density at infinity}}, \tag{22.26}$$

*Note that it is not advisable to use this approximation for general velocity distributions. If one e.g. has a lower limit on possible velocities, u_{min}, for heavy WIMPs capture will then only be possible very close to the central core. Replacing the actual distribution of potentials $\phi(r)$ with the typical value ϕ_i may then introduce larger errors. We will encounter these kind of distributions shortly.

where

$$\delta_E = \frac{5.44\times10^{36}}{(v_o/220\,\mathrm{km\,s^{-1}})}\times g_{\rm tot}\,\mathrm{GeV\,cm^{-2}} = \frac{0.212}{(v_o/220\,\mathrm{km\,s^{-1}})}\,g_{\rm tot}^{(-10)}\,. \tag{22.27}$$

Here, $g_{\rm tot}^{(-10)} \equiv 10^{10}\,g_{\rm tot}(\mathrm{GeV})^3$, and $g_{\rm tot} = \sum_A (f_A/m_A)\,\sigma_A\,\phi_A^s$, where f_A is the mass fraction of element A in the Sun, and ϕ_A^s is the surface value of the capture function on the element of mass number A in the Sun [102].

The scattering rate of neutralinos in the outer layers of the Sun (which causes the fast halo neutralinos to lose enough energy to enter bound orbits close to the Earth's orbit) is proportional to $\sigma_A\phi_A^s$, which can be calculated once the parameters of the SUSY neutralino in question are fixed. (For the elemental abundances in the Sun, we use the compilation in [106].)

The values of $g_{\rm tot}^{(-10)}$ can in some cases approach unity. The spread is very large, however, and some models give orders of magnitude smaller values. As would be expected, the models with the highest values of $g_{\rm tot}^{(-10)}$ are the same models which give high scattering rates in direct detection experiments. As mentioned, the integrated effect of the new population in direct experiments is not very prominent (see refs. [101, 102]). On the other hand, they can imply a large effect on indirect detection neutrino rates.

The total capture rate is computed according to the formulas in [77], which take into account that the annihilation rates from the earth will, in general depend on time in a different way than the simple result in Eq. (22.7).

Due to this nonlinear nature of the capture rate, there is no simple scaling of the computed detection rates with the local halo density. Therefore, it is advisable that the user rescales the local halo density (see section 16.1.1) before calculating the rates in neutrino telescopes.

The new population can cause an increase of the detection rates by as much as a factor of 100 when the neutralino mass is less than around 150 GeV.

22.1.9 Effects of WIMP diffusion in the solar system

As the Earth has a rather low escape velocity, the Earth will only be able to capture WIMPs that have a rather low velocity with respect to the Earth. However, WIMPs from the halo have gained speed in the gravitaional potential from the Sun and will essentially be impossible to capture by the Earth. Hence, the Earth will only capture WIMPs that have diffused around in the solar system (by gravitational interactions with the other planets). Gould showed [187] that effectively this diffusion will lead to the same phase space distribution at the Earth as if the Earth was in free space (i.e. neglecting the solar potential). However, numerical simulations of asteroids showed that they are thrown into the Sun due to perturbations of the orbits by other planets, see e.g. [188]. These analyses led to worried that maybe the population of WIMPs diffusing around in the solar system is not as big as thought [189]. In [186], Lundberg and Edsjö investigated this issue with detailed numerical simulations of WIMP orbits in the solar system, showing that the annihilation rate in the Earth is typically reduced by up to two orders of magnitude. In DarkSUSY, we include these results for the neutrino rates from the Earth by using the velocity distribution at the Earth (as obtained in [186]). This velocity distribution is then used as input for our numerical capture rate routines instead of the usual approximation of using the halo velocity distribution directly. Using these new velocity distributions for the Earth is the default in DarkSUSY.

22.2 Neutrinos from Sun and Earth – routines

COMMENT #1: NOTE: This section is not up-to date with the current DarkSUSY release.

This set of routines contain routines to calculate the neutrino-induced muon flux from the Earth and the Sun in various models. It also includes routines that calculate the neutrino-induced muon flux from other sources, like the Sun's atmosphere, the Earth's atmosphere .

COMMENT #2: (include these???)

There are three different methods of calculation available (determined by `ntcalcmet` in `dsntcom.h`). Method 1 uses the approximate formulae for the capture rates in the Earth/Sun from the Jungman, Kamionkowski and Griest review [3]. Method 2, uses the same expression for the Sun, but the full expression from Gould [169] for capture in the Earth (this is the default). Method 3, finally, is the same as 2, but it also includes capture in the Earth from the Damour-Krauss population of WIMPs that have scattered in the outscirts of the Sun. The easiest way to select method is by calling `dsntset`, with the argument 'jkg' for method 1, 'gould' or 'default' for method 2 and 'dk' for method 3. A call to `dsntset('default')` is made in `dsinit`, but can be changed by the user by calling `dsntset` after `dsinit`.

To calculate the neutrino-induced muon flux from the Earth, you call

subroutine **dsntrates**(emuth,thmax,rtype,rateea,ratesu,istat)

Purpose: Calculate the rate of neutrinos or neutrino-induced muons in a neutrino telescope from neutralino annihilation in the Earth and the Sun.

Input:

emuth	r8	The neutrino or muon energy threshold in GeV.
thmax	r8	The half-aperture opening angle (in degrees) towards the center of the Sun or the Earth (i.e. the flux will be summed in a cone towards the center of the Sun or the Earth, where the top-angle of the cone is 2*thmax).
rtype	i	Type of flux to calculate: =1: muon neutrino-flux (neutrino and anti-neutrino summed) in units of km^{-2} yr^{-1}. =2: neutrino-to-muon conversion rate (muons and anti-muons summed) in units of km^{-3} yr^{-1}. =3: muon flux (muons and anti-muons summed) in units of km^{-2} yr^{-1}.

Output:

rateea	r8	The rate from neutralino annihilation in the Earth in the above units.
ratesu	r8	The rate from neutralino annihilation in the Sun in the above units.
istat	i	=0: Everything went OK. $\neq 0$: Some of the tables of neutrino or muon yields had to be used outside their tabulated regions. Extrapolations have been used.

subroutine **dsntdiffrates**(emu,theta,rtype,rateea,ratesu,istat)

Purpose: Calculate the differential rate of neutrinos or neutrino-induced muons in a neutrino telescope from neutralino annihilation in the Earth and the Sun.

Input:

emu	r8	The neutrino or muon energy in GeV.
theta	r8	The angle (in degrees) from the center of the Sun or the Earth.
rtype	i	Type of flux to calculate: =1: muon neutrino-flux (neutrino and anti-neutrino summed) in units of km^{-2} yr^{-1} GeV^{-1} $degrees^{-1}$. =2: neutrino-to-muon conversion rate (muons and anti-muons summed) in units of km^{-3} yr^{-1} GeV^{-1} $degrees^{-1}$. =3: muon flux (muons and anti-muons summed) in units of km^{-2} yr^{-1} GeV^{-1} $degrees^{-1}$.

Output:

rateea	r8	The rate from neutralino annihilation in the Earth in the above units.
ratesu	r8	The rate from neutralino annihilation in the Sun in the above units.
istat	i	=0: Everything went OK. $\neq 0$: Some of the tables of neutrino or muon yields had to be used outside their tabulated regions. Extrapolations have been used.

Chapter 23

src/pb: Antiproton fluxes from the halo

23.1 Antiprotons – theory

Neutralinos can annihilate each other in the halo producing leptons, quarks, gluons, gauge bosons and Higgs bosons. The quarks, gauge bosons and Higgs bosons will decay and/or form jets that will give rise to antiprotons (and antineutrons which decay shortly to antiprotons). Since antiprotons are not very abundant in the Universe, this could in principle be a good signature for supersymmetric dark matter. However, the cosmic rays (mainly protons) may produce secondary antiprotons in collisions with the interstellar medium, giving an important background. It was hoped that the difference in kinematics between such secondary antiprotons and the primary ones generated in neutralino annihilations would give an unambiguous signature at low antiproton energy. However, recent calculations indicate that other effects spoil this picture to a large degree [108, 109]. It still remains true, however, that present measurements and upper limits to the antiproton flux may be used as a constraint to rule out some MSSM configurations with large rates.

Unfortunately, there is a larger uncertainty in limits thus obtained than, for example, for the signal from neutrinos from the Earth and Sun. This is due to the severe astrophysical uncertainties about the phase space structure of the dark matter halo, in particular the density profile towards the Galactic center. This uncertainty will plague all indirect detection signals from the halo: antiprotons, positrons and gamma-rays. Therefore, the limits that can be put generally involve a combination of MSSM and halo model parameters, and are therefore of limited use constraining the MSSM alone.

At tree level the relevant final states for $\bar{p}$ production are $q\bar{q}$, $\ell\bar{\ell}$, W^+W^-, Z^0Z^0, W^+H^-, ZH_1^0, ZH_2^0, $H_1^0H_3^0$ and $H_2^0H_3^0$. We have included in DarkSUSY all the heavier quarks (c, b and t), gauge bosons and Higgs boson final states. In addition, we have included the $Z\gamma$ ([110]) and the 2 gluon ([111]; [112]) final states which occur at one loop-level.

The hadronization and/or decay of all final states (including) gluons is simulated with Pythia as described in section **??**. A word of caution should be raised, however, that antiproton data is not very abundant, in particular not at the lowest antiproton lab energies which tend to dominate the signal. Therefore an uncertainty in normalization, probably of the order of a factor 2, cannot be excluded at least in the low energy region.

23.1.1 The Antiproton Source Function

The source function $Q_{\bar{p}}^{\chi}$ gives the number of antiprotons per unit time, energy and volume element produced in annihilation of neutralinos locally in space. It is given by

$$Q_{\bar{p}}^{\chi}(T,\vec{x}\,) = (\sigma_{\rm ann} v)\left(\frac{\rho_{\chi}(\vec{x}\,)}{m_{\chi}}\right)^2 \sum_f \frac{dN^f}{dT} B^f \tag{23.1}$$

where T is the $\bar{p}$ kinetic energy. For a given annihilation channel f, B^f and dN^f/dT are, respectively, the branching ratio and the fragmentation function, and $(\sigma_{\rm ann} v)$ is the annihilation rate at $v = 0$ (which is very good approximation since the velocity of the neutralinos in the halo is so low). As dark matter neutralinos annihilate in pairs, the source function is proportional to the square of the neutralino number density $n_{\chi} = \rho_{\chi}/m_{\chi}$. Assuming that most of the dark matter in the Galaxy is made up of neutralinos and that these are smoothly distributed in the halo, one can directly relate the neutralino number density to the dark matter density profile in the galactic halo ρ. Although what is implemented is a smooth distribution of dark matter particles in the halo, an extension to a clumpy distribution is potentially interesting as well ([114]; [115]).

23.1.2 Propagation model

In the absence of a well established theory to describe the interactions of charged particles with the magnetic field of the Galaxy and the interstellar medium, the propagation of cosmic rays has generally been treated by postulating a semiempirical model and fitting the necessary set of unknown parameters to available data. A common approach is to use a diffusion approximation defined by a transport equation and an appropriate choice of boundary conditions (see e.g. [116]; [117] and references therein).

We have chosen to compute the propagation of cosmic rays in the Galaxy by means of a transport equation of the diffusion type (see [116]; [117]). In the case of a stationary solution, the number density N of a stable cosmic ray species whose distribution of sources is defined by the function of energy and space $Q(E,\vec{x})$, is given by:

$$\frac{\partial N(E,\vec{x})}{\partial t} = 0 = \nabla\cdot(D(R,\vec{x})\,\nabla N(E,\vec{x})) - \nabla\cdot(\vec{u}(\vec{x})\,N(E,\vec{x})) - p(E,\vec{x})\,N(E,\vec{x}) + Q(E,\vec{x}) \ . \tag{23.2}$$

On the right hand side of Eq. (23.2) the first term implements the diffusion approximation for a given diffusion coefficient D, generally assumed to be a function of rigidity R, while the second term describes a large-scale convective motion of velocity $\vec{u}$. The third term is added to take into account losses due to to collisions with the interstellar matter. It is a very good approximation to include in this term only the interactions with interstellar hydrogen, in this case p is given by:

$$p(E,\vec{x}) = n^H(\vec{x})\,v(E)\,\sigma_{cr\,p}^{\rm in}(E) \tag{23.3}$$

where n^H is the hydrogen number density in the Galaxy, v is the velocity of the cosmic ray particle considered '*cr*', while $\sigma_{cr\,p}^{\rm in}$ is the inelastic cross section for *cr*-proton collisions.

The propagation region is assumed to have a cylindrical symmetry: the Galaxy is split into two parts, a disk of radius R_h and height $2\cdot h_g$, where most of the interstellar gas is confined, and a halo of height $2\cdot h_h$ and the same radius. We assume that the diffusion coefficient is isotropic with possibly two different values in the disk and in the halo, reflecting the fact that in the disk there may be a larger random component of the magnetic fields. The spatial dependence is then:

$$D(\vec{x}) = D(z) = D_g\,\theta(h_g - |z|) + D_h\,\theta(|z| - h_g) \ . \tag{23.4}$$

Regarding the rigidity dependence, we consider the same functional form as in [118] and [119]:

$$D_l(R) = D_l^0\left(1 + \frac{R}{R_0}\right)^{0.6} \tag{23.5}$$

where $l = g, h$.

The convective term has been introduced in Eq. (23.2) to describe the effect of particle motion against the wind of cosmic rays leaving the disk, assuming a galactic wind of velocity

$$\vec{u}(\vec{x}) = (0, 0, u(z)) \tag{23.6}$$

where

$$u(z) = \mathrm{sign}(z)\, u_h\, \theta(|z| - h_g) \quad . \tag{23.7}$$

An analytic solution is possible also in the case of a linearly increasing wind ([115]). The distribution of gas in the Galaxy is for convenience assumed to have the very simple z dependence

$$n^H(\vec{x}) = n^H(z) = n_g^H\, \theta(h_g - |z|) + n_h^H\, \theta(|z| - h_g) \tag{23.8}$$

where $n_h \ll n_g$ (in practice, $n_h = 0$ is taken) and an average in the radial direction is performed.

As boundary condition, it is usually assumed that cosmic rays can escape freely at the border of the propagation region, i.e.

$$N(R_h, z) = N(r, h_h) = N(r, -h_h) = 0 \tag{23.9}$$

as the density of cosmic rays is assumed to be negligibly small in the intergalactic space.

The cylindrical symmetry and the free escape at the boundaries makes it possible to solve in DarkSUSY the transport equation expanding the number density distribution N in a Fourier-Bessel series:

$$N(r, z, \theta) = \sum_{k=0}^{\infty} \sum_{s=1}^{\infty} J_k\left(\nu_s^k \frac{r}{R_h}\right) \cdot \left[M_s^k(z)\cos(k\theta) + \tilde{M}_s^k(z)\sin(k\theta)\right] \tag{23.10}$$

which automatically satisfies the boundary condition at $r = R_h$, ν_s^k being the s-th zero of J_k (the Bessel function of the first kind and of order k). In the same way the source function can be expanded as:

$$Q(r, z, \theta) = \sum_{k=0}^{\infty} \sum_{s=1}^{\infty} J_k\left(\nu_s^k \frac{r}{R_h}\right) \cdot \left[Q_s^k(z)\cos(k\theta) + \tilde{Q}_s^k(z)\sin(k\theta)\right] \tag{23.11}$$

where

$$Q_s^k(z) = \frac{2}{{R_h}^2\, {J_{k+1}}^2(\nu_s^k)} \int_0^{R_h} dr'\; r' J_k\left(\nu_s^k \frac{r'}{R_h}\right) \frac{1}{\alpha_k\, \pi} \int_{-\pi}^{\pi} d\theta'\; \cos(k\theta')\, Q(r', z, \theta') \quad . \tag{23.12}$$

The equation relevant for the propagation in the z direction is [108]:

$$\frac{\partial}{\partial z} D(z) \frac{\partial}{\partial z} M_s^k(z) - D(z)\left(\frac{\nu_s^k}{R_h}\right)^2 M_s^k(z) - \frac{\partial}{\partial z}\left(u(z)\, M_s^k(z)\right) - p(z) M_s^k(z) + Q_s^k(z) = 0 \quad . \tag{23.13}$$

For $-h_g \le z \le h_g$ the solution is given by:

$$M_s^k(z) = M_s^k(0)\cosh(\lambda_g^{ks} z) - \frac{1}{D_g\, \lambda_g^{ks}} \int_0^z dz' \sinh\left(\lambda_g^{ks}(z - z')\right) Q_s^k(z') \tag{23.14}$$

where

$$\begin{aligned} M_s^k(0) \quad = \quad & \frac{1}{\cosh(\lambda_g^{ks} h_g)} \left\{ \frac{I_H}{\sinh\left(\lambda_h^{ks}(h_h - h_g)\right)} + \frac{D_h\, I_{GS}}{D_g\, \lambda_g^{ks}} \left[\gamma_h + \lambda_h^{ks} \coth\left(\lambda_h^{ks}(h_h - h_g)\right)\right] + I_{GC} \right\} \\ & \times \left[D_g\, \lambda_g^{ks}\, \tanh\left(\lambda_g^{ks} h_g\right) + D_h\, \gamma_h + D_h\, \lambda_h^{ks}\, \coth\left(\lambda_h^{ks}(h_h - h_g)\right)\right]^{-1} \end{aligned} \tag{23.15}$$

with

$$\lambda_g^{ks} = \sqrt{\left(\frac{\nu_s^k}{R_h}\right)^2 + \frac{n_g^H v\sigma_{cr\,p}^{\rm in}}{D_g}}\,, \qquad \lambda_h^{ks} = \sqrt{\left(\frac{\nu_s^k}{R_h}\right)^2 + \frac{n_h^H v\sigma_{cr\,p}^{\rm in}}{D_h} + {\gamma_h}^2}\,, \qquad \gamma_h = \frac{u_h}{2\,D_h} \tag{23.16}$$

and

$$\begin{aligned} I_H &= \int_{h_g}^{h_h} dz'\, \sinh\left(\lambda_h^{ks}(h_h - z')\right) \exp\left(\gamma_h(h_g - z')\right) \cdot \frac{Q_s^k(z') + Q_s^k(-z')}{2} \\ I_{GS} &= \int_0^{h_g} dz'\, \sinh\left(\lambda_g^{ks}(h_g - z')\right) \cdot \frac{Q_s^k(z') + Q_s^k(-z')}{2} \\ I_{GC} &= \int_0^{h_g} dz'\, \cosh\left(\lambda_g^{ks}(h_g - z')\right) \cdot \frac{Q_s^k(z') + Q_s^k(-z')}{2}\,. \end{aligned} \tag{23.17}$$

In DarkSUSY we have also as an option included the propagation models by Chardonnay et al. [166] and Bottino et al. [167].

23.1.3 Solar Modulation

A complication when comparing predictions of a theoretical model with data on cosmic rays taken at Earth is given by the solar modulation effect. During their propagation from the interstellar medium through the solar system, charged particles are affected by the solar wind and tend to lose energy. The net result of the modulation is a shift in energy between the interstellar spectrum and the spectrum at the Earth and a substantial depletion of particles with non-relativistic energies.

The simplest way to describe the phenomenon is the analytical force-field approximation by Gleeson & Axford [160] for a spherically symmetric model. The prescription of this effective treatment is that, given an interstellar flux at the heliospheric boundary, $d\Phi_{\rm b}/dT_{\rm b}$, the flux at the Earth is related to this by

$$\frac{d\Phi_\oplus}{dT_\oplus}(T_\oplus) = \frac{p_\oplus^2}{p_{\rm b}^2}\frac{d\Phi_{\rm b}}{dT_{\rm b}}(T_{\rm b}) \tag{23.18}$$

where the energy at the heliospheric boundary is given by

$$E_{\rm b} = E_\oplus + |Ze|\phi_F \tag{23.19}$$

and $p_\otimes$ and $p_{\rm b}$ are the momenta at the Earth and the heliospheric boundary respectively. Here e is the absolute value of the electron charge and Z the particle charge in units of e (e.g. $Z = -1$ for antiprotons).

An alternative approach is to solve numerically the propagation equation of the spherically symmetric model ([120]): the solar modulation parameter one has to introduce with this method roughly corresponds to ϕ_F as given above. When computing solar modulated antiproton fluxes, the two treatments seem not to be completely equivalent in the low energy regime. Keeping this in mind, we have anyway implemented the force field approximation in DarkSUSY avoiding the CPU time-consuming problem of having to solve a partial differential equation for each supersymmetric model.

23.2 Antiprotons from the halo – routines

.....

Chapter 24

src/rd: Relic density routines (general)

24.1 Relic density – theoretical background

24.1.1 The Boltzmann equation and thermal averaging

Griest and Seckel [171] have worked out the Boltzmann equation when coannihilations are included. We start by reviewing their expressions and then continue by rewriting them into a more convenient form that resembles the familiar case without coannihilations. This allows us to use similar expressions for calculating thermal averages and solving the Boltzmann equation whether coannihilations are included or not. The implementation in DarkSUSY is based upon the work done in [35]. We will later in this chapter, for the sake of clarification, assume that we work with supersymmetric dark matter with the lightest neutralino being the LSP. The routines here are completely general though and the interface between supersymmetry and the relic density routines is handled by the routines in **src/rn**.

24.1.2 Review of the Boltzmann equation with coannihilations

Consider annihilation of N supersymmetric particles χ_i $(i = 1, \ldots, N)$ with masses m_i and internal degrees of freedom (statistical weights) g_i. Also assume that $m_1 \leq m_2 \leq \cdots \leq m_{N-1} \leq m_N$ and that R-parity is conserved. Note that for the mass of the lightest neutralino we will use the notation m_χ and m_1 interchangeably.

The evolution of the number density n_i of particle i is

$$\begin{aligned}\frac{dn_i}{dt} &= -3Hn_i - \sum_{j=1}^{N}\langle\sigma_{ij}v_{ij}\rangle\left(n_in_j - n_i^{\rm eq}n_j^{\rm eq}\right)\\ &\quad -\sum_{j\neq i}\left[\langle\sigma'_{Xij}v_{ij}\rangle\left(n_in_X - n_i^{\rm eq}n_X^{\rm eq}\right) - \langle\sigma'_{Xji}v_{ij}\rangle\left(n_jn_X - n_j^{\rm eq}n_X^{\rm eq}\right)\right]\\ &\quad -\sum_{j\neq i}\left[\Gamma_{ij}\left(n_i - n_i^{\rm eq}\right) - \Gamma_{ji}\left(n_j - n_j^{\rm eq}\right)\right]. \end{aligned} \tag{24.1}$$

The first term on the right-hand side is the dilution due to the expansion of the Universe. H is the Hubble parameter. The second term describes $\chi_i\chi_j$ annihilations, whose total annihilation cross section is

$$\sigma_{ij} = \sum_X \sigma(\chi_i\chi_j \to X). \tag{24.2}$$

The third term describes $\chi_i \to \chi_j$ conversions by scattering off the cosmic thermal background,

$$\sigma'_{Xij} = \sum_Y \sigma(\chi_i X \to \chi_j Y) \tag{24.3}$$

being the inclusive scattering cross section. The last term accounts for χ_i decays, with inclusive decay rates

$$\Gamma_{ij} = \sum_X \Gamma(\chi_i \to \chi_j X). \tag{24.4}$$

In the previous expressions, X and Y are (sets of) standard model particles involved in the interactions, v_{ij} is the 'relative velocity' defined by

$$v_{ij} = \frac{\sqrt{(p_i \cdot p_j)^2 - m_i^2 m_j^2}}{E_i E_j} \tag{24.5}$$

with p_i and E_i being the four-momentum and energy of particle i, and finally $n_i^{\rm eq}$ is the equilibrium number density of particle χ_i,

$$n_i^{\rm eq} = \frac{g_i}{(2\pi)^3} \int d^3\mathbf{p}_i f_i \tag{24.6}$$

where $\mathbf{p}_i$ is the three-momentum of particle i, and f_i is its equilibrium distribution function. In the Maxwell-Boltzmann approximation it is given by

$$f_i = e^{-E_i/T}. \tag{24.7}$$

The thermal average $\langle \sigma_{ij} v_{ij} \rangle$ is defined with equilibrium distributions and is given by

$$\langle \sigma_{ij} v_{ij} \rangle = \frac{\int d^3\mathbf{p}_i d^3\mathbf{p}_j f_i f_j \sigma_{ij} v_{ij}}{\int d^3\mathbf{p}_i d^3\mathbf{p}_j f_i f_j} \tag{24.8}$$

Normally, the decay rate of supersymmetric particles χ_i other than the lightest which is stable is much faster than the age of the universe. Since we have assumed R-parity conservation, all of these particles decay into the lightest one. So its final abundance is simply described by the sum of the density of all supersymmetric particles,

$$n = \sum_{i=1}^{N} n_i. \tag{24.9}$$

For n we get the following evolution equation

$$\frac{dn}{dt} = -3Hn - \sum_{i,j=1}^{N} \langle \sigma_{ij} v_{ij} \rangle \left(n_i n_j - n_i^{\rm eq} n_j^{\rm eq} \right) \tag{24.10}$$

where the terms on the second and third lines in Eq. (24.1) cancel in the sum.

The scattering rate of supersymmetric particles off particles in the thermal background is much faster than their annihilation rate, because the scattering cross sections σ'_{Xij} are of the same order of magnitude as the annihilation cross sections σ_{ij} but the background particle density n_X is much larger than each of the supersymmetric particle densities n_i when the former are relativistic and the latter are non-relativistic, and so suppressed by a Boltzmann factor. In this case, the χ_i distributions remain in thermal equilibrium, and in particular their ratios are equal to the equilibrium values,

$$\frac{n_i}{n} \simeq \frac{n_i^{\rm eq}}{n^{\rm eq}}. \tag{24.11}$$

We then get

$$\frac{dn}{dt} = -3Hn - \langle \sigma_{\rm eff} v \rangle \left(n^2 - n_{\rm eq}^2 \right) \tag{24.12}$$

where

$$\langle \sigma_{\rm eff} v \rangle = \sum_{ij} \langle \sigma_{ij} v_{ij} \rangle \frac{n_i^{\rm eq}}{n^{\rm eq}} \frac{n_j^{\rm eq}}{n^{\rm eq}}. \tag{24.13}$$

24.1.3 Thermal averaging

So far the reviewing. Now let's continue by reformulating the thermal averages into more convenient expressions.

We rewrite Eq. (24.13) as

$$\langle \sigma_{\rm eff} v \rangle = \frac{\sum_{ij} \langle \sigma_{ij} v_{ij} \rangle n_i^{\rm eq} n_j^{\rm eq}}{n_{\rm eq}^2} = \frac{A}{n_{\rm eq}^2}. \tag{24.14}$$

For the denominator we obtain, using Boltzmann statistics for f_i,

$$n^{\rm eq} = \sum_i n_i^{\rm eq} = \sum_i \frac{g_i}{(2\pi)^3} \int d^3 p_i e^{-E_i/T} = \frac{T}{2\pi^2} \sum_i g_i m_i^2 K_2 \left(\frac{m_i}{T} \right) \tag{24.15}$$

where K_2 is the modified Bessel function of the second kind of order 2.

The numerator is the total annihilation rate per unit volume at temperature T,

$$A = \sum_{ij} \langle \sigma_{ij} v_{ij} \rangle n_i^{\rm eq} n_j^{\rm eq} = \sum_{ij} \frac{g_i g_j}{(2\pi)^6} \int d^3 \mathbf{p}_i d^3 \mathbf{p}_j f_i f_j \sigma_{ij} v_{ij} \tag{24.16}$$

It is convenient to cast it in a covariant form,

$$A = \sum_{ij} \int W_{ij} \frac{g_i f_i d^3 \mathbf{p}_i}{(2\pi)^3 2E_i} \frac{g_j f_j d^3 \mathbf{p}_j}{(2\pi)^3 2E_j}. \tag{24.17}$$

W_{ij} is the (unpolarized) annihilation rate per unit volume corresponding to the covariant normalization of $2E$ colliding particles per unit volume. W_{ij} is a dimensionless Lorentz invariant, related to the (unpolarized) cross section through*

$$W_{ij} = 4 p_{ij} \sqrt{s} \sigma_{ij} = 4 \sigma_{ij} \sqrt{(p_i \cdot p_j)^2 - m_i^2 m_j^2} = 4 E_i E_j \sigma_{ij} v_{ij}. \tag{24.18}$$

Here

$$p_{ij} = \frac{\left[s - (m_i + m_j)^2 \right]^{1/2} \left[s - (m_i - m_j)^2 \right]^{1/2}}{2\sqrt{s}} \tag{24.19}$$

is the momentum of particle χ_i (or χ_j) in the center-of-mass frame of the pair $\chi_i \chi_j$.

Averaging over initial and summing over final internal states, the contribution to W_{ij} of a general n-body final state is

$$W_{ij}^{n-\rm body} = \frac{1}{g_i g_j S_f} \sum_{\text{internal d.o.f.}} \int |\mathcal{M}|^2 (2\pi)^4 \delta^4 (p_i + p_j - \textstyle\sum_f p_f) \displaystyle\prod_f \frac{d^3 \mathbf{p}_f}{(2\pi)^3 2E_f}, \tag{24.20}$$

where S_f is a symmetry factor accounting for identical final state particles (if there are K sets of N_k identical particles, $k = 1, \ldots, K$, then $S_f = \prod_{k=1}^K N_k!$). In particular, the contribution of a two-body final state can be written as

$$W_{ij \to kl}^{2-\rm body} = \frac{p_{kl}}{16\pi^2 g_i g_j S_{kl} \sqrt{s}} \sum_{\text{internal d.o.f.}} \int |\mathcal{M}(ij \to kl)|^2 \, d\Omega, \tag{24.21}$$

*The quantity w_{ij} in Ref. [65] is $W_{ij}/4$.

where p_{kl} is the final center-of-mass momentum, S_{kl} is a symmetry factor equal to 2 for identical final particles and to 1 otherwise, and the integration is over the outgoing directions of one of the final particles. As usual, an average over initial internal degrees of freedom is performed.

We now reduce the integral in the covariant expression for A, Eq. (24.17), from 6 dimensions to 1. Using Boltzmann statistics for f_i (a good approximation for $T \lesssim m$)

$$A = \sum_{ij} \int g_i g_j W_{ij} e^{-E_i/T} e^{-E_j/T} \frac{d^3\mathbf{p}_i}{(2\pi)^3 2E_i} \frac{d^3\mathbf{p}_j}{(2\pi)^3 2E_j}, \tag{24.22}$$

where $\mathbf{p}_i$ and $\mathbf{p}_j$ are the three-momenta and E_i and E_j are the energies of the colliding particles. Following the procedure in Ref. [68] we then rewrite the momentum volume element as

$$d^3\mathbf{p}_i d^3\mathbf{p}_j = 4\pi |\mathbf{p}_i| E_i dE_i \, 4\pi |\mathbf{p}_j| E_j dE_j \, \frac{1}{2} d\cos\theta \tag{24.23}$$

where θ is the angle between $\mathbf{p}_i$ and $\mathbf{p}_j$. Then we change integration variables from E_i, E_j, θ to E_+, E_- and s, given by

$$\left\{ \begin{array}{lcl} E_+ &=& E_i + E_j \\ E_- &=& E_i - E_j \\ s &=& m_i^2 + m_j^2 + 2E_iE_j - 2|\mathbf{p}_i||\mathbf{p}_j|\cos\theta, \end{array} \right. \tag{24.24}$$

whence the volume element becomes

$$\frac{d^3\mathbf{p}_i}{(2\pi)^3 2E_i} \frac{d^3\mathbf{p}_j}{(2\pi)^3 2E_j} = \frac{1}{(2\pi)^4} \frac{dE_+ dE_- ds}{8}, \tag{24.25}$$

and the integration region $\{E_i \geq m_i, E_j \geq m_j, |\cos\theta| \leq 1\}$ transforms into

$$s \geq (m_i + m_j)^2, \tag{24.26}$$

$$E_+ \geq \sqrt{s}, \tag{24.27}$$

$$\left| E_- - E_+ \frac{m_j^2 - m_i^2}{s} \right| \leq 2p_{ij} \sqrt{\frac{E_+^2 - s}{s}}. \tag{24.28}$$

Notice now that the product of the equilibrium distribution functions depends only on E_+ and not E_- due to the Maxwell-Boltzmann approximation, and that the invariant rate W_{ij} depends only on s due to the neglect of final state statistical factors. Hence we can immediately integrate over E_-,

$$\int dE_- = 4p_{ij} \sqrt{\frac{E_+^2 - s}{s}}. \tag{24.29}$$

The volume element is now

$$\frac{d^3\mathbf{p}_i}{(2\pi)^3 2E_i} \frac{d^3\mathbf{p}_j}{(2\pi)^3 2E_j} = \frac{1}{(2\pi)^4} \frac{p_{ij}}{2} \sqrt{\frac{E_+^2 - s}{s}} dE_+ ds \tag{24.30}$$

We now perform the E_+ integration. We obtain

$$A = \frac{T}{32\pi^4} \sum_{ij} \int_{(m_i+m_j)^2}^{\infty} ds g_i g_j p_{ij} W_{ij} K_1\left(\frac{\sqrt{s}}{T}\right) \tag{24.31}$$

where K_1 is the modified Bessel function of the second kind of order 1.

We can take the sum inside the integral and define an effective annihilation rate $W_{\rm eff}$ through

$$\sum_{ij} g_i g_j p_{ij} W_{ij} = g_1^2 p_{\rm eff} W_{\rm eff} \tag{24.32}$$

with

$$p_{\text{eff}} = p_{11} = \frac{1}{2}\sqrt{s - 4m_1^2}. \tag{24.33}$$

In other words

$$W_{\text{eff}} = \sum_{ij} \frac{p_{ij}}{p_{11}} \frac{g_i g_j}{g_1^2} W_{ij} = \sum_{ij} \sqrt{\frac{[s-(m_i-m_j)^2][s-(m_i+m_j)^2]}{s(s-4m_1^2)}} \frac{g_i g_j}{g_1^2} W_{ij}. \tag{24.34}$$

Because $W_{ij}(s) = 0$ for $s \leq (m_i + m_j)^2$, the radicand is never negative.

In terms of cross sections, this is equivalent to the definition

$$\sigma_{\text{eff}} = \sum_{ij} \frac{p_{ij}^2}{p_{11}^2} \frac{g_i g_j}{g_1^2} \sigma_{ij}. \tag{24.35}$$

Eq. (24.31) then reads

$$A = \frac{g_1^2 T}{32\pi^4} \int_{4m_1^2}^{\infty} ds p_{\text{eff}} W_{\text{eff}} K_1 \left(\frac{\sqrt{s}}{T}\right) \tag{24.36}$$

This can be written in a form more suitable for numerical integration by using p_{eff} instead of s as integration variable. From Eq. (24.33), we have $ds = 8 p_{\text{eff}} dp_{\text{eff}}$, and

$$A = \frac{g_1^2 T}{4\pi^4} \int_0^{\infty} dp_{\text{eff}} p_{\text{eff}}^2 W_{\text{eff}} K_1 \left(\frac{\sqrt{s}}{T}\right) \tag{24.37}$$

with

$$s = 4p_{\text{eff}}^2 + 4m_1^2 \tag{24.38}$$

So we have succeeded in rewriting A as a 1-dimensional integral.

From Eqs. (24.37) and (24.15), the thermal average of the effective cross section results

$$\langle \sigma_{\text{eff}} v \rangle = \frac{\int_0^{\infty} dp_{\text{eff}} p_{\text{eff}}^2 W_{\text{eff}} K_1 \left(\frac{\sqrt{s}}{T}\right)}{m_1^4 T \left[\sum_i \frac{g_i}{g_1} \frac{m_i^2}{m_1^2} K_2 \left(\frac{m_i}{T}\right)\right]^2}. \tag{24.39}$$

This expression is very similar to the case without coannihilations, the differences being the denominator and the replacement of the annihilation rate with the effective annihilation rate. In the absence of coannihilations, this expression correctly reduces to the formula in Gondolo and Gelmini [68].

The definition of an effective annihilation rate independent of temperature is a remarkable calculational advantage. As in the case without coannihilations, the effective annihilation rate can in fact be tabulated in advance, before taking the thermal average and solving the Boltzmann equation.

In the effective annihilation rate, coannihilations appear as thresholds at $\sqrt{s}$ equal to the sum of the masses of the coannihilating particles. We show an example in Fig. 24.1 where it is clearly seen that the coannihilation thresholds appear in the effective invariant rate just as final state thresholds do. For the same example, Fig. 24.2 shows the differential annihilation rate per unit volume dA/dp_{eff}, the integrand in Eq. (24.37), as a function of p_{eff}. We have chosen a temperature $T = m_\chi/20$, a typical freeze-out temperature. The Boltzmann suppression contained in the exponential decay of K_1 at high p_{eff} is clearly visible. At higher temperatures the peak shifts to the right and at lower temperatures to the left. For the particular model shown in Figs. 24.1–24.2, the relic density results $\Omega_\chi h^2 = 0.030$ when coannihilations are included and $\Omega_\chi h^2 = 0.18$ when they are not. Coannihilations have lowered $\Omega_\chi h^2$ by a factor of 6.

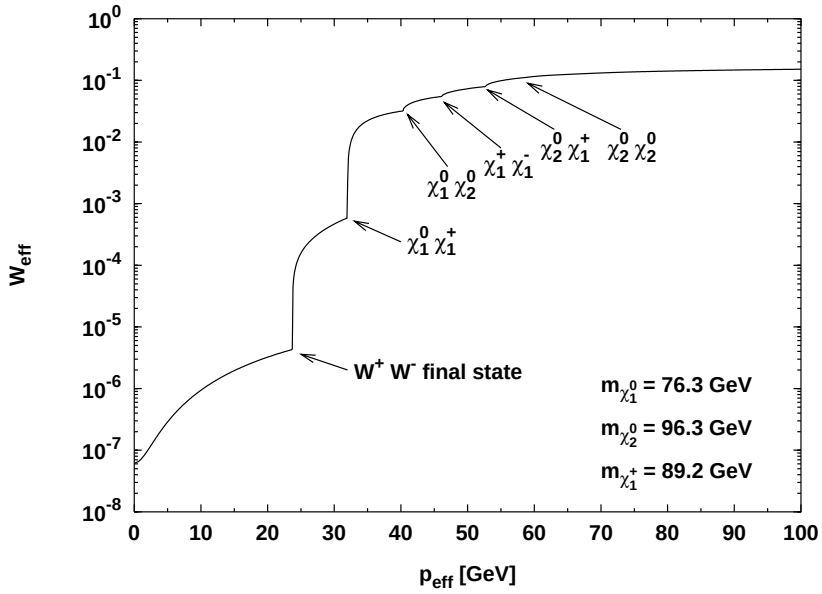

Figure 24.1: The effective invariant annihiliation rate $W_{\rm eff}$ as a function of $p_{\rm eff}$ for an example model. The final state threshold for annihilation into W^+W^- and the coannihilation thresholds, as given by Eq. (24.34), are indicated. The $\chi_2^0\chi_2^0$ coannihilation threshold is too small to be seen.

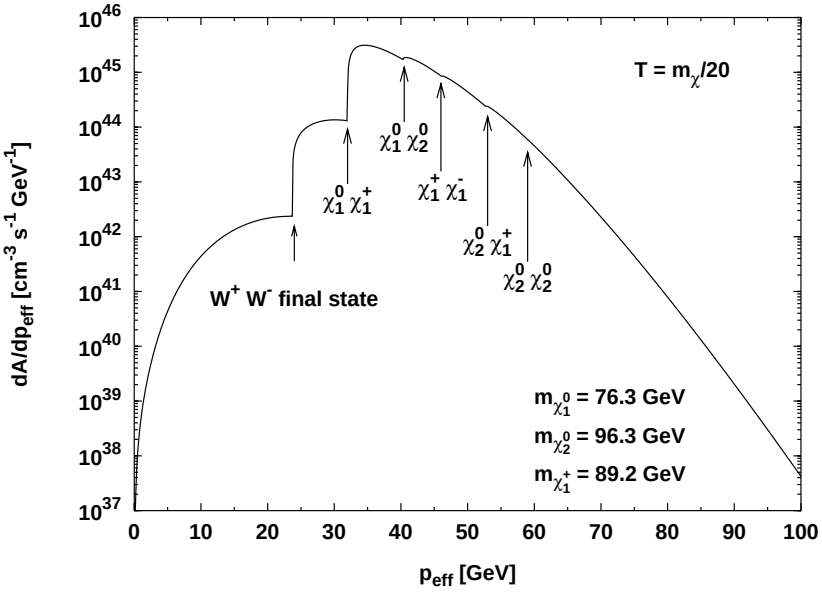

Figure 24.2: Total differential annihilation rate per unit volume $dA/dp_{\rm eff}$ for the same model as in Fig. 24.1, evaluated at a temperature $T = m_\chi/20$, typical of freeze-out. Notice the Boltzmann suppression at high $p_{\rm eff}$.

24.1.4 Internal degrees of freedom

If we look at Eqs. (24.34) and (24.39) we see that we have a freedom on how to treat particles degenerate in mass, e.g. a chargino can be treated either

a) as two separate species χ_i^+ and χ_i^-, each with internal degrees of freedom $g_{\chi^+} = g_{\chi^-} = 2$, or,

b) as a single species $\chi_i^\pm$ with $g_{\chi_i^\pm} = 4$ internal degrees of freedom.

Of course the two views are equivalent, we just have to be careful including the g_i's consistently whichever view we take. In a), we have the advantage that all the W_{ij} that enter into Eq. (24.34) enter as they are, i.e. without any correction factors for the degrees of freedom. On the other hand we get many terms in the sum that are identical and we need some book-keeping machinery to avoid calculating identical terms more than once. On the other hand, with option b), the sum over W_{ij} in Eq. (24.34) is much simpler only containing terms that are not identical (except for the trivial identity $W_{ij} = W_{ji}$ which is easily taken care of). However, the individual W_{ij} will be some linear combinations of the more basic W_{ij} entering in option a), where the coefficients have to be calculated for each specific type of initial condition.

Below we will perform this calculation to show how the W_{ij} look like in option b) for different initial states. We will use a prime on the W_{ij} when they refer to these combined states to indicate the difference.

Neutralino-chargino annihilation

The starting point is Eq. (24.34) which we will use to define the W_{ij} in option b) such that W_{eff} is the same as in option a). Eq. (24.39) is then guaranteed to be the same in both cases since the sum in the denominator is linear in g_i.

Now consider annihilation between χ_i^0 and χ_c^+ or χ_c^-. The corresponding terms in Eq. (24.34) does for option a) read

$$\begin{aligned} W_{\text{eff}} &= \sum_{ij} \frac{p_{ij}}{p_{11}} \frac{g_i g_j}{g_1^2} W_{ij} = \frac{p_{ic}}{p_{11}} \frac{2 \cdot 2}{2^2} \left[W_{\chi_i^0 \chi_c^+} + W_{\chi_i^0 \chi_c^-} + \underbrace{W_{\chi_c^+ \chi_i^0}}_{W_{\chi_i^0 \chi_c^+}} + \underbrace{W_{\chi_c^- \chi_i^0}}_{W_{\chi_i^0 \chi_c^-}} \right] \\ &= 2 \frac{p_{ic}}{p_{11}} \left[W_{\chi_i^0 \chi_c^+} + \underbrace{W_{\chi_i^0 \chi_c^-}}_{W_{\chi_i^0 \chi_c^+}} \right] = 4 \frac{p_{ic}}{p_{11}} W_{\chi_i^0 \chi_c^+} \end{aligned} \tag{24.40}$$

For option b), we instead get

$$W_{\text{eff}} = \sum_{ij} \frac{p_{ij}}{p_{11}} \frac{g_i g_j}{g_1^2} W_{ij} = \frac{p_{ic}}{p_{11}} \frac{2 \cdot 4}{2^2} \left[W'_{\chi_i^0 \chi_c^\pm} + \underbrace{W'_{\chi_c^\pm \chi_i^0}}_{W'_{\chi_i^0 \chi_c^\pm}} \right] = 4 \frac{p_{ic}}{p_{11}} W'_{\chi_i^0 \chi_c^\pm} \tag{24.41}$$

Comparing Eq. (24.41) and Eq. (24.40) we see that they are indentical if we make the identification

$$W'_{\chi_i^0 \chi_c^\pm} \equiv W_{\chi_i^0 \chi_c^+} \tag{24.42}$$

Chargino-chargino annihilation

First consider the case where we include the terms in the sum for which we have annihilation between χ_c^+ or χ_c^- and χ_d^+ or χ_d^- with $c \neq d$.

In option a), the corresponding terms in Eq. (24.34) reads

$$\begin{aligned} W_{\rm eff} &= \sum_{ij} \frac{p_{ij}}{p_{11}} \frac{g_i g_j}{g_1^2} W_{ij} \\ &= \frac{p_{cd}}{p_{11}} \frac{2\cdot 2}{2^2} \Big[W_{\chi_c^+\chi_d^+} + W_{\chi_c^+\chi_d^-} + W_{\chi_c^-\chi_d^+} + W_{\chi_c^-\chi_d^-} \\ &\quad + \underbrace{W_{\chi_d^+\chi_c^+}}_{W_{\chi_c^+\chi_d^+}} + \underbrace{W_{\chi_d^+\chi_c^-}}_{W_{\chi_c^-\chi_d^+}} + \underbrace{W_{\chi_d^-\chi_c^+}}_{W_{\chi_c^+\chi_d^-}} + \underbrace{W_{\chi_d^-\chi_c^-}}_{W_{\chi_c^-\chi_d^-}} \Big] \\ &= 2\frac{p_{cd}}{p_{11}} \Big[W_{\chi_c^+\chi_d^+} + W_{\chi_c^+\chi_d^-} + \underbrace{W_{\chi_c^-\chi_d^+}}_{W_{\chi_c^+\chi_d^-}} + \underbrace{W_{\chi_c^-\chi_d^-}}_{W_{\chi_c^+\chi_d^+}} \Big] \\ &= 4\frac{p_{cd}}{p_{11}} \Big[W_{\chi_c^+\chi_d^+} + W_{\chi_c^+\chi_d^-} \Big] \end{aligned} \tag{24.43}$$

In option b), the corresponding terms would instead read

$$W_{\rm eff} = \sum_{ij} \frac{p_{ij}}{p_{11}} \frac{g_i g_j}{g_1^2} W'_{ij} = \frac{p_{cd}}{p_{11}} \frac{4\cdot 4}{2^2} \Big[W'_{\chi_c^\pm\chi_d^\pm} + \underbrace{W'_{\chi_d^\pm\chi_c^\pm}}_{W'_{\chi_c^\pm\chi_d^\pm}} \Big] = 8\frac{p_{cd}}{p_{11}} W'_{\chi_c^\pm\chi_d^\pm} \tag{24.44}$$

Comparing Eq. (24.43) and Eq. (24.44) we see that they are identical if we make the following identifcation

$$W'_{\chi_c^\pm\chi_d^\pm} \equiv \frac{1}{2}\Big[W_{\chi_c^+\chi_d^+} + W_{\chi_c^+\chi_d^-} \Big] \tag{24.45}$$

For clarity, let's also consider the case where $c = d$. In option a), the terms in $W_{\rm eff}$ are

$$\begin{aligned} W_{\rm eff} &= \sum_{ij} \frac{p_{ij}}{p_{11}} \frac{g_i g_j}{g_1^2} W_{ij} = \frac{p_{cc}}{p_{11}} \frac{2\cdot 2}{2^2} \Big[W_{\chi_c^+\chi_c^+} + W_{\chi_c^+\chi_c^-} + \underbrace{W_{\chi_c^-\chi_c^+}}_{W_{\chi_c^+\chi_c^-}} + \underbrace{W_{\chi_c^-\chi_c^-}}_{W_{\chi_c^+\chi_c^+}} \Big] \\ &= 2\frac{p_{cc}}{p_{11}} \Big[W_{\chi_c^+\chi_c^+} + W_{\chi_c^+\chi_c^-} \Big] \end{aligned} \tag{24.46}$$

In option b), the corresponding term would instead read

$$W_{\rm eff} = \sum_{ij} \frac{p_{ij}}{p_{11}} \frac{g_i g_j}{g_1^2} W'_{ij} = \frac{p_{cc}}{p_{11}} \frac{4\cdot 4}{2^2} W'_{\chi_c^\pm\chi_c^\pm} + = 4\frac{p_{cc}}{p_{11}} W'_{\chi_c^\pm\chi_c^\pm} \tag{24.47}$$

Comparing Eq. (24.46) and Eq. (24.47) we see that they are identical if we make the following identifcation

$$W'_{\chi_c^\pm\chi_c^\pm} \equiv \frac{1}{2}\Big[W_{\chi_c^+\chi_c^+} + W_{\chi_c^+\chi_c^-} \Big] \tag{24.48}$$

i.e. the same identification as in the case $c \neq d$.

Neutralino-sfermion annihilation

For each sfermion we have in total four different states, $\tilde{f}_1$, $\tilde{f}_2$, $\tilde{f}_1^*$ and $\tilde{f}_2^*$. Of these, the $\tilde{f}_1$ and $\tilde{f}_2$ in general have different masses and have to be treated separately. Considering only one mass eigenstate $\tilde{f}_k$, option a) then means that we treat $\tilde{f}_k$ and $\tilde{f}_k^*$ as two separate species with $g_i = 1$ degree of freedom each, whereas option b) means that we treat them as one species $\tilde{f}'_k$ with

$g_i = 2$ degrees of freedom. As before, the prime indicates that we mean both the particle and the antiparticle state.

Note, that for squarks we also have the number of colours $N_c = 3$ to take into account. In option a) we should choose to treat even colour state differently, i.e. $g_i = 1$, whereas $g_i = 6$ in case b). The expressions would be the same as above except that both the expression in a) and b) would be multiplied by the colour factor $N_c = 3$. The expression relating case a) and case b) is thus unaffected by this colour factor. Note however, that in option b) we take the average over the squark colours (or in this case calculate it only for one colour. See sections 24.1.4 and 24.1.4 below for more details.

For option a), Eq. (24.34) then reads

$$\begin{aligned} W_{\text{eff}} &= \sum_{ij} \frac{p_{ij}}{p_{11}} \frac{g_i g_j}{g_1^2} W_{ij} = \frac{p_{ik}}{p_{11}} \frac{2 \cdot 1}{2^2} \left[W_{\chi_i^0 \tilde{f}_k} + W_{\chi_i^0 \tilde{f}_k^*} + \underbrace{W_{\tilde{f}_k \chi_i^0}}_{W_{\chi_i^0 \tilde{f}_k}} + \underbrace{W_{\tilde{f}_k^* \chi_i^0}}_{W_{\chi_i^0 \tilde{f}_k^*}} \right] \\ &= \frac{p_{ik}}{p_{11}} \left[W_{\chi_i^0 \tilde{f}_k} + \underbrace{W_{\chi_i^0 \tilde{f}_k^*}}_{W_{\chi_i^0 \bar{f}_k}} \right] = 2 \frac{p_{ik}}{p_{11}} W_{\chi_i^0 \tilde{f}_k} \end{aligned} \tag{24.49}$$

whereas for option b), Eq. (24.34) reads

$$W_{\text{eff}} = \sum_{ij} \frac{p_{ij}}{p_{11}} \frac{g_i g_j}{g_1^2} W'_{ij} = \frac{p_{ik}}{p_{11}} \frac{2 \cdot 2}{2^2} \left[W'_{\chi_i^0 \tilde{f'}_k} + \underbrace{W'_{\tilde{f'}_k \chi_i^0}}_{W'_{\chi_i^0 \tilde{f'}_k}} \right] = 2 \frac{p_{ik}}{p_{11}} W'_{\chi_i^0 \tilde{f'}_k} \tag{24.50}$$

Comparing Eq. (24.50) and Eq. (24.49) we see that they are indentical if we make the identification

$$W'_{\chi_i^0 \tilde{f'}_k} \equiv W_{\chi_i^0 \tilde{f}_k} \tag{24.51}$$

For clarity, for squarks the corresponding expression would be

$$W'_{\chi_i^0 \tilde{q'}_k} \equiv \frac{1}{3} \sum_{a=1}^{3} W_{\chi_i^0 \tilde{q}_k^a} \tag{24.52}$$

where a is a colour index.

Chargino-sfermion annihilation

In option a) the chargino has $g_i = 2$ and the sfermion has $g_i = 1$ degrees of freedom, whereas in option b), the chargino has $g_i = 4$ and the sfermion has $g_i = 2$ degrees of freedom

For option a), Eq. (24.34) then reads

$$\begin{aligned} W_{\text{eff}} &= \sum_{ij} \frac{p_{ij}}{p_{11}} \frac{g_i g_j}{g_1^2} W_{ij} \\ &= \frac{p_{ck}}{p_{11}} \frac{2 \cdot 1}{2^2} \Big[W_{\chi_c^+ \tilde{f}_k} + W_{\chi_c^+ \tilde{f}_k^*} + W_{\chi_c^- \tilde{f}_k} + W_{\chi_c^- \tilde{f}_k^*} \\ &\quad + \underbrace{W_{\tilde{f}_k \chi_c^+}}_{W_{\chi_c^+ \tilde{f}_k}} + \underbrace{W_{\tilde{f}_k^* \chi_c^+}}_{W_{\chi_c^+ \tilde{f}_k^*}} + \underbrace{W_{\tilde{f}_k \chi_c^-}}_{W_{\chi_c^- \tilde{f}_k}} + \underbrace{W_{\tilde{f}_k^* \chi_c^-}}_{W_{\chi_c^- \tilde{f}_k^*}} \Big] \\ &= \frac{p_{ck}}{p_{11}} \left[W_{\chi_c^+ \tilde{f}_k} + W_{\chi_c^+ \tilde{f}_k^*} + \underbrace{W_{\chi_c^- \tilde{f}_k}}_{W_{\chi_c^+ \bar{f}_k^*}} + \underbrace{W_{\chi_c^- \tilde{f}_k^*}}_{W_{\chi_c^+ \bar{f}_k}} \right] = 2 \frac{p_{ck}}{p_{11}} \left[W_{\chi_c^+ \tilde{f}_k} + W_{\chi_c^+ \tilde{f}_k^*} \right] \end{aligned} \tag{24.53}$$

In option b), Eq. (24.34) reads

$$W_{\rm eff} = \sum_{ij} \frac{p_{ij}}{p_{11}} \frac{g_i g_j}{g_1^2} W'_{ij} = \frac{p_{ck}}{p_{11}} \frac{4 \cdot 2}{2^2} \left[W'_{\chi_c^\pm \tilde{f}'_k} + \underbrace{W'_{\tilde{f}'_k \chi_c^\pm}}_{W'_{\chi_c^\pm \tilde{f}'_k}} \right] = 4 \frac{p_{ck}}{p_{11}} W'_{\chi_c^\pm \tilde{f}'_k} \tag{24.54}$$

Comparing Eq. (24.54) and Eq. (24.53) we see that they are indentical if we make the identification

$$W'_{\chi_c^\pm \tilde{f}'_k} \equiv \frac{1}{2} \left[W_{\chi_c^+ \tilde{f}_k} + W_{\chi_c^+ \tilde{f}_k^*} \right] \tag{24.55}$$

For clarity, for squarks the corresponding expression would be

$$W'_{\chi_c^\pm \tilde{q}'_k} \equiv \frac{1}{2} \frac{1}{3} \sum_{a=1}^{3} \left[W_{\chi_c^+ \tilde{q}_k^a} + W_{\chi_c^+ \tilde{q}_k^{a*}} \right] \tag{24.56}$$

where a is a colour index.

Sfermion-sfermion annihilation

First consider the case where we have annihilation between sfmerions of different types, i.e. annihilation between $\tilde{f}_k$ or $\tilde{f}_k^*$ and $\tilde{f}_l$ or $\tilde{f}_l^*$.

For option a), Eq. (24.34) then reads

$$\begin{aligned} W_{\rm eff} &= \sum_{ij} \frac{p_{ij}}{p_{11}} \frac{g_i g_j}{g_1^2} W_{ij} \\ &= \frac{p_{kl}}{p_{11}} \frac{1 \cdot 1}{2^2} \Big[W_{\tilde{f}_k \tilde{f}_l} + W_{\tilde{f}_k \tilde{f}_l^*} + W_{\tilde{f}_k^* \tilde{f}_l} + W_{\tilde{f}_k^* \tilde{f}_l^*} \\ &\quad + \underbrace{W_{\tilde{f}_l \tilde{f}_k}}_{W_{\tilde{f}_k \tilde{f}_l}} + \underbrace{W_{\tilde{f}_l \tilde{f}_k^*}}_{W_{\tilde{f}_k^* \tilde{f}_l}} + \underbrace{W_{\tilde{f}_l^* \tilde{f}_k}}_{W_{\tilde{f}_k \tilde{f}_l^*}} + \underbrace{W_{\tilde{f}_l^* \tilde{f}_k^*}}_{W_{\tilde{f}_k^* \tilde{f}_l^*}} \Big] \\ &= \frac{1}{2} \frac{p_{kl}}{p_{11}} \left[W_{\tilde{f}_k \tilde{f}_l} + W_{\tilde{f}_k \tilde{f}_l^*} + \underbrace{W_{\tilde{f}_k^* \tilde{f}_l}}_{W_{\tilde{f}_k \tilde{f}_l^*}} + \underbrace{W_{\tilde{f}_k^* \tilde{f}_l^*}}_{W_{\tilde{f}_k \tilde{f}_l}} \right] = \frac{p_{kl}}{p_{11}} \left[W_{\tilde{f}_k \tilde{f}_l} + W_{\tilde{f}_k \tilde{f}_l^*} \right] \end{aligned} \tag{24.57}$$

In option b) we would get

$$\begin{aligned} W_{\rm eff} &= \sum_{ij} \frac{p_{ij}}{p_{11}} \frac{g_i g_j}{g_1^2} W'_{ij} \\ &= \frac{p_{kl}}{p_{11}} \frac{2 \cdot 2}{2^2} \left[W'_{\tilde{f}'_k \tilde{f}'_l} + \underbrace{W'_{\tilde{f}'_l \tilde{f}'_k}}_{W'_{\tilde{f}'_k \tilde{f}'_l}} \right] = 2 \frac{p_{kl}}{p_{11}} \left[W'_{\tilde{f}'_k \tilde{f}'_l} \right] \end{aligned} \tag{24.58}$$

Comparing Eq. (24.58) and Eq. (24.57) we see that they are indentical if we make the identification

$$W'_{\tilde{f}'_k \tilde{f}'_l} \equiv \frac{1}{2} \left[W_{\tilde{f}_k \tilde{f}_l} + W_{\tilde{f}_k \tilde{f}_l^*} \right] \tag{24.59}$$

It is easy to show that this relation holds true even if $k = l$.

Squark-squark annihilation

Even though we treated sfermion-sfermion annihilation in the previous subsection, squarks have colour which can complicate things, so let's for clarity consider squarks separately.

Let's denote the squarks $\tilde{q}_k^a$ where a is now a colour index. In option a) we will let each colour be a seprate species, which means that $g_i = 1$ in this case. In option b) we will instead have $g_i = 6$.

In option a) we would have

$$\begin{aligned} W_{\text{eff}} &= \sum_{ij} \frac{p_{ij}}{p_{11}} \frac{g_i g_j}{g_1^2} W_{ij} \\ &= \frac{p_{kl}}{p_{11}} \frac{1 \cdot 1}{2^2} \sum_{a,b=1}^{3} \Big[W_{\tilde{q}_k^a \tilde{q}_l^b} + W_{\tilde{q}_k^a \tilde{q}_l^{b*}} + W_{\tilde{q}_k^{a*} \tilde{q}_l^b} + W_{\tilde{q}_k^{a*} \tilde{q}_l^{b*}} \\ &\quad + \underbrace{W_{\tilde{q}_l^a \tilde{q}_k^b}}_{W_{\tilde{q}_k^a \tilde{q}_l^b}} + \underbrace{W_{\tilde{q}_l^a \tilde{q}_k^{b*}}}_{W_{\tilde{q}_k^{a*} \tilde{q}_l^b}} + \underbrace{W_{\tilde{q}_l^{a*} \tilde{q}_k^b}}_{W_{\tilde{q}_k^a \tilde{q}_l^{b*}}} + \underbrace{W_{\tilde{q}_l^{a*} \tilde{q}_k^{b*}}}_{W_{\tilde{q}_k^{a*} \tilde{q}_l^b}} \Big] \\ &= \frac{1}{2} \frac{p_{kl}}{p_{11}} \sum_{a,b=1}^{3} \Big[W_{\tilde{q}_k^a \tilde{f}_l^b} + W_{\tilde{q}_k^a \tilde{f}_l^{b*}} + \underbrace{W_{\tilde{q}_k^{a*} \tilde{q}_l^b}}_{W_{\tilde{q}_k^a \tilde{q}_l^{b*}}} + \underbrace{W_{\tilde{q}_k^{a*} \tilde{q}_l^{b*}}}_{W_{\tilde{q}_k^a \tilde{q}_l^b}} \Big] = \frac{p_{kl}}{p_{11}} \sum_{a,b=1}^{3} \Big[W_{\tilde{q}_k^a \tilde{q}_l^b} + W_{\tilde{q}_k^a \tilde{q}_l^{b*}} \Big] \end{aligned} \tag{24.60}$$

In option b) we would get

$$\begin{aligned} W_{\text{eff}} &= \sum_{ij} \frac{p_{ij}}{p_{11}} \frac{g_i g_j}{g_1^2} W'_{ij} \\ &= \frac{p_{kl}}{p_{11}} \frac{6 \cdot 6}{2^2} \Big[W'_{\tilde{q'}_k \tilde{q'}_l} + \underbrace{W'_{\tilde{q'}_l \tilde{q'}_k}}_{W'_{\tilde{q'}_k \tilde{q'}_l}} \Big] = 18 \frac{p_{kl}}{p_{11}} \Big[W'_{\tilde{q'}_k \tilde{q'}_l} \Big] \end{aligned} \tag{24.61}$$

Comparing Eq. (24.61) and Eq. (24.60) we see that they are indentical if we make the identification

$$W'_{\tilde{q'}_k \tilde{q'}_l} \equiv \frac{1}{2} \frac{1}{9} \sum_{a,b=1}^{3} \Big[W_{\tilde{q}_k^a \tilde{q}_l^b} + W_{\tilde{q}_k^a \tilde{q}_l^{b*}} \Big] \tag{24.62}$$

i.e. we get the same relation as for other sfermions, the only difference being that we in option b) should also take the average over the colour states.

Sfermion-squark annihilation

For clarity, if we have annihilation between a non-coloured sfermion and a squark, we would in the same way as in the previous subsection get

$$W'_{\tilde{f'}_k \tilde{q'}_l} \equiv \frac{1}{2} \frac{1}{3} \sum_{b=1}^{3} \Big[W_{\tilde{f}_k \tilde{q}_l^b} + W_{\tilde{f}_k \tilde{q}_l^{b*}} \Big] \tag{24.63}$$

Summary of degrees of freedom

We have found above the following relations between option b) and option a),

$$\begin{cases} W'_{\chi_i^0\chi_j^\pm} & \equiv & W_{\chi_i^0\chi_j^+} = W_{\chi_i^0\chi_j^-} \quad , \quad \forall\ i=1,\ldots,4,\ j=1,2 \\ W'_{\chi_i^\pm\chi_j^\pm} & \equiv & \frac{1}{2}\left[W_{\chi_i^+\chi_j^+} + W_{\chi_i^+\chi_j^-}\right] = \frac{1}{2}\left[W_{\chi_i^-\chi_j^-} + W_{\chi_i^-\chi_j^+}\right] \quad , \quad \forall\ i=1,2,\ j=1,2 \\ W'_{\chi_i^0\tilde{f}'_k} & \equiv & W_{\chi_i^0\tilde{f}_k} \quad , \quad \forall i=1,\ldots 4,\ k=1,2 \\ W'_{\chi_c^\pm\tilde{f}'_k} & \equiv & \frac{1}{2}\left[W_{\chi_c^+\tilde{f}_k} + W_{\chi_c^+\tilde{f}_k^*}\right] \quad , \quad \forall c=1,2,\ k=1,2 \\ W'_{\tilde{f}'_k\tilde{f}'_l} & \equiv & \frac{1}{2}\left[W_{\tilde{f}_k\tilde{f}_l} + W_{\tilde{f}_k\tilde{f}_l^*}\right] \quad , \quad \forall k=1,2,\ l=1,2 \\ W'_{\tilde{q}'_k\tilde{q}'_l} & \equiv & \frac{1}{2}\frac{1}{9}\sum_{a,b=1}^{3}\left[W_{\tilde{q}_k^a\tilde{q}_l^b} + W_{\tilde{q}_k^a\tilde{q}_l^{b*}}\right] \quad , \quad \forall k=1,2,\ l=1,2 \end{cases} \tag{24.64}$$

We don't list all the possible cases with squarks explicitly, the principle being that we in option b) should take the *average* over the squark colour states (see the squark-squark entry in the list above).

We will choose option b) and the code (dsandwdcoscn, dsandwdcoscn, dsasdwdcossfsf and dsasdwdcossfchi) should thus return W' as defined above. Note again that squarks are assumed to have $g_i = 6$ degrees of freedom in this convention and the summing over colours should also be taken into account in the code.

24.1.5 Reformulation of the Boltzmann equation

We now follow Gondolo and Gelmini [68] to put Eq. (24.12) in a more convenient form by considering the ratio of the number density to the entropy density,

$$Y = \frac{n}{s}. \tag{24.65}$$

Consider

$$\frac{dY}{dt} = \frac{d}{dt}\left(\frac{n}{s}\right) = \frac{\dot{n}}{s} - \frac{n}{s^2}\dot{s} \tag{24.66}$$

where dot means time derivative. In absence of entropy production, $S = R^3 s$ is constant (R is the scale factor). Differentiating with respect to time we see that

$$\dot{s} = -3\frac{\dot{R}}{R}s = -3Hs \tag{24.67}$$

which yields

$$\dot{Y} = \frac{\dot{n}}{s} + 3H\frac{n}{s}. \tag{24.68}$$

Hence we can rewrite Eq. (24.12) as

$$\dot{Y} = -s\langle\sigma_{\rm eff}v\rangle\left(Y^2 - Y_{\rm eq}^2\right). \tag{24.69}$$

The right-hand side depends only on temperature, and it is therefore convenient to use temperature T instead of time t as independent variable. Defining $x = m_1/T$ we have

$$\frac{dY}{dx} = -\frac{m_1}{x^2}\frac{1}{3H}\frac{ds}{dT}\langle\sigma_{\rm eff}v\rangle\left(Y^2 - Y_{\rm eq}^2\right). \tag{24.70}$$

where we have used

$$\frac{1}{\dot{T}} = \frac{1}{\dot{s}}\frac{ds}{dT} = -\frac{1}{3Hs}\frac{ds}{dT} \tag{24.71}$$

which follows from Eq. (24.67). With the Friedmann equation in a radiation dominated universe

$$H^2 = \frac{8\pi G\rho}{3}, \tag{24.72}$$

where G is the gravitational constant, and the usual parameterization of the energy and entropy densities in terms of the effective degrees of freedom $g_{\rm eff}$ and $h_{\rm eff}$,

$$\rho = g_{\rm eff}(T)\frac{\pi^2}{30}T^4, \quad s = h_{\rm eff}(T)\frac{2\pi^2}{45}T^3, \tag{24.73}$$

we can cast Eq. (24.70) into the form [68]

$$\frac{dY}{dx} = -\sqrt{\frac{\pi}{45G}}\frac{g_*^{1/2}m_1}{x^2}\langle\sigma_{\rm eff}v\rangle\left(Y^2 - Y_{\rm eq}^2\right) \tag{24.74}$$

where $Y_{\rm eq}$ can be written as

$$Y_{\rm eq} = \frac{n_{\rm eq}}{s} = \frac{45x^2}{4\pi^4 h_{\rm eff}(T)}\sum_i g_i\left(\frac{m_i}{m_1}\right)^2 K_2\left(x\frac{m_i}{m_1}\right), \tag{24.75}$$

using Eqs. (24.15), (24.65) and (24.73).

The parameter $g_*^{1/2}$ is defined as

$$g_*^{1/2} = \frac{h_{\rm eff}}{\sqrt{g_{\rm eff}}}\left(1 + \frac{T}{3h_{\rm eff}}\frac{dh_{\rm eff}}{dT}\right) \tag{24.76}$$

For $g_{\rm eff}$, $h_{\rm eff}$ and $g_*^{1/2}$ DarkSUSY has the option of either using the results of Gondolo and Gelmini [68] with a QCD phase-transition temperature $T_{QCD} = 150$ MeV or the later results of Hindmarsh and Philipsen [201]. The default in DarkSUSY is to use the results for equation of state B in Hindmarsh and Philipsen. The user can change this default choice with a call to dsrdset (see header of that file for explanation of how to call it). Using the Hindmarsh and Philipsen equation of state B (default) gives about 1.5–3.5% higher relic densities than the Gondolo and Gelmini degrees of freedom.

To obtain the relic density we integrate Eq. (24.79) from $x = 0$ to $x_0 = m_\chi/T_0$ where T_0 is the photon temperature of the Universe today. The relic density today in units of the critical density is then given by

$$\Omega_\chi = \rho_\chi^0/\rho_{\rm crit} = m_\chi s_0 Y_0/\rho_{\rm crit} \tag{24.77}$$

where $\rho_{\rm crit} = 3H^2/8\pi G$ is the critical density, s_0 is the entropy density today and Y_0 is the result of the integration of Eq. (24.79). With a background radiation temperature of $T_0 = 2.726$ K we finally obtain

$$\Omega_\chi h^2 = 2.755\times 10^8\frac{m_\chi}{\rm GeV}Y_0. \tag{24.78}$$

24.2 Relic density – numerical integration of the density equation

Let us write the evolution equation for the density,

$$\frac{dY}{dx} = -\sqrt{\frac{\pi}{45G}}\frac{g_*^{1/2}m_1}{x^2}\langle\sigma_{\rm eff}v\rangle\left(Y^2 - Y_{\rm eq}^2\right) \tag{24.79}$$

as

$$\frac{dY}{dx} = \lambda(Y^2 - q^2), \tag{24.80}$$

where λ contains the annihilation rate and q represents the thermal-equilibrium density.

This equation is stiff and an explicit method, like Euler or Runge-Kutta, fails to converge. To obtain a numerical solution, we use an adaptive implicit trapezoidal method which we explain in the following. Basically we discretize the equation first with a trapezoidal then with an Euler method, and adapt the step size according to the difference in the updated function values.

For simplicity we denote the right hand wide of eq. (24.80) as $f(x)$. We further write $f_i = f(x_i)$ and similarly for the other functions $\lambda(x)$ and $q(x)$. Given $Y_i = Y(x_i)$ we find $Y_{i+1} = Y(x_{i+1})$ with $x_{i+1} = x_i + h$ as follows.

First we discretize the evolution equation as

$$Y_{i+1} - Y_i = h\frac{f_i + f_{i+1}}{2}. \tag{24.81}$$

We insert

$$f_i = \lambda_i \left(Y_i^2 - q_i^2\right), \tag{24.82}$$
$$f_{i+1} = \lambda_{i+1} \left(Y_{i+1}^2 - q_{i+1}^2\right), \tag{24.83}$$

and solve the resulting quadratic equation for Y_{i+1} to obtain

$$Y_{i+1} = \frac{c}{1 + \sqrt{1 + uc}}, \tag{24.84}$$

where

$$c = 2Y_i + u\left[(q_{i+1}^2 + \rho q_i^2) - \rho Y_i^2\right], \tag{24.85}$$
$$u = h\lambda_{i+1}, \tag{24.86}$$
$$\rho = \lambda_i/\lambda_{i+1}. \tag{24.87}$$

In the expression for c we have explicitly indicated the order of evaluation which we found avoids round-off errors. If in eq. (24.84) $1 + uc$ is negative, we simply reduce the step h to $h/2$ and try again.

Secondly we discretize the evolution equation as

$$Y_{i+1} - Y_i = hf_{i+1}. \tag{24.88}$$

We insert the expression for f_{i+1} and solve the quadratic equation for Y_{i+1} to obtain

$$Y'_{i+1} = \frac{1}{2}\,\frac{c'}{1 + \sqrt{1 + uc'}}, \tag{24.89}$$

where

$$c' = 4\left(Y_i + uq_{i+1}^2\right). \tag{24.90}$$

Again if in eq. (24.89) $1 + uc' < 0$, we reduce the step h to $h/2$ and try again.

We then adapt the step size according to the relative difference of Y_{i+1} and Y'_{i+1},

$$d = \left|\frac{Y_{i+1} - Y'_{i+1}}{Y_{i+1}}\right|. \tag{24.91}$$

If the difference is larger than a prefixed ϵ, set at 0.01, we reduce the step size h to $hs/\sqrt{\epsilon}$ but never to less than $h/10$. s is a safety factor set to 0.9. If $d < \epsilon$, we increase the step size by a factor $s/\sqrt{\epsilon}$ but never by more than a factor of 5. We do not allow the step size to become smaller than $h_{\min} = 10^{-9}$. Error code 5 is reported if this happens. Error code 4 occurs when x_{i+1} is numerically equal to x_i because of round-off. Error code 6 occurs when the number of steps exceeds a maximum of 100000. Finally the initial step size is taken to be 0.01.

24.3 Relic density – routines

In src/rd, the general relic density routines are found. These routines can be used for any dark matter candidate and the interface to neutralino dark matter is in src/rn. We will first discuss how the routines for neutralino relic density are used and then how the general routines work.

24.3.1 Neutralino relic density

function **dsrdomega**(coann,fast,xf,ierr,iwar,nfc) r8

Purpose: Calculate the relic density of the lightest neutralino, possibly including coannihilations between different neutralinos, neutralinos and charginos and between charginos.

Input:

coann	i	=0: do not include coannihilations. =1: include all coannihilations =2: include coannihilations between neutralino–neutralino, neutralino–chargino and chargino–chargino.
fast	i	=1: Do a faster calculation, with slightly less accuracy in the numerical integrations and only including coannihilations (if coann=1) with other particles up to 1.3 times heavier than the lightest neutralino. =2: Do a more accurate calculation, with higher accuracy in the numerical integrations and including coannihilations (if coann=1) with other particles up to 2.1 times heavier than the lightest neutralino.

Output:

xf	r8	x is defined as $x = m_\chi/T$ and xf is the x at which freeze-out occurs (defined as the temperature at which the number density is a factor of two higher than the equilibrium density).
ierr	i	=0: Calculation went OK. $\neq 0$: Somethig went wrong.
iwar	i	=0: Calculation went OK. $\neq 0$: A slight inaccuracy may have occured at a resonance or threshold for numerical reasons. Usually, this doesn't affect the result, but one should keep it in mind in case the returned relic density seems strange.
nfc	i	The number of points (in $p_{\rm eff}$) at which the cross section was evaluated.

subroutine **dsrdwrate**(unit1,unit2,ich)

Purpose: Writes a table of the partial annihilation rates $W_F(p, \cos\theta)$ into each final channel F as a function of the center-of-mass momentum p and at $\cos\theta = 0.1$ to unit2.

Inputs:

unit1	i	What is this?
unit2	i	Unit number to write output to.
ich	i	What initial state channel to use: =1: neutralino–neutralino annihilation =2: neutralino–chargino coannihilation =3: chargino–chargino coannihilations.

Comment: Only annihilation between the *lightest* neutralinos and charginos are included.

24.3.2 General relic density routines

The routine that performs the actual relic density calculation is

subroutines **dsrdens**(wx,ncoann,mcoann,dof,nrs,rm,rw,nt,tm,oh2,tf,ierr,iwar)

Purpose: Calculate the relic density of a dark matter candidte.

Input:

wx	r8	User-defined function that returns the effective invariant annihilation rate, $W_{\rm eff}$, as a function of the effective momentum $p_{\rm eff}$. The function has to be declared external in the calling routine.
ncoann	i	Number of particles that coannihilate.
mcoann	r8	An array with the masses (in GeV) that can coannihilate.
dof	r8	Number of internal degrees of freedom for the coannihilating particles.
nrs	i	Number of resonances.
rm	r8	An array with the masses of the resonances (in GeV).
rw	r8	An array with the widths of the resonances (in GeV).
nt	i	Number of thresholds.
tm	r8	An array with the $\sqrt{s}$ (in GeV) at which the thresholds occur.

Output:

oh2	r8	The relic density, Ωh^2 where h is the Hubble constant in units of 100 km s^{-1} Mpc^{-1}.
tf	r8	The temperature (in GeV) at which the freeze-out occured. Freeze-out is defined to occur when the number density is 2 times the equlibrium density.
ierr	i	=0: Calculation went OK. $\neq 0$: Somethig went wrong.
iwar	i	=0: Calculation went OK. $\neq 0$: A slight inaccuracy may have occured at a resonance or threshold for numerical reasons. Usually, this doesn't affect the result, but one should keep it in mind in case the returned relic density seems strange.

It is up to the user to prepare the input function and arrays accordingly before calling the routine.

All internal settings of the relic density routines are set in common blocks in dsrdcom.h. The most important parameters that can be changed by the user are

Important parameters in **dsrdcom.h**

Purpose:		Provide a set of parameters, with which the internal behaviour of the relic density routines can be changed.
Parameters		
tharsi	i	Size of the coannihilation, resonance and threshold arrays (default=50). Increase this size if you have more than 50 coannihilating particles, more than 50 resonances or more than 50 thresholds.
rdluerr	i	Logical unit number where error messages are printed.
rdtag	c*12	Idtag that is printed in case of errors.
cosmin	r8	...
waccd	r8	...
dpminr	r8	...
dpthr	r8	...
wdiffr	r8	...
wdifft	r8	...
hstep	r8	...

When the relic density has been calculated, the integer variable copart in dsandwcom.h is set to indicate which coannihilating particles that have been included in the calculation. In Table 24.1, the meaning if this variable is shown.

24.3.3 Brief description of the internal routines

Below, the remaining routines related to the relic density calculation are briefly mentioned. For more details, we refer to the routines themselves.

Routine	**Purpose**

copart			PAW variables		
Bit set	Octal value	Decimal value	cop1 bit	cop2 bit	Particle
0	1	1	0	–	$\tilde{\chi}_1^0$
1	2	2	1	–	$\tilde{\chi}_2^0$
2	4	4	2	–	$\tilde{\chi}_3^0$
3	10	8	3	–	$\tilde{\chi}_4^0$
4	20	16	4	–	$\tilde{\chi}_1^\pm$
5	40	32	5	–	$\tilde{\chi}_2^\pm$
6	100	64	6	–	$\tilde{e}_1$
7	200	128	7	–	$\tilde{\mu}_1$
8	400	256	8	–	$\tilde{\tau}_1$
9	1 000	512	9	–	$\tilde{e}_2$
10	2 000	1 024	10	–	$\tilde{\mu}_2$
11	4 000	2 048	11	–	$\tilde{\tau}_2$
12	10 000	4 096	12	–	$\tilde{\nu}_e$
13	20 000	8 192	13	–	$\tilde{\nu}_\mu$
14	40 000	16 384	14	–	$\tilde{\nu}_\tau$
15	100 000	32 768	–	0	$\tilde{u}_1$
16	200 000	65 536	–	1	$\tilde{c}_1$
17	400 000	131 072	–	2	$\tilde{t}_1$
18	1 000 000	262 144	–	3	$\tilde{u}_2$
19	2 000 000	524 288	–	4	$\tilde{c}_2$
20	4 000 000	1 048 576	–	5	$\tilde{t}_2$
21	10 000 000	2 097 152	–	6	$\tilde{d}_1$
22	20 000 000	4 197 304	–	7	$\tilde{s}_1$
23	40 000 000	8 388 608	–	8	$\tilde{b}_1$
24	100 000 000	16 777 216	–	9	$\tilde{d}_2$
25	200 000 000	33 554 432	–	10	$\tilde{s}_2$
26	400 000 000	67 108 864	–	11	$\tilde{b}_2$

Table 24.1: The bits of copart are set to indicate which initial states that are included in the coannihilation calculation. In the output file *.omegaco, the value of copart is written in octal format. In PAW cop1 and cop2 are available. Check if a bit is set with btest(cop1,bit).

dsrdaddpt To add one point in the $W_{\rm eff}$-$p_{\rm eff}$ table.

dsrdcom To initialize parameters in the common blocks in dsrdcom.h. If you want to change these parameters yourself, include dsrdcom.h in your code and change the parameters you want.

dsrddof150 To prepare a table of the degrees of freedom as a function of the temperature in the early Universe.

dsrddpmin To return the allowed minimal distance in $p_{\rm eff}$ between two points in the $W_{\rm eff}$-$p_{\rm eff}$ plane. The returned value depends on if there is a resonance present or not at the given $p_{\rm eff}$.

dsrdeqn To solve the relic density equation by means of an implicit trapezoidal method with adaptive stepsize and termination.

dsrdfunc To return the invariant annihilation rate times the thermal distribution.

dsrdfuncs To provide dsrdfunc in a form suitable for numerical integration.

dsrdlny To return ln($W_{\rm eff}$ for a given $p_{\rm eff}$.

dsrdnormlz To return a unit vector in a given direction.

dsrdqad To calculate the relic density with a quick-and-dirty method. It uses the approximative expressions in Kolb & Turner with the cross section expaned in v.

dsrdqrkck To numerically integrate a function with a Runge-Kutta method

dsrdrhs To calculate terms on the right-hand side in the Boltzmann equation.

dsrdset To set the control parameters for the relic density calculation. Currently, only the choice of effective degrees of freedom is implemented through dsrdset; the other parameters are passed as arguments to dsrdomega.

dsrdspline To set up the table $W_{\rm eff}$-$p_{\rm eff}$ for spline interpolation.

dsrdstart To sort and store information about coannihilations, resonances and thresholds in common blocks.

dsrdtab To set up the table $W_{\rm eff}$-$p_{\rm eff}$.

dsrdthav To calculate the thermally averaged annihilation cross section at a given temperature.

dsrdthclose ...

dsrdthlim To determine the end-points for the thermal average integration.

dsrdthtest To check if a given entry in the $W_{\rm eff}$-$p_{\rm eff}$ table is at a threshold.

dsrdwdwdcos To write out a table of $dW_{\rm eff}/d\cos\theta$ as a function of $\cos\theta$ for a given $p_{\rm eff}$.

dsrdwfunc To write out dsrdfunc for a given $x = m_\chi/T$.

dsrdwintp To return the invariant rate $W_{\rm eff}$ for any given $p_{\rm eff}$ by performing a spline interpolation in the $W_{\rm eff}$-$p_{\rm eff}$ table.

dsrdwintpch To check the spline interpolation in the $W_{\rm eff}$-$p_{\rm eff}$ table and compare with a linear interpolation.

dsrdwintrp To write out a table of the invariant rate $W_{\rm eff}$ and some internal integration variables and expressions.

dsrdwres To write out the table $W_{\rm eff}$-$p_{\rm eff}$.

Below are brief descriptions of routines in src/rn not mentioned above

Routine	Purpose
dsrdres	To prepare the array of resonances needed before the call to dsrdens.
dsrdthr	To prepare the array of thresholds needed before the call to dsrdens.

Chapter 25

src/rge: mSUGRA interface (Isasugra) to DarkSUSY

25.1 mSUGRA (ISASUGRA) interface to DarkSUSY

If Isasugra is available, DarkSUSY can use Isasugra to generate mSUGRA models. In **src/rge/**, routines are avaible to transfer the mSUGRA parameters from DarkSUSY to Isasugra, call Isasugra and then transfer back the results to DarkSUSY. The philosophy of this interface is that whenever a user uses Isasugra, we should use all the results of Isasugra also in DarkSUSY. That means that instead of calculating the mass spectrum from the low-energy parameters obtained from Isasugra, we extract the masses and mixings from Isasugra.

Chapter 26

src/rn: Relic density of neutralinos (wrapper for rd routines)

26.1 Relic density of neutralinos

The relic density routines in **src/rd** solve the Boltzmann equation for any cold dark matter particle and it is up to us to tell it what kind of particles that can participate in coannihilations and what the effective annihilation rate is. This set-up for neutralino dark matter is done in **dsrdomega**. This routine is therefor the main routine the user should call, when the relic density of neutralinos is wanted.

What it does internally is the following:

- It determines which particles that can coannihilate (based on their mass differences) and puts these particles into a common block for the annihlation rate routines (**dsanwx**) and an array for the relic density routines. The relic density routines need to know their masses and internal degrees of freedom.
- It checks where we have resonances and thresholds and adds these to an array, which is passed to the relic density routines. The relic density routines then use this knowledge to make sure the tabulation of the cross section and the integrations are performed correctly at these difficult points.
- It then calls the relic density routines to calculate the relic density.

The returned value is $\Omega_\chi h^2$.

Chapter 27

src/slha: SUSY Les Houches Accord interface

27.1 SUSY Les Houches Accord

DarkSUSY includes routines to read and write SUSY Les Houches Accord [202, 203] files (SLHA files). This is done with the help of SLHALIB by T. Hahn [204].

DarkSUSY will write SLHA2 files and expect to get SLHA2 as well. The implementation right now takes a middle path between dumping everything or just a minimal set of inputs to the SLHA2 file. This choice was made to make most other SLHA2-aware programs able to exchange SLHA2 files with DarkSUSY.

However, we have not made a careful testing with lots of other codes, so if you try this out, please let us know if there are some things that don't work or could work better.

Chapter 28

src/su: General SUSY model setup: masses, vertices etc

28.1 Supersymmetric model

We will here review the definition of the MSSM as given in [1].

28.1.1 Parameters

In our notation, the superpotential and the soft supersymmetry-breaking scalar potential minimal supersymmetric standard model (MSSM) with R-parity conservation [4] read respectively

$$W = \epsilon_{ij}\left(-\hat{\mathbf{e}}_R^*\mathbf{h}_E\hat{\mathbf{l}}_L^i\hat{H}_1^j - \hat{\mathbf{d}}_R^*\mathbf{h}_D\hat{\mathbf{q}}_L^i\hat{H}_1^j + \hat{\mathbf{u}}_R^*\mathbf{h}_U\hat{\mathbf{q}}_L^i\hat{H}_2^j - \mu\hat{H}_1^i\hat{H}_2^j\right), \tag{28.1}$$

$$\begin{aligned} V_{\rm soft} = {} & \epsilon_{ij}\left(-\tilde{\mathbf{e}}_R^*\mathbf{A}_E\mathbf{h}_E\tilde{\mathbf{l}}_L^iH_1^j - \tilde{\mathbf{d}}_R^*\mathbf{A}_D\mathbf{h}_D\tilde{\mathbf{q}}_L^iH_1^j + \tilde{\mathbf{u}}_R^*\mathbf{A}_U\mathbf{h}_U\tilde{\mathbf{q}}_L^iH_2^j - B\mu H_1^iH_2^j\right. \\ & \left.+\text{h.c.}\right) \\ & +H_1^{i*}m_1^2H_1^i + H_2^{i*}m_2^2H_2^i \\ & +\tilde{\mathbf{q}}_L^{i*}\mathbf{M}_Q^2\tilde{\mathbf{q}}_L^i + \tilde{\mathbf{l}}_L^{i*}\mathbf{M}_L^2\tilde{\mathbf{l}}_L^i + \tilde{\mathbf{u}}_R^*\mathbf{M}_U^2\tilde{\mathbf{u}}_R + \tilde{\mathbf{d}}_R^*\mathbf{M}_D^2\tilde{\mathbf{d}}_R + \tilde{\mathbf{e}}_R^*\mathbf{M}_E^2\tilde{\mathbf{e}}_R. \end{aligned} \tag{28.2}$$

Here i and j are SU(2) indices ($\epsilon_{12} = +1$), $\mathbf{h}$'s, $\mathbf{A}$'s and $\mathbf{M}$'s are 3×3 matrices in generation space, and the other boldface letters are vectors in generation space.

The current version of DarkSUSY uses only a restricted set of parameters. Namely the number of free parameters (a grand total of 124 [9]) is reduced by setting the off-diagonal elements of the $\mathbf{A}$'s and $\mathbf{M}$'s to zero and imposing CP conservation (except in the CKM matrix).

28.1.2 Mass spectrum

For easy reference, we now give the particle mass matrices, together with our convention for the mixing matrices.

Concerning the Higgs sector, we choose as independent parameters $\tan\beta$ and the mass m_A of the CP-odd Higgs boson. The code provides six options for the calculation of the Higgs masses: higloop=0: tree level formulas; higloop=1: the effective potential approach in [10, 11] (correcting the sign of μ in eq. (4) of [11]); higloop=2: the effective potential approach in [12] with addition

	Higgs boson			
Channel	H_1^0	H_2^0	H_3^0	H^+
i=	j=1	j=2	j=3	j=4
1	$c\bar{c}$	$c\bar{c}$	$c\bar{c}$	ud
2	$b\bar{b}$	$b\bar{b}$	$b\bar{b}$	$u\bar{s}$
3	$t\bar{t}$	$t\bar{t}$	$t\bar{t}$	$u\bar{b}$
4	$\tau^+\tau^-$	$\tau^+\tau^-$	$\tau^+\tau^-$	$c\bar{d}$
5	W^+W^-	W^+W^-	–	$c\bar{s}$
6	Z^0Z^0	Z^0Z^0	–	cb
7	–	$H_1^0H_1^0$	–	$t\bar{d}$
8	$H_2^0H_2^0$	–	–	$t\bar{s}$
9	$H_3^0H_3^0$	$H_3^0H_3^0$	–	$t\bar{b}$
10	H^+H^-	H^+H^-	–	$\nu_e e^+$
11	–	–	ZH_1^0	$\nu_\mu\mu^+$
12	–	–	ZH_2^0	$\nu_\tau\tau^+$
13	ZH_3^0	ZH_3^0	–	$W^+H_1^0$
14	W^+H^-/W^-H^+	W^+H^-/W^-H^+	W^+H^-/W^-H^+	$W^+H_2^0$
15	$\mu^+\mu^-$	$\mu^+\mu^-$	$\mu^+\mu^-$	$W^+H_3^0$
16	$s\bar{s}$	$s\bar{s}$	$s\bar{s}$	–
17	gg	gg	gg	–
18	$\gamma\gamma$	$\gamma\gamma$	$\gamma\gamma$	–
19	$Z^0\gamma$	$Z^0\gamma$	$Z^0\gamma$	–
20	$\tilde{f}\tilde{f}'$	$\tilde{f}\tilde{f}'$	$\tilde{f}\tilde{f}'$	$\tilde{f}\tilde{f}'$

Table 28.1: Higgs partial widths hdwidth(i,j). Index i refers to the decay channel and index j to the Higgs boson. All widths are given in GeV. Note that typically we have that $m_{H_2} < m_{H_3} < m_{H^+} < m_{H_1}$ so many of these decay channels are not kinematically allowed, but included for completeness. If the HDECAY interface is used, the channels where $m_{H_2} < m_{H_3} < m_{H^+} < m_{H_1}$ is not satisfied are not included. Channels 16–19 are only included if HDECAY is used.

of D-terms and correction of some signs and numerical factors; higloop=3: the analytical approximations to the RGE-improved effective potential in [13]; higloop=4: the pole mass calculation in [14]; higloop=5: FeynHiggs (requires FeynHiggs to be installed) [163]; higloop=6: FeynHiggsFast (default) [164].

The masses of the Higgs bosons are obtained from

$$\mathcal{M}_H^2 = \begin{pmatrix} m_Z^2\cos^2\beta + m_A^2\sin^2\beta + \Delta_{11} & -\sin\beta\cos\beta(m_Z^2+m_A^2) + \Delta_{12} \\ -\sin\beta\cos\beta(m_Z^2+m_A^2) + \Delta_{21} & m_Z^2\sin^2\beta + m_A^2\cos^2\beta + \Delta_{22} \end{pmatrix} \tag{28.3}$$

$$m_{H^\pm}^2 = m_A^2 + m_W^2 + \Delta_\pm. \tag{28.4}$$

The quantities Δ_{ij} and $\Delta_\pm$ are the one-loop radiative corrections, calculated acording to the value of higloop as described above. Diagonalization of $\mathcal{M}_H^2$ gives the two CP-even Higgs boson masses, $m_{H_{1,2}}$, and their mixing angle α ($-\pi/2 < \alpha < 0$). For higloop=4, the pole masses are then obtained solving $m_{H_i}^{2\text{pole}} = m_{H_i}^2 + \Pi_{ii}(m_{H_i}^{2\text{pole}}) - \Pi_{ii}(0)$, where $\Pi_{ii}(p^2)$ is H_iH_i the self-energy. In this case, m_{H_3} is the pole mass and m_A is the running mass.

The Higgs widths are calculated at tree level, but with QCD corrections [165]. The decays to supersymmetric particles are also included in the total width, so the sum of the partial widths in Table 28.1 does not necessarily sum up to the total width given in width(k). The loop corrections are also available via an interface to HDECAY.

The neutralinos $\tilde{\chi}_i^0$ are linear combinations of the neutral gauginos $\tilde{B}$, $\tilde{W}_3$ and of the neutral

higgsinos $\tilde{H}_1^0$, $\tilde{H}_2^0$. In this basis, we write their mass matrix as

$$\mathcal{M}_{\tilde{\chi}^0_{1,2,3,4}} = \begin{pmatrix} M_1 & 0 & -m_Z s_W c_\beta & +m_Z s_W s_\beta \\ 0 & M_2 & +m_Z c_W c_\beta & -m_Z c_W s_\beta \\ -m_Z s_W c_\beta & +m_Z c_W c_\beta & \delta_{33} & -\mu \\ +m_Z s_W s_\beta & -m_Z c_W s_\beta & -\mu & \delta_{44} \end{pmatrix}, \tag{28.5}$$

with $c_W = \cos\theta_W$, $s_W = \sin\theta_W$, $c_\beta = \cos\beta$, and $s_\beta = \sin\beta$. Here δ_{33} and δ_{44} are radiative corrections important when two higgsinos are close in mass. Their explicit expressions are from ref. [15]. To neglect these radiative corrections set neuloop=0 instead of neuloop=1 (default). The neutralino mass eigenstates are written as

$$\tilde{\chi}_i^0 = N_{i1}\tilde{B} + N_{i2}\tilde{W}^3 + N_{i3}\tilde{H}_1^0 + N_{i4}\tilde{H}_2^0. \tag{28.6}$$

The phases of N_{ij} are chosen so that the neutralino masses $m_{\tilde{\chi}_i^0} \geq 0$.

The charginos are linear combinations of the charged gauge bosons $\tilde{W}^\pm$ and of the charged higgsinos $\tilde{H}_1^-$, $\tilde{H}_2^+$. Their mass matrix,

$$\mathcal{M}_{\tilde{\chi}^\pm} = \begin{pmatrix} M_2 & \sqrt{2}m_W \sin\beta \\ \sqrt{2}m_W \cos\beta & \mu \end{pmatrix}, \tag{28.7}$$

is diagonalized by the following linear combinations

$$\tilde{\chi}_i^- = U_{i1}\tilde{W}^- + U_{i2}\tilde{H}_1^-, \tag{28.8}$$

$$\tilde{\chi}_i^+ = V_{i1}\tilde{W}^+ + V_{i2}\tilde{H}_1^+. \tag{28.9}$$

We choose $\det(U) = 1$ and $U^* \mathcal{M}_{\tilde{\chi}^\pm} V^\dagger = \mathrm{diag}(m_{\tilde{\chi}_1^\pm}, m_{\tilde{\chi}_2^\pm})$ with non-negative chargino masses $m_{\tilde{\chi}_i^\pm} \geq 0$.

When discussing the squark mass matrix including mixing, it is convenient to choose a basis where the squarks are rotated in the same way as the corresponding quarks in the standard model. We follow the conventions of the particle data group [32] and put the mixing in the left-handed d-quark fields, so that the definition of the Cabibbo-Kobayashi-Maskawa matrix is $\mathbf{K} = \mathbf{V}_1 \mathbf{V}_2^\dagger$, where $\mathbf{V}_1$ ($\mathbf{V}_2$) rotates the interaction left-handed u-quark (d-quark) fields to mass eigenstates. For sleptons we choose an analogous basis, but due to the masslessness of neutrinos no analog of the CKM matrix appears.

We then obtain the general 6×6 $\tilde{u}$- and $\tilde{d}$-squark mass matrices:

$$\mathcal{M}^2_{\tilde{u}} = \begin{pmatrix} \mathbf{M}_Q^2 + \mathbf{m}_u^\dagger \mathbf{m}_u + D^u_{LL}\mathbf{1} & \mathbf{m}_u^\dagger (\mathbf{A}_U^\dagger - \mu^* \cot\beta) \\ (\mathbf{A}_U - \mu \cot\beta)\mathbf{m}_u & \mathbf{M}_U^2 + \mathbf{m}_u \mathbf{m}_u^\dagger + D^u_{RR}\mathbf{1} \end{pmatrix}, \tag{28.10}$$

$$\mathcal{M}^2_{\tilde{d}} = \begin{pmatrix} \mathbf{K}^\dagger \mathbf{M}_Q^2 \mathbf{K} + \mathbf{m}_d \mathbf{m}_d^\dagger + D^d_{LL}\mathbf{1} & \mathbf{m}_d^\dagger (\mathbf{A}_D^\dagger - \mu^* \tan\beta) \\ (\mathbf{A}_D - \mu \tan\beta)\mathbf{m}_d & \mathbf{M}_D^2 + \mathbf{m}_d^\dagger \mathbf{m}_d + D^d_{RR}\mathbf{1} \end{pmatrix}, \tag{28.11}$$

and the general sneutrino and charged slepton mass matrices

$$\mathcal{M}^2_{\tilde{\nu}} = \mathbf{M}_L^2 + D^\nu_{LL}\mathbf{1} \tag{28.12}$$

$$\mathcal{M}^2_{\tilde{e}} = \begin{pmatrix} \mathbf{M}_L^2 + \mathbf{m}_e \mathbf{m}_e^\dagger + D^e_{LL}\mathbf{1} & \mathbf{m}_e^\dagger (\mathbf{A}_E^\dagger - \mu^* \tan\beta) \\ (\mathbf{A}_E - \mu \tan\beta)\mathbf{m}_e & \mathbf{M}_E^2 + \mathbf{m}_e^\dagger \mathbf{m}_e + D^e_{RR}\mathbf{1} \end{pmatrix}. \tag{28.13}$$

Here

$$D^f_{LL} = m_Z^2 \cos 2\beta (T_{3f} - e_f \sin^2\theta_w), \tag{28.14}$$

$$D^f_{RR} = m_Z^2 \cos 2\beta e_f \sin^2\theta_w. \tag{28.15}$$

In the chosen basis, $\mathbf{m}_u = \mathrm{diag}(m_\mathrm{u}, m_\mathrm{c}, m_\mathrm{t})$, $\mathbf{m}_d = \mathrm{diag}(m_\mathrm{d}, m_\mathrm{s}, m_\mathrm{b})$ and $\mathbf{m}_e = \mathrm{diag}(m_e, m_\mu, m_\tau)$.

Table 28.2: Particle codes (synonyms are separated by commas).

ν_e	knue,knu(1)	γ	kgamma	$\tilde{\chi}_i^0$	kn(i) $i = 1 \ldots 4$	$\tilde{u}_1$	ksu(1),ksqu(1)
e	ke,kl(1)	$W^\pm$	kw	$\tilde{\chi}_k^\pm$	kcha(k) $k = 1, 2$	$\tilde{u}_2$	ksu(2),ksqu(4)
ν_μ	knumu,knu(2)	Z^0	kz	$\tilde{g}$	kgluin	$\tilde{d}_1$	ksd(1),ksqd(1)
μ	kmu,kl(2)	g	kgluon	$\tilde{\nu}_e$	ksnue,ksnu(1)	$\tilde{d}_2$	ksd(2),ksqd(4)
ν_τ	knutau,knu(3)			$\tilde{e}_1$	kse(1),ksl(1)	$\tilde{c}_1$	ksc(1),ksqu(2)
τ	ktau,kl(3)			$\tilde{e}_2$	kse(2),ksl(4)	$\tilde{c}_2$	ksc(2),ksqu(5)
u	ku,kqu(1)	H^0	kh1	$\tilde{\nu}_\mu$	ksnumu,ksnu(2)	$\tilde{s}_1$	kss(1),ksqd(2)
d	kd,kqd(1)	h^0	kh2	$\tilde{\mu}_1$	ksmu(1),ksl(2)	$\tilde{s}_2$	kss(2),ksqd(5)
c	kc,kqu(2)	A^0	kh3	$\tilde{\mu}_2$	ksmu(2),ksl(5)	$\tilde{b}_1$	ksb(1),ksqd(3)
s	ks,kqd(2)	$H^\pm$	khc	$\tilde{\nu}_\tau$	ksnuta,ksnu(3)	$\tilde{b}_2$	ksb(2),ksqd(6)
b	kb,kqd(3)	G^0	kgold0	$\tilde{\tau}_1$	kstau(1),ksl(3)	$\tilde{t}_1$	kst(1),ksqu(3)
t	kt,kqu(3)	$G^\pm$	kgoldc	$\tilde{\tau}_2$	kstau(2),ksl(6)	$\tilde{t}_2$	kst(2),ksqu(6)

The slepton and squark mass eigenstates $\tilde{f}_k$ ($\tilde{\nu}_k$ with $k = 1, 2, 3$ and $\tilde{e}_k$, $\tilde{u}_k$ and $\tilde{d}_k$ with $k = 1, \ldots, 6$) diagonalize the previous mass matrices and are related to the current sfermion eigenstates $\tilde{\mathbf{f}}_L$ and $\tilde{\mathbf{f}}_R$ via ($a = 1, 2, 3$)

$$\tilde{f}_{La} = \sum_{k=1}^{6} \tilde{f}_k \mathbf{\Gamma}_{FL}^{*ka}, \tag{28.16}$$

$$\tilde{f}_{Ra} = \sum_{k=1}^{6} \tilde{f}_k \mathbf{\Gamma}_{FR}^{*ka}. \tag{28.17}$$

The squark and charged slepton mixing matrices $\mathbf{\Gamma}_{UL,R}$, $\mathbf{\Gamma}_{DL,R}$ and $\mathbf{\Gamma}_{EL,R}$ have dimension 6×3, while the sneutrino mixing matrix $\mathbf{\Gamma}_{\nu L}$ has dimension 3×3.

This version of DarkSUSY allows only for diagonal matrices $\mathbf{A}_U$, $\mathbf{A}_D$, $\mathbf{A}_E$, $\mathbf{M}_Q$, $\mathbf{M}_U$, $\mathbf{M}_D$, $\mathbf{M}_E$, and $\mathbf{M}_L$. This ansatz, while not being the most general one, implies the absence of tree-level flavor changing neutral currents in all sectors of the model. In this case, the squark mass matrices can be diagonalized analytically. For example, for the top squark one has, in terms of the top squark mixing angle $\theta_{\tilde{t}}$,

$$\Gamma_{UL}^{\tilde{t}_1\tilde{t}} = \Gamma_{UR}^{\tilde{t}_2\tilde{t}} = \cos\theta_{\tilde{t}}, \qquad \Gamma_{UL}^{\tilde{t}_2\tilde{t}} = -\Gamma_{UR}^{\tilde{t}_1\tilde{t}} = \sin\theta_{\tilde{t}}. \tag{28.18}$$

Special values of the sfermion masses can be set with the parameters `msquarks`, and msleptons. If msquarks=msleptons=0, the sfermion masses are obtained with the diagonalization described above. If `msquarks`>0 (or msleptons>0), all squark masses are set to `msquarks` (or all slepton masses to msleptons). Finally, if `msquarks`<0 (or msleptons<0), the squark (or slepton) masses are set equal to the neutralino mass but never less than |msquarks| (or |msleptons|). This is to provide the lightest possible sfermions compatible with a neutralino LSP. In all of these cases, there is no mixing between sfermions.

The particle masses are available in an array mass(p), where p is the particle code from table 28.1.2. Similarly, particle decay width are available as width(p), but currently only the width of the Higgs bosons are calculated, the other particles having fictitious widths of 1 or 5 GeV (for the sole purpose of regularizing annihilation amplitudes close to poles).

28.1.3 Three-particle vertices

We define three-particle vertices gl(i,j,k)= g_{ijk}^L and gr(i,j,k)= g_{ijk}^R as follows. We adopt the convention that the order of the particles in the indices is the order in which they appear in the

corresponding lagrangian term, so the last particle is always entering. If there are charged particles in the vertex, they are both assumed positively charged, and the particle that exits the vertex is indexed before the particle that enters.

- Three scalar bosons:
$$\mathcal{L}_{\rm int} = g_{\phi_i\phi_j\phi_k} m_W \phi_i\phi_j\phi_k \tag{28.19}$$
where ϕ_i is a Higgs or a Goldstone boson. In this case, gl=gr=g. Available vertices are $\phi_i\phi_j\phi_k$ = $H_i^0H_j^0H_k^0$, $H_i^0H^-H^+$, $H_i^0A^0A^0$, $H_i^0G^0G^0$, $H_i^0G^-G^+$, $H_i^0G^-H^+$, $H_i^0G^-G^+$, $A^0G^-H^+$, $A^0G^0H_i^0$, and permutations.

- Two scalar and one vector bosons:
$$\mathcal{L}_{\rm int} = g_{V\phi_1\phi_2} V^\mu \phi_1 i\overleftrightarrow{\partial}_\mu \phi_2. \tag{28.20}$$
Available vertices are $V\phi_1\phi_2 = Z^0H_i^0A^0$, $Z^0H^-H^+$, γH^-H^+, $W^-H^+A^0$, $W^-H^+H_i^0$, and permutations.

- One scalar and two vector bosons:
$$\mathcal{L}_{\rm int} = g_{\phi V_1V_2} m_W g_{\mu\nu} \phi V_1^\mu V_2^\nu \tag{28.21}$$
Available vertices are $\phi V_1V_2 = H_i^0W^-W^+$, $H_i^0Z^0Z^0$.

- Three vector bosons:
$$ig_{V_1V_2V_3}\left[(k_1-k_3)_\nu g_{\mu\lambda} + (k_3-k_2)_\mu g_{\lambda\nu} + (k_2-k_1)g_{\mu\nu}\right] \tag{28.22}$$
with all momenta incoming and assigned as $V_1^\mu(k_1)$, $V_2^\nu(k_2)$ and $V_3^\lambda(k_3)$. Available vertices are $Z^0W^-W^+$ and γW^-W^+.

- One scalar boson and two Dirac fermions:
$$\mathcal{L}_{\rm int} = \phi\overline{\psi}_1(g^L_{\phi\psi_1\psi_2}P_L + g^R_{\phi\psi_1\psi_2}P_R)\psi_2 \tag{28.23}$$
Available vertices are $\phi\psi_1\psi_2$ =

- One vector boson and two Dirac fermions:
$$\mathcal{L}_{\rm int} = V_\mu\overline{\psi}_1\gamma^\mu(g^L_{V\psi_1\psi_2}P_L + g^R_{V\psi_1\psi_2}P_R)\psi_2 \tag{28.24}$$
Available vertices are $V\psi_1\psi_2$ =

- One scalar boson, one Dirac and one Majorana fermion:
$$\mathcal{L}_{\rm int} = \phi\overline{\psi}(g^L_{\phi\psi\chi}P_L + g^R_{\phi\psi\chi}P_R)\chi \tag{28.25}$$
Available vertices are $\phi\psi\chi$ =

- One vector boson, one Dirac and one Majorana fermion:
$$\mathcal{L}_{\rm int} = V_\mu\overline{\psi}\gamma^\mu(g^L_{V\psi\chi}P_L + g^R_{V\psi\chi}P_R)\chi \tag{28.26}$$
Available vertices are $V\psi\chi$ =

- One scalar boson and two Majorana fermions:
$$\mathcal{L}_{\rm int} = \tag{28.27}$$
Available vertices are...

- One vector boson and two Majorana fermions:

$$\mathcal{L}_{\rm int} = \tag{28.28}$$

Explicit expressions for the coupling constants g_{ijk} can be obtained in [4], with radiative corrections to trilinear scalar couplings in [33]. We have rederived from the superpotential all vertices we have implemented.

Implemented vertices: those listed above plus $Z^0W^\pm W^\mp$, $Z^0H_i^0H_i^0$, $W^\pm H^\mp A^0$, $W^\pm H^\mp H_i^0$, $H_i^0W^\pm W^\mp$, $H_i^0Z^0Z^0$, Z^0A^0H, $H_i^0A^0A^0$, A^0ff, H_i^0ff, Z^0ff, $Z^0\tilde{\chi}^0\tilde{\chi}^0$, $H_i^0\tilde{\chi}^0\tilde{\chi}^0$, $Z^0\tilde{\chi}^0\tilde{\chi}^0$, $W^\mp\tilde{\chi}^0\tilde{\chi}^\pm$, $H^\mp\tilde{\chi}^0\tilde{\chi}^\pm$, $\tilde{q}\tilde{g}q$, $\tilde{f}\tilde{\chi}^0f$, $H_i^0\tilde{\chi}^\pm\tilde{\chi}^\mp$, $A^0\tilde{\chi}^\pm\tilde{\chi}^\mp$, $W^\pm ff'$, $H^\pm ff'$, $\gamma W^\pm W^\mp$, $\gamma H^\pm H^\mp$, $Z^0\tilde{\chi}^\pm\tilde{\chi}^\mp$, $\gamma\tilde{\chi}^\pm\tilde{\chi}^\mp$, γff, GHH, GGH, $G^\mp\tilde{\chi}^0\tilde{\chi}^\pm$.

In appendix **??**, most of the Feynman rules and the explicit expressions for the g's are found.

28.1.4 Accelerator bounds

Accelerator bounds can be checked by a call to dsacbnd(p), where p=0 checks all implemented bounds, p=1 leaves out the bound from $b \to s\gamma$, and p=2 checks only $b \to s\gamma$. The accelerator bounds implemented in version 3.10.2 (July 1999) are listed in table 28.3. The branching ratio BR($b \to s\gamma$) is calculated to 1-loop using the expressions in ref. [16], including or not including 1-loop QCD corrections according to the switch bsgqcd (=0 without, =1 with [default]).

Table 28.3: Accelerator bounds implemented in version 3.10.2 (July 1999). **COMMENT #4: NOTE: These are not up to date with the latest version of DarkSUSY.**

Bound	Ref.
$m_{H^\pm} > 59.5$GeV	[17]
$m_h > [82.5 + 10.5\sin^2(\beta-\alpha)]$GeV	[18]
$m_{\tilde{\chi}_2^+} > 91$GeV if $m_{\tilde{\chi}_1^0} - m_{\tilde{\chi}_2^+} > 4$GeV	[19]
$m_{\tilde{\chi}_2^+} > 64$GeV if $m_{\tilde{\chi}_1^0} > 43$GeV and $m_{\tilde{\chi}_2^+} > m_{\tilde{\chi}_2^0}$	[20]
$m_{\tilde{\chi}_2^+} > 47$GeV if $m_{\tilde{\chi}_1^0} > 41$GeV	[21]
$m_{\tilde{\chi}_1^+} > 99$GeV	[22]
$m_{\tilde{\chi}_1^0} > 23$GeV if $\tan\beta > 3$	[23]
$m_{\tilde{\chi}_1^0} > 20$GeV if $\tan\beta > 2$	[23]
$m_{\tilde{\chi}_1^0} > 12.8$GeV if $m_{\tilde{\nu}} < 200$GeV	[24]
$m_{\tilde{\chi}_1^0} > 10.9$GeV	[25]
$m_{\tilde{\chi}_2^0} > 44$GeV	[26]
$m_{\tilde{\chi}_3^0} > 102$GeV	[26]
$m_{\tilde{\chi}_4^0} > 127$GeV	[23]
$m_{\tilde{g}} > 212$GeV if $m_{\tilde{q}_k} < m_{\tilde{g}}$	[27]
$m_{\tilde{g}} > 162$GeV	[28]
$m_{\tilde{q}_k} > 90$GeV if $m_{\tilde{g}} < 410$GeV	[29]
$m_{\tilde{q}_k} > 176$GeV if $m_{\tilde{g}} < 300$GeV	[27]
$m_{\tilde{q}_k} > 224$GeV if $m_{\tilde{g}} > m_{\tilde{g}}$	[30]
$m_{\tilde{e}} > 78$GeV if $m_{\tilde{\chi}_1^0} < 73$GeV	[31]
$m_{\tilde{\mu}} > 71$GeV if $m_{\tilde{\chi}_1^0} < 66$GeV	[31]
$m_{\tilde{\tau}} > 65$GeV if $m_{\tilde{\chi}_1^0} < 55$GeV	[31]
$m_{\tilde{\nu}} > 44.4$GeV	[32]
$1\times10^{-4} < \mathrm{BR}(b\to s\gamma) < 4\times10^{-4}$	[32]
$\Gamma_Z^{\rm inv} < 502.4$MeV	[32]

28.2 General supersymmetry – routines

Input parameters, options, results, etc. are contained in common blocks in the file dsmssm.h, which the user has to include. The input parameters are ($a = 1, 2, 3$)

ma= m_A,	tanbe= $\tan\beta$,	mu= μ,	m1= M_1,
m2= M_2,	m3= M_3,	asofte(a)= A_{Eaa},	asoftu(a)= A_{Uaa},
asoftd(a)= A_{Daa},	mass2q(a)= M^2_{Qaa},	mass2l(a)= M^2_{Laa},	mass2u(a)= M^2_{Uaa},
mass2d(a)= M^2_{Daa},	mass2e(a)= M^2_{Eaa}.		

The options are (see previous subsections for a description)
higloop choice of tree-level or radiatively corrected Higgs boson masses;
neuloop choice of tree-level or radiatively corrected neutralino masses;
msquarks,msleptons choice of squark and slepton masses.

To initialize DarkSUSY for a new model, you should call

subroutine **dssusy**(unphys,hwarning)

Purpose: To calculate the particle spectrum, widths and couplings.
Output:
- unphys i — non-zero if the model is unphysical
- hwarning i — non-zero if the Higgs code has issued a warning.

which calculates couplings, masses and some basic cross sections.

The following subroutines specify the values of the model parameters, and read/write them to a file. The user should create his own versions by editing a copy of them. Please call them with a different name.

subroutine **dsgive_model**(mu,m2,ma,tanbe,msq,atm,abm)

Purpose: Set the MSSM parameters as specified by the arguments.
Inputs:
- mu r8 — The μ parameter in GeV.
- m2 r8 — The M_2 parameter in GeV.
- ma r8 — The mass of the CP-odd Higgs boson, m_A in GeV.
- tanbe r8 — $\tan\beta$.
- msq r8 — Sets $\mathbf{M}^Q$, etc. to a common mass scale m_0 in GeV.
- atm r8 — Sets A_t in units of m_0 (range: -3 — 3).
- abm r8 — Sets A_b in units of m_0 (range: -3 — 3).

subroutine **dsrndm_model**(mftyp)

Purpose: Sets the susy parameters in a random way. Parameter ranges and probability distributions are set inside.
Inputs:
- mftyp i — =1: M_1 is related to M_2 through GUT relations.
  =2: M_1 and M_2 are generated independently.

function **rnduni**(iseed,a,b) r8

Purpose: To give a random number uniformly distributed between a and b.
Inputs:
- iseed i — Seed for the random number generator. Must be a negative number at the first call and should not be changed from call to call.
- a r8 — Lower limit of returned number.
- b r8 — Upper limit of returned number.

function **rndlog**(iseed,a,b) r8

Purpose: To give a random number logarithmically distributed between a and b.
Inputs:
- iseed i — Seed for the random number generator. Must be a negative number at the first call and should not be changed from call to call.

a	r8	Lower limit of returned number.
b	r8	Upper limit of returned number.

function **rndsgn**(iseed) r8

Purpose: Returns ± 1 with equal probability.

Inputs:

iseed	i	Seed for the random number generator. Must be a negative number at the first call and should not be changed from call to call.

subroutine **write_model**(lunit,mftyp)

Purpose: Writes out the model parameters to the file opened as unit lunit (formatted).

Inputs:

lunit	i	Unit number to write output to.
mftyp	i	=1: Only M_2 is written since M_1 is related to M_2 through GUT relations. =2: Both M_1 and M_2 are written.

subroutine **read_model**(lunit,nmodel,mftyp)

Purpose: Reads in the model parameters from the file opened as unit unit (formatted).

Inputs:

lunit	i	Unit number to read from.
nmodel	i	=0: The next model is read. =n: Only the n:th model is read.
mftyp	i	=1: Only M_2 is read since M_1 is related to M_2 through GUT relations. =2: Both M_1 and M_2 are read.

The following subroutines are useful in the analysis.

subroutine **widtag**(unit)

Purpose: Write the model identification tag to unit unit.

Inputs:

unit	i	Unit number to write to.

subroutine **wspctm**(unit)

Purpose: Write the particle mass spectrum and mixing matrices to unit unit.

Inputs:

unit	i	Unit number to write to.

subroutine **wvertx**(unit)

Purpose: Write all non-vanishing three-particle vertices to unit unit.

Inputs:

unit	i	Unit number to write to.

subroutine **wunph**(unit)

Purpose: Write the reason for which the model is not physically acceptable (tachyons, etc.) to unit unit.

Inputs:

unit	i	Unit number to write to.

subroutine **wexcl**(unit)

Purpose: Write the reason(s) for which the model is experimentally excluded to unit unit.

Inputs:

unit	i	Unit number to write to.

subroutine **dswhwar**(unit)

Purpose: Write the reason(s) for which the Higgs calculation issued warnings to unit unit.

Inputs:

unit	i	Unit number to write to.

Chapter 29

src/xcern: CERN routines needed by DarkSUSY

Chapter 30

src/xcmlib: CMLIB routines needed by DarkSUSY

Chapter 31

src/xfeynhiggs: FeynHiggs interface to DarkSUSY

Acknowledgements

P. Gondolo created DarkSUSY in 1994, took care of its organization, arranged it for release, and prepared the documentation. He contributed [34] the routines on the supersymmetric spectrum and mixing, the original calculation of the neutralino relic density without coannihilations, the direct detection rates and the accelerator bounds. P. Gondolo and J. Edsjö [35] included coannihilations in the relic density routines. J. Edsjö contributed the package for the neutrino–induced muons from the Sun and the Earth [36], and organized the routines for annihilations in the galactic halo, incorporating the code for the gamma-ray continuum by himself, for the antiprotons [37] and the gamma-ray lines [38] by P. Ullio, and for the positrons by E. Baltz [39]. Finally, DarkSUSY includes adapted versions of (1) routines by Carena, Quirós and Wagner on the Higgs boson masses, (2) routines from CMLIB (URL: http://www.netlib.org), specifically dqagse and its dependencies, (3) routines from CERNLIB, specifically gpindp by X and gadap by T. Johansson.

Bibliography

[1] P. Gondolo, J. Edsjö, L. Bergström, P. Ullio and E.A. Baltz, JCAP 07 (2004) 008 [astro-ph/0406204].

[2] The original papers for the different processes in DarkSUSY are

General MSSM, direct detction L. Bergström and P. Gondolo, Astrop. Phys. **5** (1996) 263.

Relic density P. Gondolo and G. Gelmini, Nucl. Phys. **B360** (1991) 145; J. Edsjö and P. Gondolo, Phys. Rev. **D56** (1997) 1879; J. Edsjö, M. Schelke, P. Ullio and P. Gondolo, JCAP **04** (2003) 001.

Neutrino telescopes L. Bergström, J. Edsjö and P. Gondolo, Phys. Rev. **D58** (1998) 103519.

Positrons E.A. Baltz and J. Edsjö, Phys. Rev. **D59** (1999) 023511.

Antiprotons L. Bergström, J. Edsjö and P. Ullio, ApJ **526** (1999) 215.

Gamma lines L. Bergström and P. Ullio, Nucl. Phys. **B504** (1997) 27; P. Ullio and L. Bergström, Phys. Rev. **D57** (1998) 1962.

Internal bremsstrahlung T. Bringmann, L. Bergström and J. Edsjö, JHEP **0801** (2008) 049.

Continuous gammas L. Bergström, J. Edsjö and P. Ullio, Phys. Rev. **D58** (1998) 083507.

Kinetic decoupling and microhalos T. Bringmann and S. Hofmann, JCAP **0407** (2007) 16; T. Bringmann, NJP **11** (2009) 10527.

[3] G. Jungman, M. Kamionkowski and K. Griest, Phys. Rep. **267** (1996) 195.

[4] H.E. Haber and G.L. Kane, Phys. Rep. 117 (1985) 75; J.F. Gunion and H.E. Haber, Nucl. Phys. B272 (1986) 1 [Erratum: ibid. B402 91993) 567]; H.E. Haber and D. Wyler, Nucl. Phys. B323 (1989) 267.

[5] H.E. Haber and G.L. Kane, Phys. Rep. 117 (1985) 75.

[6] J.F. Gunion and H.E. Haber, Nucl. Phys. B272 (1986) 1 [Erratum: ibid. B402 91993) 567].

[7] Derived from the rules in Fig. 83 in Ref. [5] or directly from the Lagrangian.

[8] F. Mandl and G. Shaw, *Quantum Field Theory*, John Wiley & Sons, 1984.

[9] S. Dimopoulos and D. Sutter, Nucl. Phys. B465 (1995) 23.

[10] J. Ellis, G. Ridolfi and F. Zwirner, Phys. Lett. B257 (1991) 83; ibid. B262 (1991) 477.

[11] A. Brignole, J. Ellis, G. Ridolfi and F. Zwirner, Phys. Lett. B271 (1991) 123.

[12] M. Drees, M. Nojiri, Phys. Rev. D45 (1992) 2482.

[13] M. Carena, Espinosa, M. Quirós, and C. Wagner, Phys. Lett. B355 (1995) 209.

[14] M. Carena, M. Quirós, and C. Wagner, Nucl. Phys. B461 (1996) 407.

[15] M. Drees, M. Nojiri, Yamada, (1997) astro-ph/970129

[16] S. Bertolini, F. Borzumati, A. Masiero and G. Ridolfi, Nucl. Phys. B353 (1991) 591.

[17] Abbiendi et al. (OPAL Collab.), Europ. Phys. J. C7 (1999) 407.

[18] Gao and Gay (ALEPH Collab.), in "High Energy Physics 99," Tampere, Finland, July 1999.

[19] J. Carr et al. (ALEPH Collab.), talk to LEPC, 31 March 1998 (URL: http://alephwww.cern.ch/ALPUB/seminar/carrlepc98/index.html).

[20] Acciarri et al. (L3 Collab.), Phys. Lett. B377 (1996) 289.

[21] Decamp et al. (ALEPH Collab.), Phys. Rep. 216 (1992) 253.

[22] Hidaka, Phys. Rev. D44 (1991) 927.

[23] Acciarri et al. (L3 Collab.), Phys. Lett. B350 (1995) 109.

[24] Buskulic et al. (ALEPH Collab.), Zeitschrift für Physik C72 (1996) 549.

[25] Acciarri et al. (L3 Collab.), Europ. Phys. J. C4 (1998) 207.

[26] Abbiendi et al. (OPAL Collab.), Europ. Phys. J. C8 (1999) 255.

[27] Abachi et al. (D0 Collab.), Phys. Rev. Lett. 75 (1995) 618.

[28] Abe et al. (CDF Collab.), Phys. Rev. D56 (1997) R1357.

[29] Abe et al. (CDF Collab.), Phys. Rev. Lett. 69 (1992) 3439.

[30] Abe et al. (CDF Collab.), Phys. Rev. Lett. 76 (1996) 2006.

[31] Barate et al. (ALEPH Collab.), Phys. Lett. B433 (1998) 176.

[32] C. Caso et al. (Particle Data Group), Europ. Phys. J. C3 (1998) 1, and 1999 partial update for edition 2000 (URL: http://pdg.lbl.gov)

[33] H.E. Haber, in *Perspectives on Higgs Physics II*, ed. G. Kane (World Scientific, Singapore, 1997).

[34] L. Bersgström and P. Gondolo, Astropart. Phys. 5 (1996) 263.

[35] J. Edsjö and P. Gondolo, Phys. Rev. D56 (1997) 1879.

[36] J. Edsjö, Diploma Thesis, Uppsala University preprint TSL/ISV-93-0091 (1993); J. Edsjö, Nucl. Phys. Proc. Suppl. 43 (1995) 265; J. Edsjö and P. Gondolo, Phys. Lett. B357 (1995) 595; L. Bergström, J. Edsjö, and P. Gondolo, Phys. Rev. D55 (1997) 1765; ibid. D58 (1998) 103519.

[37] L. Bergström, J. Edsjö, and P. Ullio, astro-ph/9902012.

[38] L. Bergström and P. Ullio, Nucl. Phys. B504 (1997) 27; Phys. Rev. D57 (1998) 1962.

[39] E. Baltz and J. Edsjö, Phys. Rev. D59 (1999) 023511.

[40] N. Bahcall, J.P. Ostriker, S. Perlmutter and P.J. Steinhardt, Science **284**, 1481 (1999).

[41] L. Bergström, Rep. Prog. Phys. **63** (2000) 793.

[42] H. Goldberg, Phys. Rev. Lett. **50** (1983) 1419.

[43] L.M. Krauss, Nucl. Phys. **B227** (1983) 556.

[44] J. Ellis et al., Nucl. Phys. **B238** (1984) 453.

[45] G. Raffelt, Nucl. Phys. Proc. Suppl. **77** (1999) 456.

[46] L. Bergström and P. Gondolo, Astrop. Phys. **5** (1996) 263.

[47] H.E. Haber and G.L. Kane, Phys. Rep. **117** (1985) 75; J.F. Gunion and H.E. Haber, Nucl. Phys. **B272** (1986) 1 [Erratum-ibid. **B402** (1993) 567].

[48] S. Dimopoulos and D. Sutter, Nucl. Phys. **B465** (1995 23.

[49] S. Heinemeyer, W. Hollik and G. Weiglein, Comp. Phys. Comm. **124** (2000) 76; hep-ph/0002213.

[50] S. Heinemeyer, W. Hollik and G. Weiglein, Phys. Rev. **D58** (1998) 091701; Eur. Phys. J. **C9** (1999) 343; Phys. Lett. **B455** (1999) 179.

[51] J. Ellis, G. Ridolfi and F. Zwirner, Phys. Lett. **B257** (1991) 83; ibid. **B262** (1991) 477; A. Brignole, J. Ellis, G. Ridolfi and F. Zwirner, Phys. Lett. **B271** (1991) 123.

[52] M. Drees, M.M. Nojiri, D.P. Roy and Y. Yamada, Phys. Rev. **D56** (1997) 276 [hep-ph/9701219].

[53] D. Pierce and A. Papadopoulos, Phys. Rev. **D50** (1994) 565, Nucl. Phys. **B430** (1994) 278; A.B. Lahanas, K. Tamvakis and N.D. Tracas, Phys. Lett. **B324** (1994) 387.

[54] M. Drees, K. Hagiwara and A. Yamada, Phys. Rev. **D45** (1992) 1725.

[55] Particle Data Group, D.E. Groom et al, The European Physical Journal **C15** (2000) 1.

[56] S. Bertolini, F. Borzumati, A. Masiero and G. Ridolfi, Nucl. Phys. B353 (1991) 591.

[57] M. Kado (Aleph Collaboration), Talk given at the XXXVth Recontre de Moriond, CERN/ALEPH PUB-2000-6.

[58] P. de Bernardis et al. Nature **404** (2000) 995; S. Hanany et al., astro-ph/0005123.

[59] A. E. Lange et al., astro-ph/0005004 (2000); M. Tegmark and M. Zaldarriaga, astro-ph/0004393 (2000); A. Balbi et al., astro-ph/0005124 (2000); W. Hu, M. Fukugita, M. Zaldarriaga, and M. Tegmark, astro-ph/0006436 (2000); A. Jaffe et al., astro-ph/0007333 (2000); W. Kinney, A. Melchiorri, and A. Riotto, astro-ph/0007375 (2000).

[60] S. Perlmutter et al., Astrophys. J. **517** (1999) 565; P.M. Garnavich et al., Astrophys. J. **509** (1998) 74.

[61] K. Griest and D. Seckel, Phys. Rev. **D43** (1991) 3191.

[62] K. Griest, Phys. Rev. **D38** (1988) 2357 [erratum ibid **D39** (1989) 3802]; J. Scherrer and M.S. Turner, Phys. Rev. **D33** (1986) 1585 [erratum ibid **D34** (1986) 3263]; M. Srednicki, R. Watkins and K.A. Olive, Nucl. Phys. **B310** (1988) 693; K. Griest, M. Kamionkowski and M.S. Turner, Phys. Rev. **D41** (1990) 3565; G.B. Gelmini, P. Gondolo, and E. Roulet, Nucl. Phys. **B351** (1991) 623; A. Bottino et al., Astropart. Phys. **1** (1992) 61, ibid. **2** (1994) 67; R. Arnowitt and P. Nath, Phys. Lett. **B299** (1993) 58, **B307** (1993) 403(E), Phys. Rev. Lett. **70** (1993) 3696; H. Baer and M. Brhlik, Phys. Rev. **D53** (1996) 597.

[63] J. McDonald, K.A. Olive and M. Srednicki, Phys. Lett. **B283** (1992) 80.

[64] S. Mizuta and M. Yamaguchi, Phys. Lett. **B298** (1993) 120.

[65] M. Srednicki, R. Watkins and K.A. Olive, Nucl. Phys. **B310** (1988) 693.

[66] M. Drees and M. Nojiri, Phys. Rev. **D47** (1993) 376.

[67] E.W. Kolb and M.S. Turner, *The Early Universe*, Addison-Wesley (1990).

[68] P. Gondolo and G. Gelmini, Nucl. Phys. B360 (1991) 145.

[69] J. Edsjö and P. Gondolo, Phys. Rev. **D56** (1997) 1879 [`hep-ph/9704361`].

[70] J. Ellis, T. Falk and K. A. Olive, Phys. Lett. **B444** (1998) 367; J. Ellis, T. Falk, K. A. Olive and M. Srednicki, Astropart. Phys. **13** (2000) 181.

[71] REDUCE 3.5. A.C. Hearn, RAND, 1993.

[72] L. Bergström, J. Edsjö and P. Ullio, astro-ph/9804050, Phys.Rev. D58 (1998) 083507.

[73] L. Bergström, P. Ullio and J. Buckley, Astrop. Phys. in press, astro-ph/9712318.

[74] L. Bergström, J. Edsjö and P. Gondolo, Phys. Rev. **D55** (1997) 1765.

[75] J. Edsjö and P. Gondolo, Phys. Lett. **B357** (1995) 595.

[76] J. Edsjö, PhD Thesis, hep-ph/9704384.

[77] L. Bergstrom, T. Damour, J. Edsjo, L. M. Krauss and P. Ullio, indirect detection rates," JHEP **9908**, 010 (1999) [hep-ph/9905446].

[78] M.W. Goodman and E. Witten, Phys. Rev. **D31** (1985) 3059.

[79] A. Bottino et al., Phys. Lett. B402 (1997) 113.

[80] A. Gould, Astrophys. J. **321** (1987) 571.

[81] A. Gould, Astrophys. J. **368** (1991) 610

[82] A. Gould, Astrophys. J. **388** (1992) 338.

[83] J. Ellis and R. Flores, Nucl. Phys. B307 (1988) 883; Phys. Lett B263 (1991) 259.

[84] J. Engel, Phys. Lett. **B264** (1991) 114.

[85] K. Griest, Phys. Rev. D28 (1988) 2357; R. Barbieri, M. Frigeni and G.F. Giudice, Nucl. Phys. B313 (1989) 725; G. Gelmini, P. Gondolo and E. Roulet, Nucl. Phys. B351 (1991) 623; M. Kamionkowski, Phys. Rev. D44 (1991) 3021; A. Bottino et al., Astropart. Phys. 2 (1994) 77.

[86] J. Gasser, H. Leutwyler and M.E. Sainio, Phys. Lett. B253 (1991) 252.

[87] D. Adams et al, Phys. Lett. B357 (1995) 248.

[88] R.L. Jaffe and A. Manohar, Nucl. Phys. **337** (1990) 509.

[89] J. Engel and P. Vogel, Phys. Rev. D40 (1989) 3132; J. Engel, S. Pittel and P. Vogel, Int. J. Mod. Phys. E1 (1992) 1.

[90] T. Sjöstrand, Comm. Phys. Comm. **82** (1994) 74; T. Sjöstrand, *PYTHIA 5.7 and JETSET 7.4. Physics and Manual*, CERN-TH.7112/93, `hep-ph/9508391` (revised version).

[91] S. Ritz and D. Seckel, Nucl. Phys. **B304** (1988) 877.

[92] J. Edsjö, Diploma Thesis, Uppsala University preprint TSL/ISV-93-0091 (ISSN 0284-2769), can be downloaded from `http://www.physto.se/~edsjo/articles/index.html`.

J. Edsjö, in *Trends in Astroparticle Physics*, Stockholm, Sweden, 1994, eds. L. Bergström, P. Carlson, P.O. Hulth and H. Snellman, Nucl. Phys. (Proc. Suppl.) **B43** (1995) 265.

[93] J. Edsjö and P. Gondolo, Phys. Lett. **B357** (1995) 595.

[94] L. Krauss, *Cold dark matter candidates and the solar neutrino problem*, Harvard preprint HUTP-85/A008a (1985);
W.H. Press and D.N Spergel, Astrophys. J. **296** (1985) 679;
J. Silk, K. Olive and M. Srednicki, Phys. Rev. Lett. **55** (1985) 257;
L. Krauss, M. Srednicki and F. Wilczek, Phys. Rev. **D33** (1986) 2079;
T. Gaisser, G. Steigman and S. Tilav, Phys. Rev. **D34** (1986) 2206;
K. Griest and S. Seckel, Nucl. Phys. **B283** (1987) 681, erratum *ibid.* **B296** (1988) 1034;
L.M. Krauss, K. Freese, D.N. Spergel and W.H. Press, Astrophys. J. **299** (1985) 1001;
J. Hagelin, K. Ng and K. Olive, Phys. Lett. **B180** (1987) 375;
K. Freese, Phys. Lett. **B167** (1986) 295;
M. Kamionkowski, Phys. Rev. **D44** (1991) 3021;
F. Halzen, T. Stelzer and M. Kamionkowski, Phys. Rev. **D45** (1992) 4439;
A. Bottino, V. de Alfaro, N. Fornengo, G. Mignola and M. Pignone, Phys. Lett. **B265** (1991) 57; A. Bottino, N. Fornengo, G. Mignola, L. Moscoso, Astropart. Phys. **3** (1995) 65 [`hep-ph/9408391`];
R. Gandhi, J.L. Lopez, D.V. Nanopoulos, K. Yuan and A. Zichichi, Phys. Rev. **D49** (1994) 3691 [`astro-ph/9309048`];
L. Bergström, J. Edsjö and P. Gondolo, Phys. Rev. **D55** (1997) 1765 [`hep-ph/9607237`];
L. Bergstrom, J. Edsjo and P. Gondolo, Phys. Rev. **D58**, 103519 (1998) [hep-ph/9806293].

[95] F. Halzen, Comments Nucl. Part. Phys. **22** (1997) 155.

[96] G.F. Giudice and E. Roulet, Nucl. Phys. **B316** (1989) 429.

F. Halzen, T. Stelzer and M. Kamionkowski, Phys. Rev. **D45** (1992) 4439.

M. Drees, G. Jungman, M. Kamionkowski and M.M. Nojiri, Phys. Rev. **D49** (1994) 636.

R. Gandhi, J.L. Lopez, D.V. Nanopoulos, K. Yuan and A. Zichichi, Phys. Rev. **D49** (1994) 3691.

A. Bottino, N. Fornengo, G. Mignola and L. Moscoso, Astropart. Phys. **3** (1995) 65.

G. Jungman and M. Kamionkowski, Phys. Rev. **D51** (1995) 328.

V. Berezinsky, A. Bottino, J. Ellis, N. Fornengo, G. Mignola and S. Scopel, hep-ph/9603342.

[97] L. Bergström, J. Edsjö and P. Gondolo, Phys. Rev. **D58**

[98] M. Kamionkowski, G. Jungman, K. Griest and B. Sadoulet, Phys. Rev. Lett. **74** (1995) 5174.

[99] J. Edsjö and P. Gondolo, Phys. Lett. **B357** (1995) 595.

[100] L. Bergström, J. Edsjö and M. Kamionkowski, Astropart. Phys. **7** (1997) 147.

[101] T. Damour and L.M. Krauss, Phys. Rev. Lett. **81** (1998) 5726 [`astro-ph/9806165`].

[102] T. Damour and L.M. Krauss, Phys. Rev. **D59** (1999) 063509 [`astro-ph/9807099`].

[103] G. Steigman, C.L. Sarazin, H. Quintana and J. Faulkner, Astrophys. J. **83** (1978) 1050;
K. Griest, Phys. Rev. **D37** (1988) 2703;
A. Gould, J.A. Frieman and K. Freese, Phys. Rev. **D39** (1989) 1029;
J.I. Collar, Phys. Rev. **D59** (1999) 063514 [`astro-ph/9808058`].

[104] A. Gould, Astrophys. J. **368** (1991) 610.

[105] A. Gould and S. M. Khairul Alam, astro-ph/9911288.

[106] J.N. Bahcall and M.H. Pinsonneault, Rev. Mod. Phys. **64** (1992) 885.

[107] *The Earth: its properties, composition, and structure.* Britannica CD, Version 99 ©1994–1999. Encyclopædia Britannica, Inc.

[108] L. Bergström, J. Edsjö and P. Ullio, Astrophys. J. **526** (1999) 215.

[109] J.W. Bieber et al., Phys. Rev. Lett. **83** (1999) 674.

[110] Ullio, P. & Bergström, L. 1998, Phys. Rev., D57, 1962.

[111] Drees, M., Jungman, G., Kamionkowski, M. & Nojiri, M.M. 1994, Phys. Rev., D49, 636.

[112] L. Bergström and P. Ullio, Nucl. Phys. **B504** (1997) 27; see also Z. Bern, P. Gondolo and M. Perelstein, Phys. Lett. **B411** (1997) 86.

[113] J.F. Navarro, C.S. Frenk and S.D.M. White, Ap. J. **462** (1996) 563.

[114] Bergström, L., Edsjö, J., Gondolo, P. & Ullio, P. 1999, Phys. Rev., D59, 043506.

[115] P. Ullio, astro-ph/9904086.

[116] Berezinskii, V.S., Bulanov, S., Dogiel, V., Ginzburg, V. & Ptuskin, V. 1990, *Astrophysics of cosmic rays*, North-Holland, Amsterdam.

[117] Gaisser, T.K. 1990, *Cosmic rays and particle physics*, Cambridge University Press, Cambridge.

[118] Chardonnet, P., Mignola, G., Salati, P. & Taillet, R. 1996, Phys. Lett., B384, 161.

[119] Bottino, A., Donato, F., Fornengo, N. & Salati, P. 1998, Phys. Rev. D58 123503.

[120] Fisk, L.A. 1971, J. Geophys. Res., 76, 221.

[121] E.A. Baltz and J. Edsjö, Phys. Rev. **D59** (1999) 023511.

[122] Bergström, L., Ullio, P. & Buckley, J.H. 1998, Astrop. Phys. 9, 137.

[123] W.R. Webber, M.A. Lee and M. Gupta, Astrophys. J. **390** (1992) 96.

[124] M. Kamionkowski and M. S. Turner, Phys. Rev. **D43** (1991) 1774.

[125] M.S. Longair, *High Energy Astrophysics*, (Cambridge University Press, New York, 1994), Vol. 2, Chap. 19.

[126] I.V. Moskalenko and A.W. Strong, Astrophys. J. **493** (1998) 694.

[127] W. Dehnen and J. Binney, astro-ph/9612059 (1997).

[128] R. Carlberg, Astrophys. J. **433** (1994) 468.

[129] A.V. Kravtsov et al., Ap. J. in press, astro-ph/9708176.

[130] B. Moore et al., astro-ph/9709051, Astrophys. J. Lett., submitted.

[131] V.S. Berezinsky, A.V. Gurevich and K.P. Zybin, Phys. Lett. **B294** (1992) 221.

[132] R.A. Flores and J.R. Primack, Astrophys. J. **427** (1994) L1.

[133] A. Burkert and J. Silk, astro-ph/9707343 (1997).

[134] T. Fukushige and J. Makino, Astrophys. J. **487** (1997) L9.

[135] N.W. Evans and J.L. Collett, astro-ph/9702085.

[136] D. N. Spergel and P. J. Steinhardt, Phys. Rev. Lett. **84** (2000) 3760.

[137] M. Kaplinghat, L. Knox and M. S. Turner, astro-ph/0005210.

[138] P. Gondolo and J. Silk, Phys. Rev. Lett. **83** (1999) 1719 [astro-ph/9906391].

[139] P. Gondolo, hep-ph/0002226.

[140] P. Ullio, PhD thesis, Physics Department, Stockholm University, 1999.

[141] C.S. Kochanek, Astrophys. J. **457** (1996) 228.

[142] D.N.C. Lin, B.F. Jones and A.R. Klemola, Astrophys. J. **439** (1995) 652.

[143] F.J. Kerr and D. Lynden-Bell, MNRAS **221** (1986) 1023.

[144] M.J. Reid, ARA&A **31** (1993) 345.

[145] R.P. Olling and M.R. Merrifield, aspro-ph/9711157, to appear in proceedings of the Workshop on Galactic Halos, Santa Cruz, August 1997 (ASP conference Series).

[146] K. Kuijken and G. Gilmore Astrophys. J. **367** (1991) L9.

[147] A. Gould, MNRAS **244** (1990) 25.

[148] J. Silk and M. Srednicki, Phys. Rev. Lett **53** (1984) 624;
J. Silk and H. Bloemen, Astrophys. J. **313** (1987) L47;
S. Rudaz and F.W. Stecker, Astrophys. J. **325** (1988) 16;
F.W. Stecker and A. Tylka, Astrophys. J. **343** (1989) 169;
H.-U. Bengtsson, P. Salati and J. Silk, Nucl Phys. **B346** (1990) 129;
E. Diehl, G.L. Kane, C. Kolda and J.D. Wells, Phys. Rev. **D52** (1994) 4223;
P. Chardonnet, P. Salati, J. Silk, I. Grenier, and G. Smoot, Astrophys. J. **454** (1995) 774.

[149] M. Srednicki, S. Theisen and J. Silk, Phys. Rev. Lett. **56**, 263 (1986); Erratum-ibid. **56**, 1883 (1986);
S. Rudaz, Phys. Rev. Lett. **56**, 2128 (1986).

[150] L. Bergström and H. Snellman, Phys. Rev. **D37** (1988) 3737;
S. Rudaz, Phys. Rev. **D39** (1989) 3549;
G.F. Giudice and K. Griest, Phys. Rev. **D40** (1989) 2549;
A. Bouquet, P. Salati and J. Silk, Phys. Rev. **D40** (1989) 3168;
V. Berezinsky, A. Bottino and V. de Alfaro, Phys. Lett. **B274** (1992) 122;
M. Urban et al., Phys. Lett. **B293** (1992) 149;
L. Bergström and J. Kaplan, Astropart. Phys. **2** (1994) 261.

[151] G. Jungman and M. Kamionkowski, Phys. Rev. **D51** (1995) 3121.

[152] K. Fujikawa, Phys. Rev. **D7** (1973) 393.

[153] M.S. Turner, Phys. Rev. **D34** (1986) 1921;
J.R. Ipser and P. Sikivie, Phys. Rev. **D35** (1987) 3695;
K. Freese and J. Silk, Phys. Rev. **D40** (1989) 3828;
V. Berezinsky, A. Bottino and G. Mignola, Phys. Lett. **B325** (1994) 136.

[154] G. Lake, Nature **346** (1990) 39;
J. Silk and A. Stebbins, Astrophys. J. **411** (1993) 439;
C. Calcaneo-Roldan and B. Moore, Phys. Rev. **D62** (2000) 123005.

[155] L. Bergström, J. Edsjö and P. Ullio, Phys. Rev. D **58**, (1998) 083507.

[156] L. Bergström, J. Edsjö and C. Gunnarsson, Phys. Rev. D **63**, 083515 (2001).

[157] E. A. Baltz, C. Briot, P. Salati, R. Taillet and J. Silk, Phys. Rev. D **61**, 023514 (2000).

[158] D.B. Cline and Y.-T. Gao, Astronomy and Astrophys. **231** (1990) L23;
Y.-T. Gao, F.W. Stecker and D.B. Cline, Astronomy and Astrophys. **249**, 1 (1991).

[159] L. Bergström, J. Edsjö and P. Ullio, Phys. Rev. Lett. (2001) in press.

[160] Gleeson, L.J. & Axford, W.I. 1967, ApJ, 149, L115.

[161] M. Kamionkowski, Phys. Rev. **D44** (1991) 3021.

[162] X. Chen, M. Kamionkowski and X. Zhang, Phys. Rev. **D64** (2001) 021302; S. Hofmann, D.J. Schwarz and H. Stocker, Phys. Rev. **D64** (2001) 083507.

[163] Feynhiggs.

[164] FeynHiggsFast.

[165] higgsqcd.

[166] chardonnay.

[167] bottinopbar.

[168] linejk.

[169] Gould321.

[170] P. Gondolo, private communication.

[171] K. Griest and D. Seckel, Phys. Rev. **D43** (1991) 3191.

[172] W.F. Mcdonough, Treatise on Geochemistry, Vol 2, Elsevier, 2003. (The values for the Earth composition are very close to those in The Encyclopedia of Geochemistry, Eds. Marshall and Fairbridge, Klower Acadmic Publ, 1998.)

[173] Perl script **form2f** to convert from Form output to Fortran output, written by J. Edsjö.

[174] L. Bergström and P. Ullio, Nucl. Phys. **B504** (1997) 27.

[175] P. Ullio and L. Bergström, Phys. Rev. **D57** (1998) 1962.

[176] L. Bergström, P. Ullio and J. Buckley, Astrop. Phys. **9** (1998) 137.

[177] J. Edsjö, ... **SFCOANN**.

[178] P. Gambino and M. Misiak, Nucl. Phys. **B611** (2001) 338.

[179] A. J. Buras, A. Czarnecki, M. Misiak and J. Urban, Nucl. Phys. **B631** (2002) 219.

[180] M. Ciuchini, G. Degrassi, P. Gambino and G. F. Giudice, Nucl. Phys. **B527** (1998) 21.

[181] G. Degrassi, P. Gambino and G. F. Giudice, JHEP **0012** (2000) 009.

[182] M. Ciuchini, G. Degrassi, P. Gambino and G. F. Giudice, Nucl. Phys. **B534** (1998) 3.

[183] K. Okumura and L. Roszkowski, hep-ph/0212007, Proceedings SUSY02.

[184] K. Hagiwara et al., Phys. Rev. **D66** (2002) 010001.

[185] F. Donato, N. Fornengo and P. Salati, Phys. Rev. **D62** (2000) 043003.

[186] J. Lundberg and J. Edsjö, Phys. Rev. **D69**(2004) 123505. [astro-ph/0401113]

[187] A. Gould, *Gravitational diffusion of solar system WIMPs*, Astrophys. J. **368** (1991) 610.

[188] P. Farinella, C. Froeschlé, C. Froeschlé, R. Gonczi, G. Hahn, A. Morbidelli and G.B. Velsecchi, *Asteroids falling into the Sun*, Nature **371** (1994) 314).

[189] A. Gould and S.M.K Alam, *Can heavy WIMPs be captured by the Earth?*, Astrophys. J. **549** (2001) 72.

[190] **BP2000 solar model.**

[191] T. Bringmann, L. Bergstrom and J. Edsjo, *New Gamma-Ray Contributions to Supersymmetric Dark Matter Annihilation*, JHEP **0801** (2008) 049 [arXiv:0710.3169 [hep-ph]].

[192] L. Bergström, T. Bringmann, M. Eriksson and M. Gustafsson, *Gamma rays from Kaluza-Klein dark matter*, Phys. Rev. Lett. **94**, 131301 (2005) [arXiv:astro-ph/0410359].

[193] A. Birkedal, K. T. Matchev, M. Perelstein and A. Spray, arXiv:hep-ph/0507194.

[194] L. Bergström, *Radiative processes in dark matter photino annihilation*, Phys. Lett. B **225**, 372 (1989).

[195] L. Bergström, T. Bringmann, M. Eriksson and M. Gustafsson, *Gamma rays from heavy neutralino dark matter*, Phys. Rev. Lett. **95** (2005) 241301 [arXiv:hep-ph/0507229].

[196] M. Misiak et al: hep-ph/0609232; M. Misiak and M. Steinhauser: hep-ph/0609241; M. Misiak and M. Steinhauser, private communication; P. Gambino, private communication.

[197] Barbiero et al, Heavy Flavour Averaging Group [arXiv: 0704:3575]

[198] WimpSim Monte Carlo, J. Edsjö, `http://www.physto.se/~edsjo/wimpsim`.

[199] nusigma neutrino-nucleon scattering Monte Carlo, J. Edsjö, `http://www.physto.se/~edsjo/wimpsim`.

[200] M. Blennow, J. Edsjö and T. Ohlsson, *Neutrinos from WIMP Annihilations Obtained Using a Full Three-Flavor Monte Carlo Approach*, JCAP **01** (2008) 021 [arXiv: 0709.3898].

[201] M. Hindmarsh and O. Philipsen, *WIMP Dark Matter and the QCD Equation of State*, Phys. Rev. **D71** (2005) 087302 [arXiV: hep-ph/0501232].

[202] P. Skands, [arXiv: hep-ph/0311123].

[203] B.C. Allanach et al, [arXiv: 0801.0045].

[204] T. Hahn, [arXiv: hep-ph/0605049].

[205] T. Bringmann and S. Hofmann, JCAP **0407** (2007) 016 [arXiv:hep-ph/0612238].

[206] T. Bringmann, New J. Phys. **11** (2009) 105027 [arXiv:0903.0189 [astro-ph.CO]].

[207] A. M. Green, S. Hofmann and D. J. Schwarz, JCAP **0508** (2005) 003 [arXiv:astro-ph/0503387].

[208] A. Loeb and M. Zaldarriaga, Phys. Rev. D **71** (2005) 103520 [arXiv:astro-ph/0504112].

[209] E. Bertschinger, Phys. Rev. D **74** (2006) 063509 [arXiv:astro-ph/0607319].

[210] J. Diemand, B. Moore and J. Stadel, Nature **433** (2005) 389 [arXiv:astro-ph/0501589].